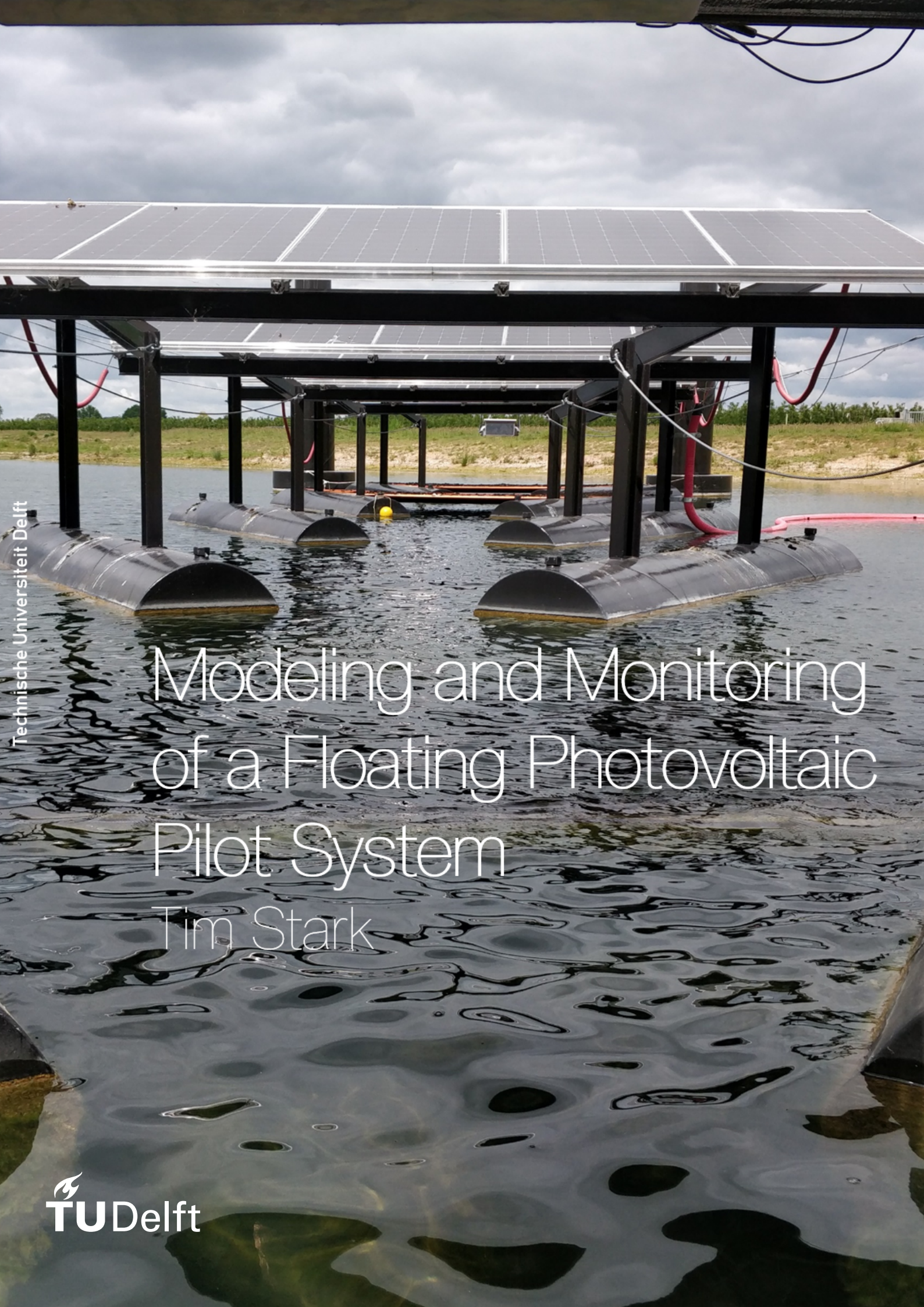

Technische Universiteit Delft

Modeling and Monitoring of a Floating Photovoltaic Pilot System

Tim Stark

TU Delft

Modeling and Monitoring of a Floating Photovoltaic Pilot System

by

Tim Stark

to obtain the degree of Master of Science
at the Delft University of Technology,
to be defended publicly on Monday August 24, 2020 at 13:00.

Student number:	4631781	
Project duration:	November 18, 2019 – August 24, 2020	
Thesis committee:	Dr. ir. O. Isabella,	TU Delft - PVMD, Supervisor
	Dr. ir. H. Ziar,	TU Delft - PVMD, Daily Supervisor
	Dr. ir. M. Cvetkovic,	TU Delft - IEPG
	Dr. ir. R. Santbergen,	TU Delft - PVMD
	Ir. B. Roeffen,	Blue21

This thesis is confidential and cannot be made public until August 24, 2022.

TU Delft

Preface

This thesis report marks the end of my master study *Sustainable Energy Technology* at the Delft University of Technology. I was very fortunate to end my studies with a fascinating thesis subject: the INNOZOWA (Innovative Sun on Water) Project. This thesis project would not have been possible without the help and support of several people.

First, I would like to thank Olindo Isabella for enabling me to carry out my research at the Photovoltaic Materials and Devices (PVMD) group. This research group proved to be a challenging and inspiring environment in which I was able to complete my research on a high level. Second, I would like to thank Hesan Ziar for his support, input, and feedback throughout the thesis project. Our biweekly meetings motivated and encouraged me repeatedly. I really appreciate the time and effort you put into this project. Third, I would like to thank several people that helped me with different aspects of the project: Rudi Santbergen, for his help with the PVMD modeling toolbox; Bjorn Prudon from Waterschap Rivierenland, and Dennis Heijkoop and Daniel van Tilborg from Hakkers, for the information they shared with me throughout the project; and Sandeep Mishra for the support with his irradiance model. Fourth, I would like to thank Milos Cvetkovic, Bart Roeffen and Rudi Santbergen for being part of the thesis committee. Lastly, I would like my thank my friends and family for their continuous support. I especially would like to thank my parents and sister for their love and support throughout this project, particularly the past seven months.

Finally, I'm pleased to announce that the project of which this thesis is part of has been selected by the *European PV Solar Energy Conference and Exhibition* (the largest international conference for photovoltaic research, technologies and applications) for possible publication in the peer-reviewed scientific journal *Progress in Photovoltaics*. The article is expected to be published later this year but a draft version of the article can be found in Appendix A of this report.

Tim Stark
Oud-Beijerland, August 2020

Abstract

Floating photovoltaic (PV) systems enable a sustainable way of generating electricity on bodies of water. Floating PV systems have several advantages over conventional roof and ground-based systems and their potential is substantial. One of the projects that aims to accelerate the development of floating PV in the Netherlands is the INNOZOWA project. Within this project, several parties are working together on the development of floating PV systems which can be utilized on bodies of inland water. To test the designed systems, a pilot project was initiated in September 2019. During the pilot project, two floating PV systems are being tested: the Tracker System and the Retractable System. In total, nine different subsystems are being evaluated, which differ in module type, orientation, and reflector utilization.

The INNOZOWA project provides the opportunity to test the PVMD modeling toolbox in detail and to improve the existing software code. The PVMD modeling toolbox is a modular MATLAB based program designed for making energy yield simulations from cell level up to module level. Considering the opportunity the INNOZOWA project provides to test the PVMD modeling toolbox to its limits and the recommendations for model as well as system improvement that may result from this, this master thesis project was initiated. Broadly, three main topics are discussed in this report: 1) The development of a new power conversion model for the PVMD modeling toolbox. 2) The process of simulating the energy yield of the nine INNOZOWA study cases and the analysis of the results. 3) Detailed performance monitoring of the INNOZOWA subsystems.

Since the INNOZOWA PV pilot system makes use of power optimizers and considering that there is no immediate way of simulating these devices in the PVMD modeling toolbox, an input model for power optimizers is developed. This input model is part of the new Power Conversion script for the PVMD modeling toolbox. Other models added to this new script are models for inverters and cables, based on industry standard models. A manual is created as well to support the user with operating the new script. The Power Conversion tool was tested and validated using INNOZOWA energy yield data.

Energy yield simulations are made for the study cases of the INNOZOWA pilot project. Initial simulations showed significant differences between simulated and monitored values. The deviations resulted from unrealistic albedo values, unsuitable thermal models, and installation faults. An on-site inspection was conducted, yielding important observations which improved the simulation results. The final simulation results showed that on-site irradiance data with a high resolution provides the most accurate results. The percentual difference between simulated data and monitored data was found to be ±10% on monthly as well as on daily basis. No correlation was found between meteorological parameters and the accuracy of the simulations. Uncertainties in the simulations mainly concern the accuracy and resolution of the monitored values, the fouling of the modules and uncertainties on the model side. The simulations yielded recommendations for model and workflow improvement.

Throughout a period of ten months, the performance of the INNOZOWA system was analyzed in detail. Results showed that the bifacial modules of the Tracker System, installed at a tilt angle of 15 degrees, outperform the ground-based reference case by about 9%. Calculations showed that the pumps consume less than 1% of the total yearly energy production per module of the Tracker System. Other important observations include the deviations in the energy yield data of the monofacial modules of the Retractable System (a difference of about 25% between the highest yielding module and the lowest yielding module) and the monofacial modules of the Tracker System, installed at a tilt angle of zero degrees (a difference of about 50% between the highest yielding module and the lowest yielding module in December 2019). The former case is explained by the shadows that are being casted by the support structure. The deviations in the energy yield of the monofacial modules of the Tracker System are expected to arise from the internal control which determines the optimizer output voltage. From the analysis of the albedo of the water and the reflectance of the reflectors it is concluded that the water albedo is low (0.05 during operating hours) and reflectors are needed for floating bifacial modules.

Contents

1 Introduction

This chapter provides an extensive introduction to the topics that are of importance in this master thesis research. First, the advantages and challenges, the current status, and the future potential of floating photovoltaic (PV) systems are discussed. Second, an introduction is given to the INNOZOWA project, which this thesis is a part of. Third, a description is given of the PVMD modeling toolbox, which is a MATLAB based simulation tool which can be used to make energy yield calculations of PV modules. When all topics are introduced, the main research question and the sub-questions of this thesis are introduced. Finally, the structure of this report is given.

1.1. Floating Photovoltaic Systems

This section gives an overview of floating photovoltaic (FPV) systems with the goal to create a better technical understanding of these systems and to illustrate their potential and remaining challenges. First a short introduction is given on the technology itself and the potential advantages and remaining challenges. Second, the current global status of FPV systems is explored. Finally, the global potential of this technology is examined.

1.1.1. What are Floating PV systems?

Over the past two decades the worldwide implementation of renewable energy sources has grown rapidly. According to the International Renewable Energy Agency, the renewable generation capacity has expanded from less than 20 GW per year in 2001 to about 160 GW per year in the last four years [1]. This growth has been accelerated by initiatives like the Paris Agreement in which almost all countries pledged to strengthen their response to the threat of climate change to prevent global warming [2]. One of the fastest growing and most promising renewable energy sources is solar PV. This technology converts light from the sun to a renewable form of electricity. The total installed solar PV capacity increased from 808 MWp in the year 2000 up to 480,000 MWp in 2018 1.1. The trend of cumulative installed solar PV capacity is shown in Figure 1.1.

There are multiple ways solar PV can be utilized. PV systems are typically build and operated on land or roofs. Other emerging forms of solar PV systems are, for example, building integrated PV and floating PV. Floating PV has gained a lot of interest in the past decade and has a huge potential. The biggest reason for this gained interest is the lack of suitable areas of land for (large-scale) ground based PV systems. Furthermore, if suitable areas *are* available, there are multiple competing uses for this land. This has lead to the development and research of the deployment of solar PV on water bodies like water basins, dredging depots, sand extraction sites, flooded coal mines, buffer sumps, and waste water treatment plants.

A floating PV system is basically an ordinary PV system but with some additional components to make the system float and to ensure it stays in the same spot. The floating system typically consist of so called pontoons. Pontoons are large flotation devices which can carry a significant number of PV modules. They consist of plastic hollow floats which are combined to form the pontoon. These floats

are typically made out of HDPE (high density poly-ethylene) known for its tensile strength, maintenance free use, and UV and corrosion resistance. Furthermore, a mooring system is used fix the floater in place and to prevent the system from floating away due to winds or currents. The requirements of this system typically depend on the nature of the water: the water depth, wave weight, distance to the shore, current, tides, etc. [3]

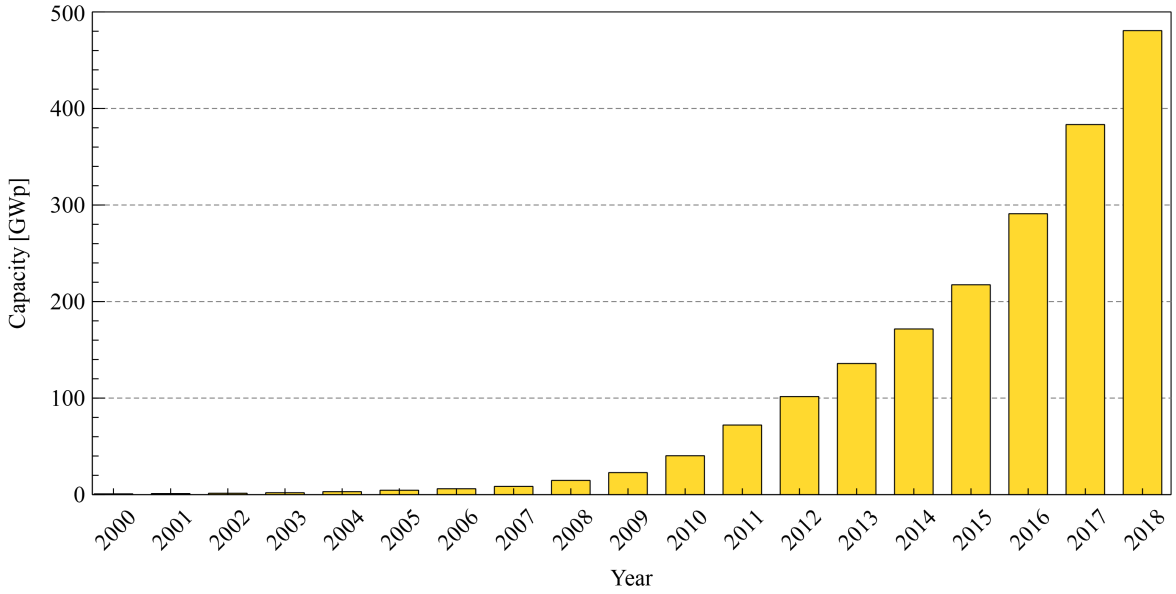

Figure 1.1: Global installed solar PV capacity. Adapted from [4].

Apart from the advantage of using floating PV in highly populated areas with competing uses for land as described earlier, there are many other advantages associated with floating PV:

- **Increased Efficiency of the PV Modules**. The surroundings of the PV modules on water are typically cooler than on land. This is the result of the reflection of light from the water and the natural cooling effect of the water. These factors lead to an increased efficiency of the PV module, since the module efficiency depends linearly on the operating temperature [5]. Several studies have been conducted to examine the efficiency increase from the cooling effect of the water. The results of these studies range from an efficiency increase of 1.5 to 2% based on theoretical research for a typical polysilicon PV module [6], to 11% based on empirical research [7].
- **Reduced Evaporation of the Water**. The shading provided by the floating PV systems reduces water evaporation. Furthermore, the system limits the evaporating effects of wind. This advantage could be utilized by water reservoirs and artificial lakes in places were water is evaporating (too quickly) due to extreme weather conditions. [3, 8]
- **Improved Water Quality**. The floating system prevents sunlight from entering the water and therefore disrupts the photosynthesis process. This could be useful for bodies of water were algae growth is undesired, like buffer sumps or reservoirs [8]. However, at natural bodies of water with an ecological significance, this could actually be a negative consequence. More information on the negative consequences of floating PV on the ecology can be found later in this section.
- **Less Dust Effects**. This could especially be an advantage for places with high solar energy potential that are dusty and arid, like dry/desert biomes, since the effect of dust on the modules can reduce the energy output significantly [9].
- **Synergy with Other Forms of Renewable Energy**. Floating PV could be used in combination with other forms of renewable energy to create a complementary energy system. An example of such a synergy is the combination of floating PV plants with large existing hydropower plants. The floating PV systems can be installed on the reservoirs of the hydropower plant, while using

the existing energy infrastructure. The solar capacity can then be used to manage periods with low water availability. Furthermore, the hydropower can be used to smoothen the variable solar output [8]. Another possible synergy is the combination of floating PV with offshore wind energy. Since solar and offshore wind energy are complementary energy sources, they can utilize the same energy infrastructure [10]. This could lower the cost for both offshore wind projects and offshore floating PV.

Floating PV systems present many advantages over ground based systems, however, floating solar is still an emerging technology with a lack of a robust track record. This means that there are several uncertainties still surrounding the technology, like costs, permitting and licensing, environmental and ecological impact, and design, building and operating. These uncertainties are described in more detailed below:

- **Costs**. The costs of floating PV systems are still slightly higher than the costs of ground based PV systems, mainly because of the floating devices and the mooring and anchoring systems. However, these costs are expected to drop due to the large projects that are being planned and the subsequent improved economies of scale [8]. Furthermore, the slightly higher costs could be balanced by the (possible) increase in energy yield. However, more long-time research is needed to get a better understanding of the economics of floating PV systems.
- **Permitting and Licensing**. There are currently no clear regulations on the permitting and licensing of floating PV systems [8]. It is therefore important to create an unambiguous policy with regards to safety, ecological aspects and water quality [10]. On a national level, the first report to assess these issues was published by the knowledge centre for water managements, STOWA. The report, called 'handreiking voor vergunningverlening drijvende zonneparken op water' (Guide for the permitting of floating solar parks on water), provides a flowchart to indicate all the necessary steps needed to get the permits for a floating PV systems in the Netherlands [11].
- **Design, Building and Operation**. Challenges regarding the design and building of floating PV systems are: The wave and wind resistance of the floating structures as well as the mooring and anchoring systems, the lifetime and reliability of the system under moist conditions and the choice for module orientation, tracking systems and module technology (e.g. the use of bifacial modules). Depending on the local conditions and the design choices, significant differences in the economics of the system can occur. Furthermore, finding the right balance between production, transport and construction is an ongoing process. [10].
- **Water Quality and Ecology**. The same report as mentioned under 'Permitting and Licensing' assessed the effects of floating PV systems on the water quality and the local ecology [11]. It concluded that floating PV systems can have a significant effect on the water temperature, the distribution of the temperature throughout the body of water, the oxygen level, the biomass, and the area that is suitable for water plants. The operation of a FPV system could therefore negatively influence the water quality and ecology. However, it should be noted that this depends on the location of the FPV system as well as on the area that the FPV system covers on the body of water. Several tools were developed to assess individual bodies of water to indicate the possible ecological effects. Monitoring of (pilot) systems is needed to get a better understanding of the aforementioned effects.

1.1.2. Current Status of Floating PV

This subsection briefly discusses the current status of FPV systems. First some historical context is provided. Second the current status of FPV on a global scale as well as the status of FPV in the Netherlands is discussed.

The first floating PV plant was build in 2007, in the country of Japan. The first commercial installation followed a year later; a 175kWp system build in the United States, California. From 2013 onward the global interest in floating PV systems increased, as more countries started to develop and test FPV systems, especially countries like Japan, South-Korea and the US. In 2016 the first larger than 10MWp plant was completed while two years later the first larger than 100MWp plant was put into use. Figure 1.2 shows the global annual and cumulative installed floating PV capacity up to September 2018 [8].

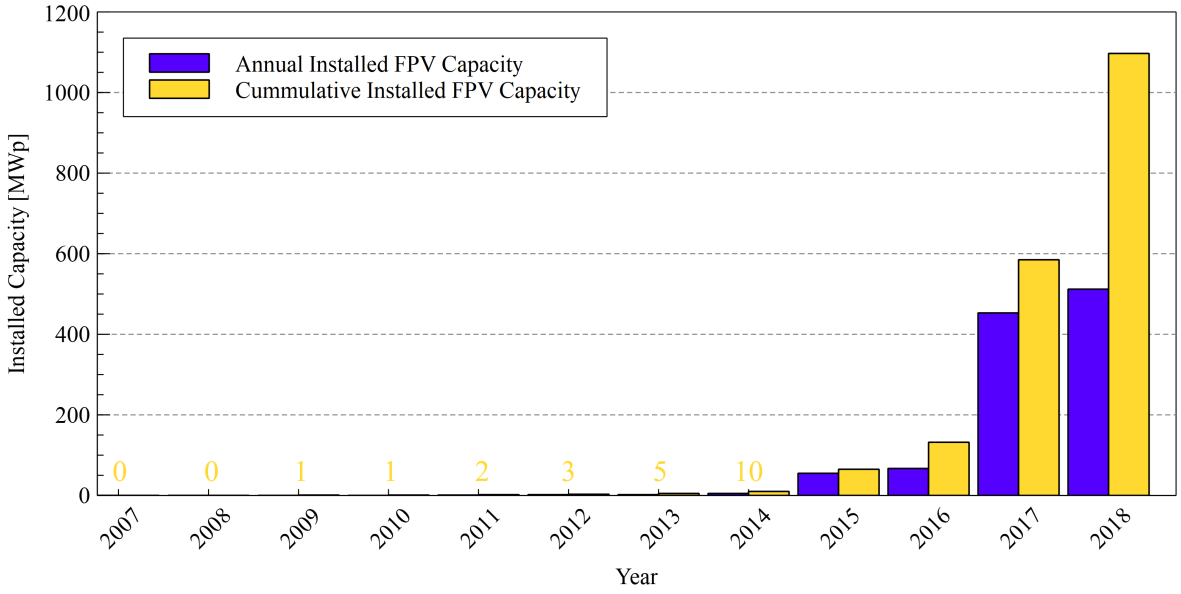

Figure 1.2: Global installed floating PV capacity. Adapted from [8].

By December 2018, the total installed capacity of floating solar was about 1.3 GWp, which is equal to the installed capacity of land based solar in 2000 [8]. According to a recent study (September 2019) by Wood Mackenzie Power & Renewables, the demand for floating Solar is expected to grow by an average of 22% from 2019 through 2024 [12]. Notable examples of planned large scale FPV projects are a 200MWp plant in Indonesia [13] and a 1GWp plant in India [14].

The main driving force behind the research and development of floating photovoltaic systems in the Netherlands is the 'Nationaal Consortium Zon op Water' (National Consortium Sun on Water), which is a partnership between more than 35 parties, including governmental institutions, companies and knowledge institutions. This consortium is involved with several (pilot) projects throughout the Netherlands to accelerate the energy transition using floating PV. One of the projects that they are involved with is 'INNOZOWA' (Innovative Sun on Water), which is introduced in Section 1.2 of this chapter. [15]

1.1.3. The Potential of Floating PV

The previous subsection showed that there is national and international interest in floating PV by giving historical context and providing an overview of the current status of this technology. However, the current installed capacity is only a small fraction of the potential global capacity. Because of the advantages of FPV and the progress made with these systems, many studies have been conducted, on national as well as international level, to assess the total potential of floating PV. A brief overview of some of these studies is given to illustrate the significant potential of this emerging technology.

According to a recent report by the World Bank Group the global potential for floating PV is exceeding 400GWp, based on their most conservative estimations [8]. This is almost equal to the total worldwide installed PV capacity in 2017 [4]. A detailed breakdown of their estimated potential can be found in Table 1.1.

Table 1.1: Peak capacity and energy generation potential of floating solar on freshwater man-made reservoirs, by continent. Adapted from [8].

Continent	**Total surface area available (km^2)**	**Number of water bodies assessed**	**Floating PV potential (GWp) [5% of total surface area used]**	**Possible annual energy generation (GWh/year) [5% of total surface area used]**
Africa	101,130	724	506	835,824
Middle East and Asia	115,621	2,041	578	643,456
Europe	20,424	1,082	102	97,868
North America	126,017	2,248	630	704,076
Australia and Oceania	4,991	254	25	33,565
South America	36,271	299	181	290,753
Total	**404,454**	**6,648**	**2,022**	**2,605,542**

In December 2018 the National Renewable Energy Laboratory (NREL) provided the first large scale potential study for floating PV in the US [16]. They estimated that by installing floating PV on suitable water bodies, about 10% of the current domestic electricity generation can be produced. Furthermore, many of these water bodies are located in water-stressed areas with high land and electricity costs, adding to the value of floating PV.

The 'Nationaal Consortium Zon op Water' made a prognosis of the potential floating solar capacity up to 2023. They estimate a total cumulative installed capacity of over 2GWp in the Netherlands by 2023. The breakdown of this estimation is shown in Figure 1.3 [10].

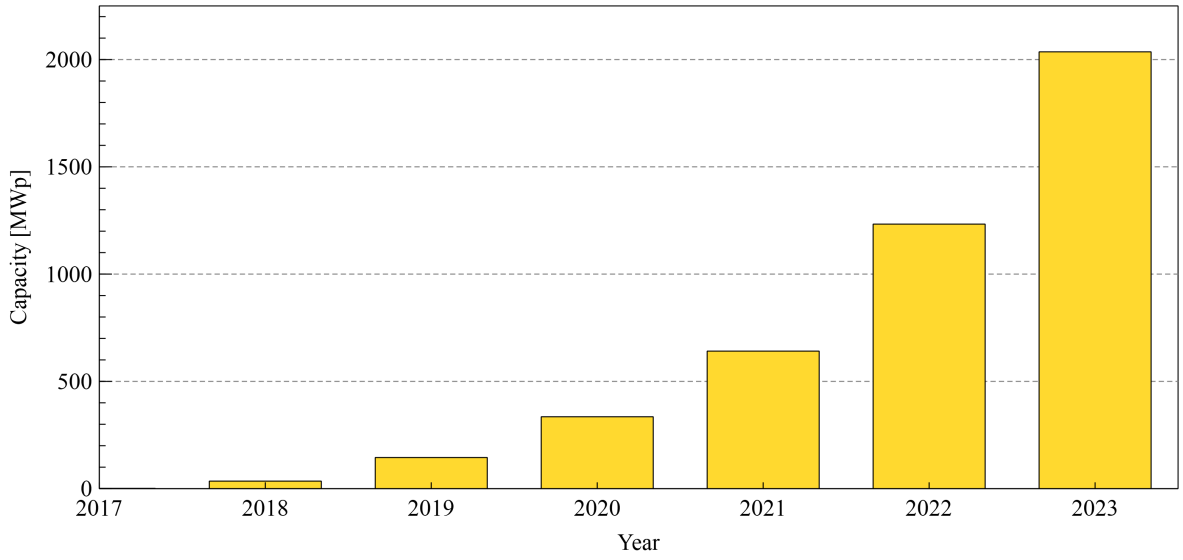

Figure 1.3: Prognosis of cumulative installed FPV capacity in the Netherlands. Adapted from [10].

In the same report an extended, long-term, prognosis is given for the total potential capacity of floating PV. The prognosis is broken down into 4 categories: wave category 1 to 4, which differentiate in wave height, wind speed and water depth. This prognosis is shown in Table 1.2

Table 1.2: Long-term prognosis of the total potential of floating photovoltaic systems in the Netherlands [10].

Wave Category	Description	GWp
1	Wastewater treatment plants, small inland water,	8
2	Slufter Maasvlakte, Tjeukemeer, Veluwe randmeren, large sand extraction sites	8
3	IJsselmeer, Markermeer, Zeeuwse wateren, lades	8
4	Sea	51
Total		**75**

From the examined sources it can be concluded that there is a significant potential for solar PV on water, globally as well as on a national level in the Netherlands. In the next subsection, the future developments of floating PV systems are discussed.

1.1.4. Future Developments of Floating PV

As described in the previous sections, progress is made with floating PV on man-made bodies of water like reservoirs and water ponds. However, the development of floating PV is advancing, and companies and governments are starting to show interest in a relatively new FPV technology: *offshore* floating PV [8]. Considering the limited availability of land, offshore floating PV might be the only viable option for small island states or populous near-shore cities. Although the concept of near-shore floating PV systems is more or less equal to floating PV on inland bodies of water, the near-shore concept comes with additional challenges:

- Due to the higher wind speed and higher waves, the water conditions are much rougher at near-shore sites. Moreover, currents and tides provide an additional challenge. These harsher water conditions impose strict requirements on the floating constructions as well on the mooring and anchoring of the system [8].
- The salinity of the water presents an extra challenge with regards to the material that can be used.
- The accumulation of organic material from local organisms (bio-fouling) can interfere with the functionality of the PV system. Furthermore, the PV system can interfere with the complex natural systems and natural habitats of these local organisms.

1.2. The INNOZOWA Project

This master thesis is part of a project called INNOZOWA. The INNOZOWA project was already briefly mentioned in Section 1.1.2. In this section, INNOZOWA is formally introduced with the aim to provide a complete overview of the project. First, background information is provided after which the objectives of the project are formulated. Second, the role of the TU Delft in this project is explained in more detail, including the research by previous master thesis students. Finally, the current status of the project is discussed.

1.2.1. Background Information and Project Objectives

INNOZOWA is a dutch acronym which stand for INNOvatieve Zon-pv op Water (Innovative Solar PV on Water). The project is initiated by the water board Rivierenland, which is a governmental body tasked with the management of water in their region. An overview of their jurisdiction is shown in Figure 1.4.

The water board identified a potential for floating PV systems on the surface water that falls under their jurisdiction. They estimated that an area of 3800 ha is available of which about 800 ha is suitable for floating PV. Most of these bodies of water are so called 'waterbergingen', which are large 'river buffer lakes' that are used for flood protection. By utilizing these flood protection lakes for floating PV, the water board aims to give substance to their energy goals and improve their water management. The main objective of the project, as formulated by the water board, is:

To accelerate the development of a solar PV system that can be utilized on bodies of inland water, which is competing and complementary for solar PV on land and has an added value for the goals of the water management. [17]

Utilizing a floating PV system on a buffer lake has additional challenges compared to the challenges that were discussed in Section 1.1.2. The first additional challenge in this project is the mowing and dredging of the buffer lakes, which needs to happen once to twice a year to keep the lake operational. This is done with (mowing) boats. Consequently, a static PV system would be inconvenient, since the boats wouldn't be able to cover the entire lake. It is therefore required to develop a system that can move around so that the buffer lake can be properly maintained. A second additional challenge is that the lake can be, at times, completely empty. The construction should therefore be amphibious; it should function both on water and on land. [18]

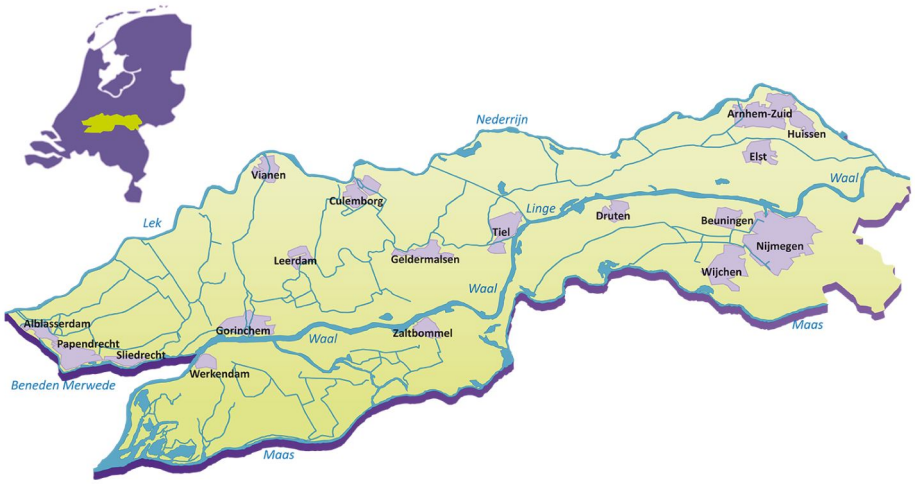

Figure 1.4: Jurisdiction of the water board Rivierenland. Reproduced from [18].

.

Based on the main goal and the additional challenges that were identified, a project plan was composed. This project plan is divided into five 'work tasks':

1. Research and development of the floating construction.
2. Optimisation of the bifacial modules.
3. Pilot research.
4. Scale-up research.
5. Project management and communication.

These tasks are carried out by several parties. These parties, as well as the work that has been done up to this point is briefly described in the next section.

1.2.2. Involved Parties and Previous Work

Within the INNOZOWA project four parties are working closely together:

- **Waterschap Rivierenland** - The water board Rivierenland is the initiator of the project and the eventual end-user of the floating PV system.
- **Blue21 B.V.** - Blue 21 is a company specialized in the design, research and realization of floating structures. They are involved with the design of the system, project management, research and monitoring and the eventual marketing of the product.
- **Hakkers B.V.** - Hakkers is a company specialized, among other things, in building on water. They are involved with the realization of the pilot installation, especially the mechanical structures.
- **TU Delft** - The TU Delft supports this project with scientific research, through the Photovoltaic Materials and Devices (PVMD) research group.

This master thesis is the next, independent, report in a series of several master thesis reports, providing academic research and support for the INNOZOWA project. This section briefly discusses some of the work that was carried out by preceding students, to give context to the current work.

The first thesis project was carried out by Elias Garcia Goma. The main goal of this thesis was to create a modular simulation toolbox which can be used to estimate the energy yield of a PV module. This toolbox will be further introduced in section 1.3. Finally, the toolbox was utilized to estimate and optimize the INNOZOWA PV system. [19]

The second project was carried out by Julen Garro Etxebarria. The main goal of this project was to investigate the validity of floating PV systems formed by bifacial modules and reflectors in the Netherlands. In order to investigate this validity, the PVMD toolbox was improved, including the addition of a thermal model using COMSOL to accurately study the thermal behaviour of bifacial modules. [20]

The third project in this series was carried out by Ignacio Narváez Alavez. The main goal of this research was to develop a monitoring system that can store historical data from the INNOZOWA pilot system. Furthermore, the PVMD toolbox was validated and used to make preliminary estimations of the INNOZOWA pilot system energy yield. [21]

1.2.3. Current Status of the Project

In Section 1.2.1, the work tasks of the project were briefly mentioned. In this section, the third work task, the pilot research, is concisely explained as this is the current phase of the project. The goal of this task, as described by the project team of INNOZOWA, is:

- To demonstrate the added value of a solar PV system on water, with bifacial panels.
- To demonstrate the robustness of the movable floating construction.
- Obtain the required knowledge for a definitive design of the floating construction.
- Monitor the maintenance of the pilot system as well as the effects on the water management and surroundings.

To achieve these goals, the pilot system needs to be tested on a significant scale. A suitable location was found near the waste water treatment plant in Weurt (Figure 1.5) which is property of the water board. At his location three systems are currently being tested. Two of these systems are floating structures, one of which has single-axis tracking capabilities. Additionally, a land-based system is used which serves as a reference case for the floating systems. In total 50 modules are deployed, including monofacial and bifacial module types. Each module is connected to a power optimizer and finally to a central inverter. The pilot started mid September 2019 and will continue for at least one year to level out seasonal fluctuations. During this period, the pilot system generates data, such as the output power, voltage and, current. This data can be analyzed and used to validate simulations. The set-up of the pilot system and all its technical specifications is described in detail in Chapter 3.

Figure 1.5: The picture on the left shows the location of the floating PV pilot system in Weurt, indicated by the red square (Adapted from [22]). The picture on the right shows a bird's-eye view of the pilot system.

.

1.3. The PVMD Modeling Toolbox

In this section, the PVMD Modeling Toolbox is introduced. The goal of this introduction is to get a better understanding of the toolbox since it will be heavily used in this master thesis project. The PVMD modeling toolbox is a modular modeling software package developed in MATLAB. It is developed internally by the PVMD research group. The goal of the toolbox is to provide a modular and detailed simulation of a PV module, from cell level up to module level based on user inputs. This section briefly introduces each of the four main scripts that are currently available in the toolbox. A flowchart, giving an overview of the toolbox, is shown in Figure 1.6.

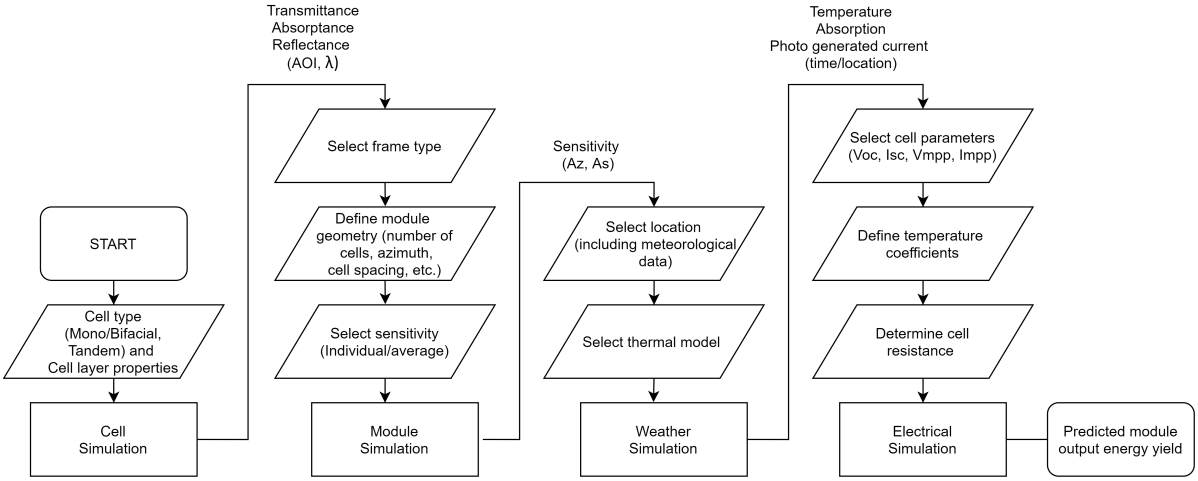

Figure 1.6: Flowchart of the PVMD toolbox. The trapezoids indicate the user inputs.

1.3.1. Cell Simulation

The first main script of the toolbox is the 'CELL' script. The user selects the type of cell: monofacial, bifacial or tandem. The cell is defined by a set of properties, such as: the thickness of the individual layers, layer texture, and reflection. The model is based on GenPro4, which is an optical model for solar cells that combines wave and ray-optics. In this optical model the solar cell is represented as a multi-layer structure. The model calculates the incident light absorbed in each layer and subsequently calculates the implied photocurrent and generation profile. The model output is the reflectance, absorptance in every layer and transmittance as a function of wavelength and angle of incidence, both for front and, in the case of a bifacial cell, rear-side illumination.

1.3.2. Module Simulation

The second main script of the toolbox is the 'MODULE' script. The goal of this script is to accurately predict the sensitivity of the cells within a module based on light coming from different azimuths and altitudes. The simulation builds a 3D geometry of the module and frame, based on parameters defined by the user. First, the module type is defined. Currently there is only one module type available in the toolbox: 'the four legged frame'. After selecting the type, the module geometry is defined (i.e. number of cell rows/columns, spacing, tilt, azimuth, etc.). Finally, the user is asked to choose between individual or average cell sensitivity. These properties are combined with the properties calculated in the previous 'CELL' script to calculate a sensitivity map of the module, which is the output of this script.

1.3.3. Weather Simulation

The third main script of the toolbox is the 'WEATHER' script. The goal of this script is to predict the irradiance absorbed by the module over a period of time. First, the model creates a sky Map showing the amount of light per every azimuth and altitude of the hemisphere, based on the input of the user. This sky map is then combined with the sensitivity map of the previous 'MODULE' script and the absorption of the 'CELL' script to estimate the generation of current in the PV module. The final step of this script is to calculate the operating cell temperature, based on a user defined thermal model. The final

output of this script is the operating cell temperature, the total absorption in every cell, and the implied photocurrent in every absorber layer.

1.3.4. Electrical Simulation

The 'ELECTRICAL' script is the fourth and final part of the current version of the PVMD toolbox. The goal of this script is to accurately assess how much electricity can be extracted out of the PV module. This is achieved by representing the solar cell with an equivalent circuit which results in an I-V curve for each point in time. From this curve the maximum power point can be calculated. The final output of the script is the predicted module output energy yield at every point in time.

1.4. Research Questions

Although there are still challenges left for floating photovoltaic systems, their potential is abundant and their advantages over traditional PV systems seem significant. Internationally, the attention for floating PV grows steadily as economies of scale drive the price of these systems down even further. In the Netherlands, the capacity of floating PV can reach multi-GWp scale in the second half of this decade. One of the pioneering projects regarding floating PV in the Netherlands is INNOZOWA. This project aims to accelerate the development of floating PV on bodies of in-land water. To reach this goal, a pilot project was initiated in September 2019 at which several systems are currently being tested. This thesis project is part of the research that is being conducted during pilot phase of the INNOZOWA project.

To asses the performance of the INNOZOWA systems, the energy yield of each individual module in the system is closely monitored. The energy yield of these modules should be accurately analyzed to check for any deficiencies or anomalies. One way of analyzing experimental data is to compare it with simulated data. Depending on the accuracy of the used models, the performance of the PV modules can be verified. There are several commercial and open-source software packages available to make these kind of energy yield simulations for PV systems, such as PVsyst, PVSOL, PVlib and the System Advisor Model (SAM). A comparable software package is currently under development in the Photovoltaic Materials and Devices Research Group of the TU Delft. This MATLAB based software package, the PVMD Modeling Toolbox, currently consists of four main scripts which enables the user to create a PV module from cell level up to module level and simulate its energy yield. The toolbox is still under development and several models are yet to be validated.

The INNOZOWA project provides an opportunity to test the current version of the PVMD modeling toolbox to its limits. Reconstructing the INNOZOWA system in the PVMD modeling toolbox is expected to provide valuable feedback and recommendations to the toolbox and the simulation procedure. Furthermore, the simulations can be validated with monitored data from the different INNOZOWA subsystems. This provides the opportunity to asses the accuracy of the toolbox. Previous research established a ±15% accuracy of the current version of the toolbox, under certain circumstances [21]. Using INNOZOWA input data, this accuracy can be put to the test . Finally, considering the accuracy that was reached with previous validations of the tool, the outcome of the simulations can provide some insight in the performance of the modules.

Considering the opportunities that the INNOZOWA pilot project provides for improving the PVMD modeling toolbox and the knowledge that can be gained about floating PV systems in general, this master thesis project was initiated. The main question this research aims to answer is:

How does the energy production of the INNOZOWA PV Pilot system compare to energy yield simulations made with an improved version of the PVMD modeling toolbox?

To answer this main question, several secondary questions need to be answered:

1. *How to model the efficiency of a power optimizer and include it as an input model in the new Power Conversion script of the PVMD modeling toolbox?*

2. *Which components are needed to build a functional and convenient power conversion tool for the PVMD modeling toolbox, how are these components modeled, and how can they be included in the PVMD modeling toolbox?*
3. *Which parameters should be used to accurately simulate the energy yield of the INNOZOWA PV pilot system in the PVMD modeling toolbox?*
4. *Which parts of the PVMD modeling toolbox can be improved based on the experience of simulating the INNOZOWA PV pilot system?*
5. *Are there any defects or deviations present in the system installation that could contribute to model and data uncertainties and how can these defects or deviations be found during an on-site inspection?*
6. *Based on a thorough data analysis of the different subsystems, are there any anomalies in the data and where do these anomalies come from?*
7. *How can the INNOZOWA PV pilot subsystems potentially be improved and which subsystem is the most likely to be used for subsequent projects and up-scaling?*

1.5. Structure of the Report

The secondary research questions mentioned in the previous section are answered in five chapters. First, the development of a new Power Conversion tool for the PVMD modeling toolbox is discussed in detail in Chapter 2. Second, the procedure of simulating the INNOZOWA subsystems in the PVMD modeling toolbox and the results of these simulations are discussed in Chapter 3. Third, the on-site inspection that was conducted is explained in Chapter 4. In Chapter 5, a thorough data analysis is made of the different INNOZOWA subsystems, including an assessment of the anomalies that are found during this analysis. Finally, the conclusions and recommendations are provided in Chapter 6.

2

Development of a Power Conversion Model for the PVMD Toolbox

One of the main goals of this thesis project is to compare the energy yield of the INNOZOWA PV pilot system with an energy yield simulated by the PVMD modeling toolbox. This simulation serves multiple purposes. One of the objectives is to improve the PVMD modeling toolbox by adding new parts of code to the toolbox which are needed to accurately simulate the INNOZOWA system. The toolbox currently consists of four main simulation scripts. These scripts were briefly introduced in Section 1.3 of the Introduction. When making a simulation in the current version of this toolbox, the final output is the energy yield of a single PV module. Furthermore, it is not possible to make a simulation of any of the 'balance of system' components. However, in the INNOZOWA pilot system power optimizers are used on module level to monitor the energy production of each individual module. Power optimizers slightly decrease the energy yield of the system due to the internal losses caused by its electrical components. In order to compare the energy yield of the INNOZOWA modules with a simulated energy yield, the efficiency of the power optimizers should be simulated as well. This chapter, therefore, aims to create a model which can simulate these power optimizer.

This model should be part of a new main script of the PVMD modeling toolbox, called: Power Conversion. This script should contain models which are used for simulating any equipment after the PV modules. After consultation with several stakeholders, a decision was made to at least include a model for inverters and cables in the new Power conversion tool. These models are added, together with the power optimizer model to the new 'main' script. The research questions that are associated with the development of the power optimizer model and the models for the other systems components are, respectively:

1. *How to model the efficiency of a power optimizer and include it as an input model in the new Power Conversion unit of the PVMD modeling toolbox?*
2. *Which components are needed to build a functional and convenient power conversion tool for the PVMD modeling toolbox, how are these components modeled and how can they be included in the PVMD modeling toolbox?*

Several boundary conditions were set at the start of this project concerning the development of the aforementioned models:

- The user should be able to make the simulations of the different components based on information from data-sheets or basic project information.
- Next to the power optimizer, at least a model for inverters and cables should be added to the newly build power conversion model.
- The power conversion model has to be fully integrated within the current version of the PVMD modeling toolbox and should be easily customizable.

- Multiple checks and warnings should be added in the code at points were the user inputs data to check if the inputted data makes sense.

This chapter consists of five parts. First, the working principles of a power optimizer as well as the advantages of a power optimizers are introduced. Second, a global description of the newly build Power Conversion model is given. After this description the underlying principles of simulating the power optimizer, the inverters, and the cable losses are discussed. Next, a validation is made of the newly build model. Finally, the conclusions and recommendations for this chapter are given.

2.1. Power Optimizers

In this section the concept of a power optimizer is introduced with the goal to get a better understanding of the role of a power optimizer in a PV system. Generally speaking, PV systems can be divided into four main groups: systems with a central inverter, systems with a string inverter, systems with a micro inverter and systems with a central inverter in combination with power optimizers [23]. The selection of architecture is based on many factors, such as local environment and system size. For this project, power optimizers are of interest because each module of the INNOZOWA PV system is connected to a SolarEdge power optimizer for continues monitoring.

Power optimizers are small devices, which are typically used on module level in a PV system. These devices contain a DC-DC converter in combination with a maximum power-point (MPP) tracker. The optimizers works in a similar way the DC-DC converter works in a typical inverter. The maximum power point tracker controls the operating point of the module while the operating point is set by the DC-DC converter. Effectively, a power optimizer forces each individual module to work at its maximum power point while a typical inverter applies the same operating point for each module in the string. Multiple power optimizers are typically connected in series and eventually connected to a central inverter.

There are many advantages associated with installing power optimizers in a PV system. Firstly, power optimizers mitigate the different working conditions of the modules in a PV system. These working conditions can be influenced by a lot of factors, such as: shading, soiling, dirtiness, mismatch between PV cells generated during the manufacturing process, mismatch due to aging, differences in orientation and inclination of the surface, and differences in temperature or irradiance [24]. These factors can limit the output current of a single or multiple cells in a module and therefore limit the current of the entire string. i.e. the weakest link determines the output of the entire string of the PV system. Installing a power optimizer would mitigate this issue as each module can operate at its own maximum power point and is not limited by e.g. a shaded cell of another module. A second advantage of power optimizers is that they provide a new level of safety in the system. Typically, the optimizer output voltage can be lowered during installation and commissioning to reduce electrocution hazards for installers [25]. The final advantage that is typically associated with power optimizers is that they enable monitoring of the performance of the module they are connected with. This is also the main reason why power optimizers are installed for the INNOZOWA pilot system. The power optimizer enables detailed analysis of each installed module.

There are several power optimizer types and manufacturers which produce these optimizers. There are optimizers which work on string level, on module level and even on cell-string level. For this project, the main focus lays on module-level optimizers, with an emphasis on the optimizers produced by the company SolarEdge, as these are installed for the INNOZOWA project.

2.2. Global Description of the Model

In this subsection, a global description of the Power Conversion tool is given. The goal of this description is to provide a concise overview of the simulation process of a newly developed model for the PVMD modeling toolbox: the Power Conversion model. The simulation process is shown, in a simplified way, in Figure 2.1.

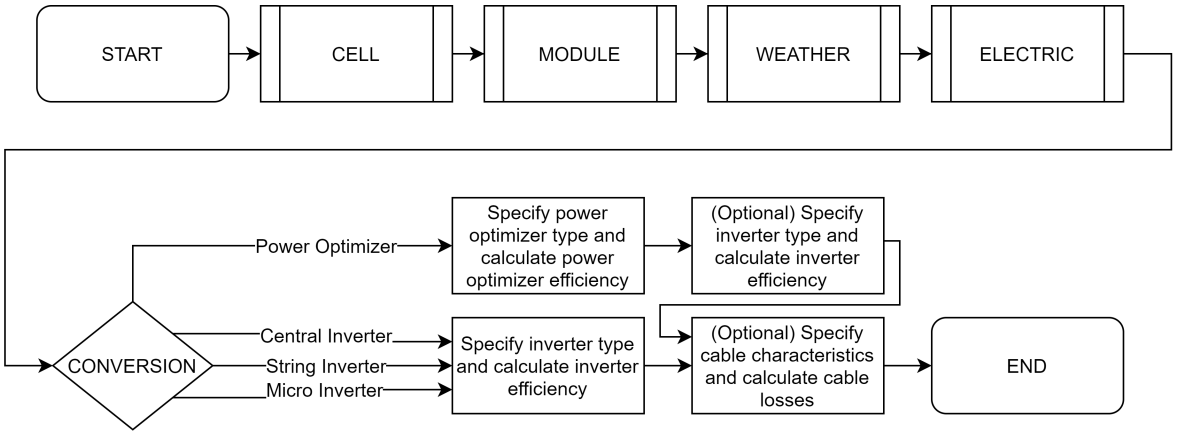

Figure 2.1: Simplified process diagram of the power conversion tool for the PVMD Modeling Toolbox.

After the 'CELL', "MODULE', 'WEATHER', and 'ELECTRIC' simulations, a new simulation option is added to the PVMD toolbox. This new option is called 'CONVERSION'. With this new option, the user has the ability to include a selection of power conversion methods as well as cable losses to the simulation of a PV system. After simulating the 'ELECTRIC' part, yielding the power, voltage and current at maximum power point, the user of the toolbox can choose from four different power conversion methods: power optimizer (with or without complementary inverter), central inverter, string inverter, or a micro inverter. The tool automatically calculates the efficiency of these devices based on several user inputs. The power optimizer efficiency is calculated based on the efficiency curves that are provided by the manufacturer. More details about this efficiency calculation procedure can be found in Section 2.3. The efficiency of the inverters is based on the Sandia Notional Laboratories (SNL) model. More details about the efficiency calculation of inverters can be found in Section 2.4

The Power Conversion tool is relatively easy to use thanks to the build-in user interfaces. These interfaces make sure that the user inputs correct data. In some places warnings are included to alert the user if their data input is not correct. Alongside the tool, a user manual is developed. This manual explains how the tool can be operated. Moreover, some of the design choices are concisely explained by the manual. The user manual can be found in Appendix B of this report.

2.3. Power Optimizer Modeling

This section describes how power optimizers are modeled in the new Power Conversion tool of the PVMD modeling toolbox. In the first subsection the underlying principles of the efficiency calculations are explained. The second subsection details the procedure of including an inverter in a system with power optimizers. Finally, in the last subsection, a note on string sizing is included.

2.3.1. Power Optimizer Efficiency

Power optimizers, already briefly introduced in Section 2.1, serve as an MPP tracker and DC-DC converter on module level. The current version of the PVMD modeling toolbox already outputs the DC power of the simulated module at maximum power point. Therefore, the power optimizer model does not simulate the actual optimization process but the power that is lost in the power optimizer due to its own conversion efficiency. To calculate this efficiency loss, the simulations makes use of efficiency curves that are specified by the power optimizer manufacturer. An example of such an efficiency curve for a power optimizer by the company *SolarEdge* is shown in Figure 2.2 [26].

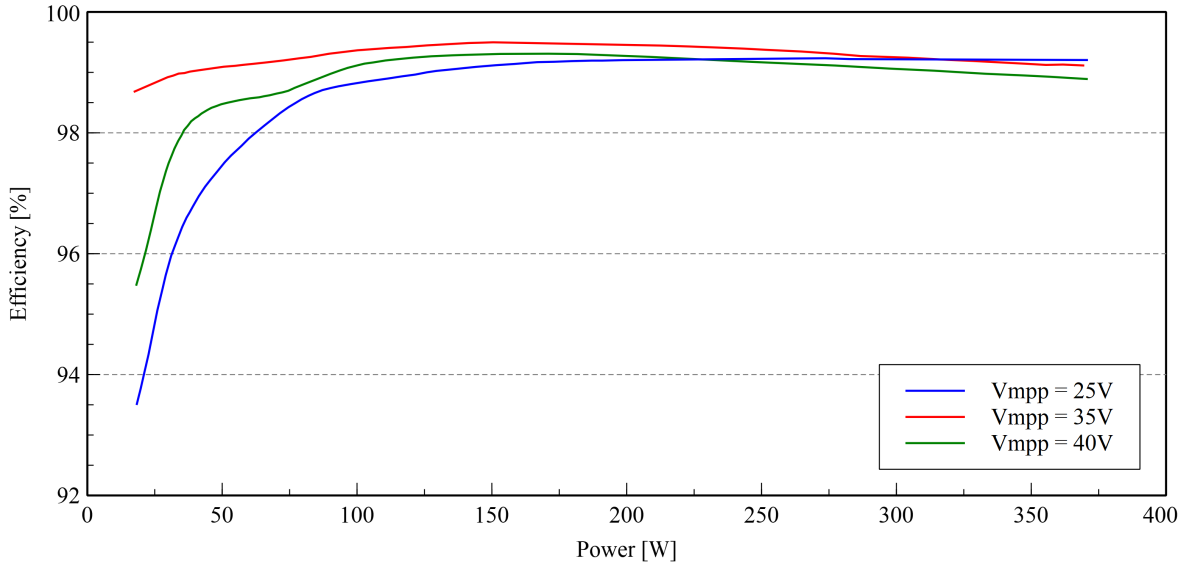

Figure 2.2: Efficiency curves at three distinct input voltages for the P300/P350/P370 from SolarEdge. Adapted from [26].

In this graph, efficiency curves are shown at three distinct input voltages. The power optimizer model has therefore two variable inputs, the power optimizer input voltage and the power optimizer input power. The graphs are digitized using a web-based tool [27] and the respective data is stored in Excel files.

The model automatically detects if the efficiency curves have a point on the y-axis at a power of 0W. If not, an additional point is calculated on the y-axis. This point is needed to calculate the efficiency at low input power. The new point is calculated assuming linearity of the efficiency curve at a low input power. The result of the new efficiency curves are shown in Figure 2.3, where the new points are indicated with the dashed lines.

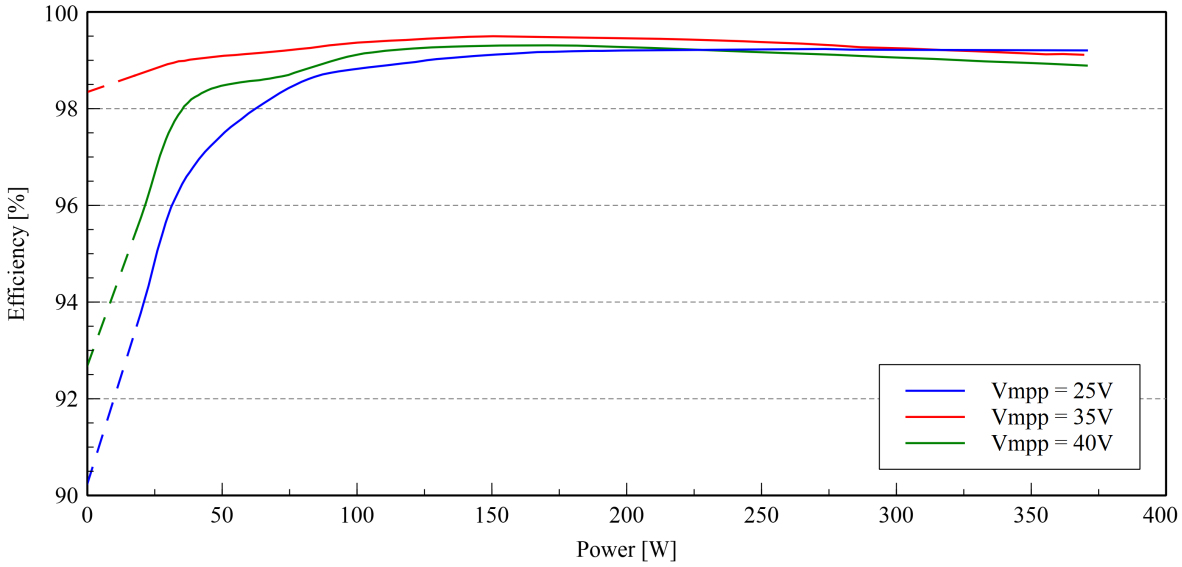

Figure 2.3: Efficiency curves of the SolarEdge P300/P350/P370, extended to the y-axis.

When all necessary points are added to the graph, the simulation calculates the efficiency of the power optimizers through linear interpolation. The interpolation is executed in two steps. First, the power optimizer efficiency at the module output power is calculated for the three, by the manufacturer

specified, voltages. These efficiencies are then used to calculate the final efficiency at the module output voltage.

2.3.2. Inverter for Systems with Power Optimizers

After selecting a power optimizer type and calculating the subsequent output power of this optimizer, the user has the option to include a complementary inverter to the system. If this inverter is included, the simulations calculate the AC output power of the inverter. There are multiple ways to calculate the AC output power of an inverter. Typical methods are the SNL model (more on this model in Subsection 2.4) and company specific efficiency curves. For the power conversion tool, company specific efficiency curves are used. The main reason for for this decision is that the SNL coefficients for the SolarEdge inverter that is used in the INNOZOWA project are unknown, while the efficiency curve of the inverter is readily available. Using a web-based tool, several efficiency curves are digitized and transformed to tabular data. An example of such an efficiency curve for the SolarEdge SE17K is shown in Figure 2.4 [28].

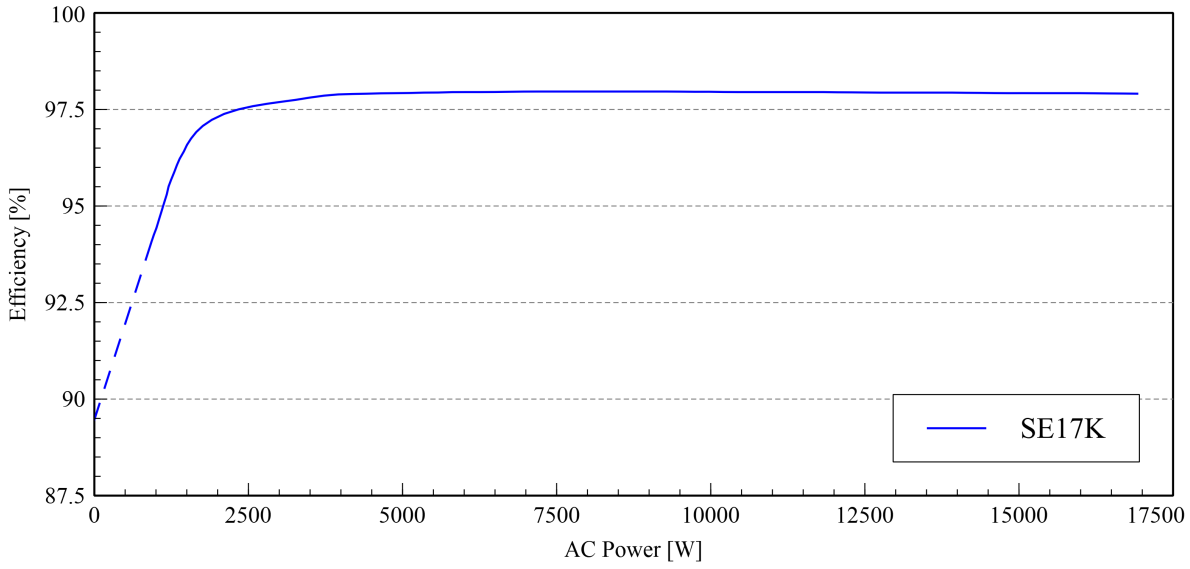

Figure 2.4: Efficiency curves of the SolarEdge SE17K, extended to the y-axis. Adapted from [28].

To calculate the efficiency of the inverter, approximately the same strategy is used as for calculating the efficiency of the power optimizer. First, the user inputs the number of modules in the string and the number of parallel strings. These inputs are needed to calculate the total number of modules and therefore the total input power that is delivered to the inverter. Second, if needed, an additional point on the y-axis of the efficiency curve is calculated. This point is needed to calculate the efficiency of the inverter at a relatively low input power. The additional points are illustrated in Figure 2.4 with a dashed line. Third, since the power in the efficiency curve is specified in AC, the DC power is calculated. Finally, the efficiency is calculated, through interpolation, based on the total inverter input power.

As an additional step, the user has the ability to select if the optimizer works in fixed voltage mode. The reason for this addition is that several manufacturers of power optimizers use inverters that utilize this mode of operation; most notably SolarEdge. This choice mainly influences the cable losses since the string current changes due to the fixed string voltage. The string current is calculated by the following equation:

$$I_{String} = \frac{P_{String}}{Vnom_{inv}} \tag{2.1}$$

Where P_{String} is the total DC power in the string and $Vmax_{inv}$ is the nominal operating voltage of the selected inverter.

2.3.3. String Sizing

Each manufacturer has its own set of design rules when it comes to string sizing. Since this project makes use of SolarEdge hardware, a string size check is added to the Power Conversion tool. The string size calculations for a SolarEdge based system are relatively straightforward thanks to its fixed voltage design. The minimum and maximum string lengths are calculated by Equation 2.2 and Equation 2.3 respectively. [29]

$$MIN = ceiling\left(\frac{Inverter\ Nom.\ DC\ Input\ Voltage}{Power\ Optimizer\ Max\ Operating\ Output\ Voltage}\right) + 2 \tag{2.2}$$

$$MAX = floor\left(\frac{Inverter\ Nom.\ DC\ Input\ Voltage * Power\ Optimizer\ Max\ Output\ Current}{Module\ Peak\ Power}\right) \tag{2.3}$$

When the user violates any of these two margins, the Power Conversion tool provides a warning. Although the Power Conversion tool is not (yet) intended as a system design tool, these warnings can help prevent users from making unnecessary mistakes in their simulations.

2.4. Inverter Modeling

The development of an input model for power optimizers answers one of the research questions discussed in this Chapter. The second research question that is answered in this chapter concerns the addition of power conversion models for other equipment. As one of the boundary conditions state at the start of this chapter, a model for inverters and cables should be included in the PVMD modeling toolbox. This section discusses how the inverter is modeled in the Power Conversion tool and the set-up of this model. The next section discusses the modeling of losses in the system wiring.

2.4.1. Inverter Performance Model

The performance of inverters is modelled with the 'Performance Model for Grid-Connected Photovoltaic Inverters', developed by the Sandia Notional Laboratories (SNL). This is an empirically based performance model which takes into account the electrical characteristics at different power and voltage levels as well as the inverter self-consumption. The model is widely used in industry and in similar power conversion tools such as those of PVsyst, SAM or PVSOL. According to SNL, the standard error of the model is about 0.1%. The model is defined by a set of equations where Equation 2.4 relates the AC power output of the inverter to the DC input power and the DC input voltage. [30]

$$P_{ac} = \left[\frac{P_{aco}}{(A-B)} - C*(A-B)\right]*(P_{dc}-B) + C*(P_{dc}-B)^2 \tag{2.4}$$

In this equation, A, B, and C are defined by Equations 2.5 to 2.7. P_{dc} is the input power of the inverter.

$$A = P_{dco}*[1 + C_1*(V_{dc} - V_{dco})] \tag{2.5}$$

$$B = P_{so}*[1 + C_2*(V_{dc} - V_{dco})] \tag{2.6}$$

$$C = C_o*[1 + C_3*(V_{dc} - V_{dco})] \tag{2.7}$$

In equations 2.5 to 2.7, C_o, C_1, C_2, and C_3 are inverter specific empirical coefficients. V_{dc} is the input voltage of the inverter. V_{dco} and P_{dco} are defined respectively as the voltage and power level at which the ac-power rating is achieved at the reference operating condition. P_{so} is the self-consumption of the inverter.

In the inverter simulation, the AC output power and the inverter efficiency are calculated for each moment in time. If the AC output power exceeds the inverter upper limit, defined by SNL as P_{aco}, the simulation automatically sets the inverter output at the value for P_{aco}. This process is typically referred

to as inverter clipping. If the DC input power is below the power level required to start the inversion process, defined by SNL as P_{so}, the output of the inverters is set to its night consumption, defined by SNL as P_{nt} . This self-consumption loss during the night is typically referred to as 'night tare' loss.

2.4.2. Inverter Model Set-up

The Power Conversion tool allows the user to choose between four distinct power conversion architectures: a central inverter, a micro inverter, a string inverter, and a power optimizer. When selecting either of the inverters, the model calculates the efficiency with the SNL model, described in detail in the previous section. The SNL constants that are used for this calculation are retrieved from the open source PV performance Modeling Collaborative, the PV LIB Toolbox [31]. In this database, no distinction is made between inverter type, so the user should select an inverter with caution. A detailed explanation of the inverter modeling procedure is found in the Power Conversion Manual in Appendix B.

2.5. Cable losses

Cables are an essential part of every photovoltaic system. The wiring of a PV system can have a significant impact on the performance of the system due to the heat that is dissipated in the cables. It is therefore important to include these cable losses in the simulation of a PV system. To simulate the cable losses, a separate 'Cable Losses Tool' is created for the PVMD modeling toolbox. Within this tool, the user can choose between a fixed loss percentage or a detailed calculation based on user specified cable characteristics. The next subsection specifies the calculation procedure of this detailed cable loss calculation. The second subsection provides information about the design considerations of the wiring in a PV system.

2.5.1. Detailed Cable Loss Calculation

The detailed cable loss calculations are based on a relatively simple cable lay-out. An example of such a lay-out is shown in Figure 2.5.

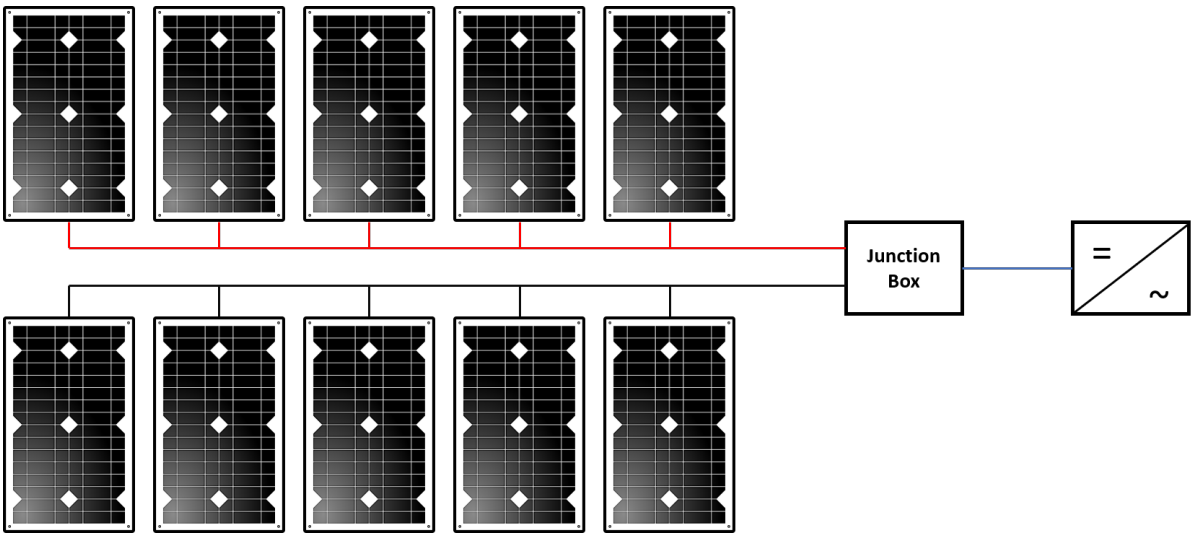

Figure 2.5: Example of a PV set-up which can be used for a detailed cable calculation. The first cable section is coloured in red, the second cable section is coloured blue.

The calculation procedure is divided in two steps. First the heat dissipated in a single string is calculated. In Figure 2.5 this cable is indicated with a red line. Using Equation 2.8, the resistance of the cable is calculated based on the cable characteristics.

$$R_{cable} = \rho * \frac{l}{A} \tag{2.8}$$

In this equation ρ is the specific resistance in $\frac{mm^2}{m^2}$, A is the cross-section of the cable in mm^2, and l is the cable length in m. Using the cable resistance, the heat dissipated in the cable can be calculated using Equation 2.9.

$$P_{cable} = I^2 * R_{cable} \tag{2.9}$$

In this equation, I is the string current. When the cable loss for a single string is known, the total cable losses for the all parallel strings can be calculated simply by multiplying the losses for a single string with the number of parallel strings.

The second step in the calculation procedure is to determine the heat dissipated in the cable from a junction box to the inverter. In Figure 2.5, this cable is indicated with a blue line. Using Equations 2.8 and 2.9, the heat dissipated in the cable is calculated. This step, however, is optional. Some PV system consist only of a single string or the inverter has the option to install multiple strings directly to the inverter. It is up to the user to include this cable section.

Finally, the losses of all cable sections can be added and the total cable loss is calculated. This loss is subtracted from the total module output power. Furthermore, the detailed cable calculation includes a check for the percentage of power that is lost in the cables. If this percentage exceeds an arbitrary level of 2%, the user is warned and, in the case of a new system, advised to select a larger cable diameter.

2.5.2. Cable Design Considerations

The detailed cable loss calculation, described in the previous subsection, is mainly useful to model existing PV systems. When designing a new system, the cable characteristics are typically not yet not known and should be selected with caution. The cable losses tool and accompanying manual provide little guidance on how to design these cables, as creating a system design tool is not within the scope of this project. However, if the tool would be used for system cable design, at least some minimum standards should be discussed. The minimum ampacity of the wiring in a PV system should confirm to the a minimum level of $1.56 * I_{sc}$, which is a standard described by the National Electrical Code (NEC), the International Electrotechnical Commission (IEC), and the Institute of Electrical and Electronics Engineers (IEEE) [32]. Table 1 in Appendix B provides an overview with wire sizes and their ampacity.

2.6. Power Conversion Tool Validation

The Power Conversion tool for the PVMD toolbox is created with the intend to use it for simulating the INNOZOWA PV system. The internal losses of the power optimizers used in the INNOZOWA system should be included in the overall energy yield simulations of the respective systems. However, after the new Power Conversion tool was created, it turned out that the power optimizer registers the voltage and current *before* the power optimizer. This effectively means that there is no need to include the efficiency simulation of a power optimizer in the energy yield simulations of the modules, since the simulated energy yield can be directly compared to the module output. Although the power optimizer model is not needed in the simulations of this project, a validation of the model might still prove useful for future users of the toolbox. This section therefore aims to validate the Power Conversion tool based on data from the INNOZOWA project. The validation focuses on two main parts: the power optimizer efficiency and the efficiency of the associated inverter. However, the models for calculating the efficiency of the power optimizer and its associated inverter cannot be validated individually. The monitoring platform which is used to monitor the INNOZOWA system registers several parameters at optimizer level: the module current, the module voltage, and the optimizer voltage. Since the monitoring platform does not measure the optimizer output current, the simulated efficiency of the optimizers cannot be compared to a monitored value. The same issue holds for the inverter, as no inverter input measurements are made, only the inverter output is measured. Therefore, only the overall system efficiency can be both calculated *and* simulated.

To simulate the overall system efficiency, first the efficiency of each individual power optimizer is simulated based on the optimizer input voltage and power which are retrieved from the SolarEdge

monitoring platform. The graphs in Figure 2.6 show the efficiency of the simulated optimizer for four distinct days during the monitoring period of the INNOZOWA project.

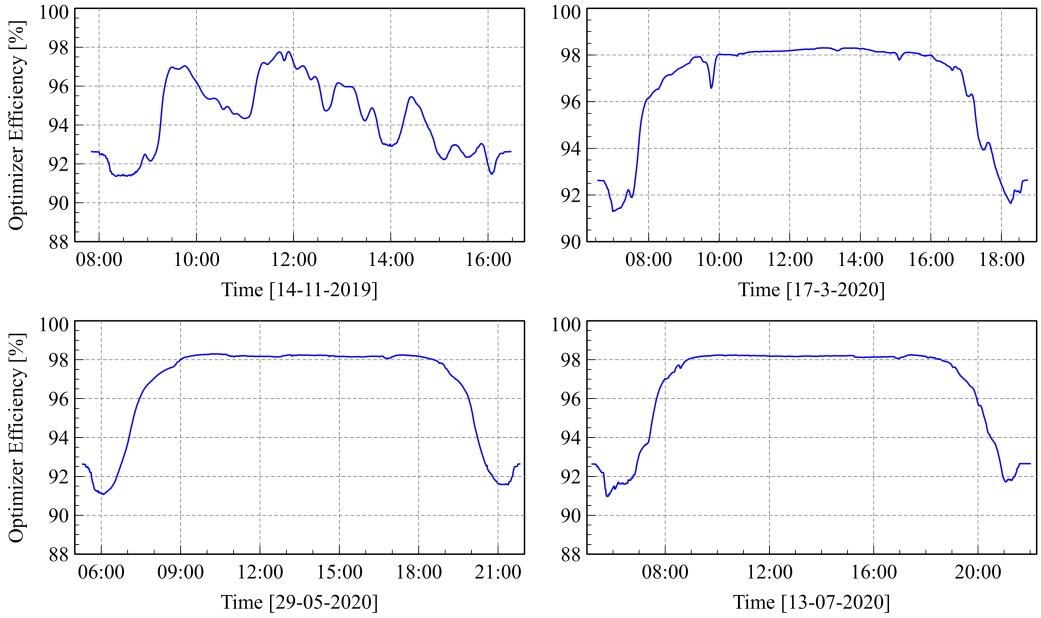

Figure 2.6: Average power optimizer efficiency simulated with the Power Conversion tool based on INNOZOWA input data.

The total DC optimizer output power is then used as an input for the efficiency simulation of the inverter. Since the SNL constants of the inverter of the INNOZOWA project are unknown, the efficiency curves of the inverter are used to simulate its efficiency. The results of this simulation can be found in Figure 2.7.

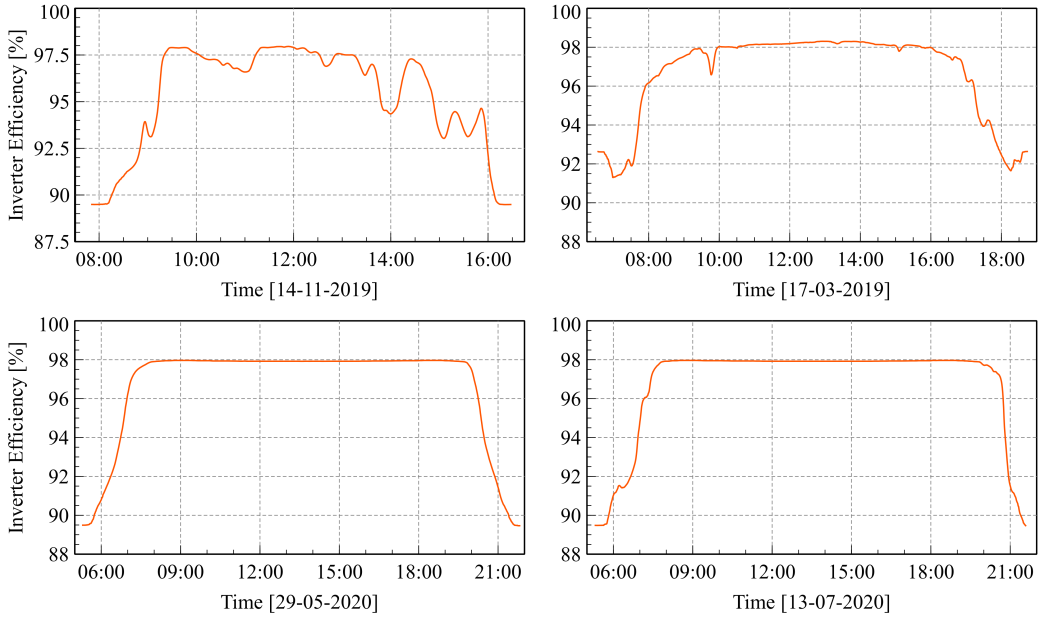

Figure 2.7: Inverter efficiency of the INNOZOWA inverter simulated with the Power Conversion tool based on INNOZOWA input data.

Using the results of both the simulated power optimizer efficiency and the simulated efficiency of the inverter the overall system efficiency can be calculated and compared to the system efficiency determined from the monitored data. The results can be found in Figure 2.8.

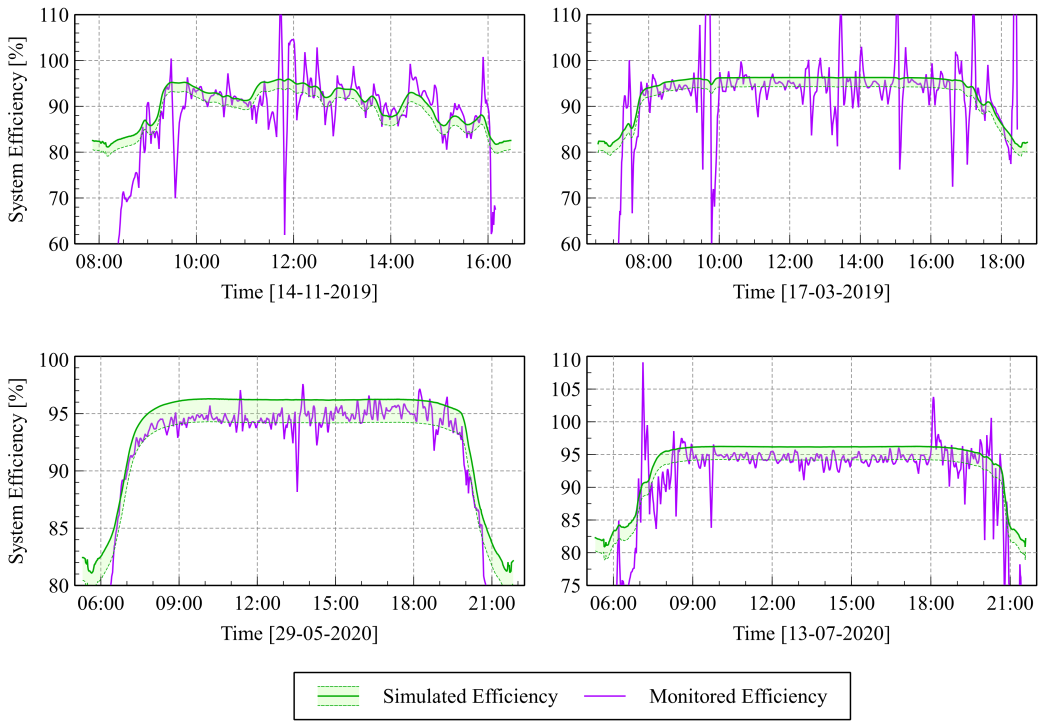

Figure 2.8: Inverter efficiency of the INNOZOWA PV system simulated with the Power Conversion tool based on INNOZOWA input data.

Figure 2.8 shows the overall system efficiency simulated with the new power conversion tool and the system efficiency calculated from monitored data. As can be noted from the graphs, the monitored efficiencies show unrealistic high values during three of the four days that are selected for this validation. These values are however easily explainable. The system efficiency is calculated by dividing the inverter AC output power by the total DC module output power. The total DC module output power is calculated by summing the DC output power of each individual module. This individual module output is however measured at a different, unevenly spaced time interval for each module in the system. Therefore, linear interpolation is used to calculate the missing values. This is not necessarily a problem on days with clear sky conditions, like the 29th of May, 2020. However, on days with changing weather conditions, like the 14th of November, 2019, or the 17th of March, 2020, the interpolated values do not correlate with the actual weather conditions. In other words, the timing of the measurements is not identical for each of the optimizers in the system which results in unrealistic values for the monitored efficiency. To make a proper comparison for days with changing weather conditions, measurements should be taken at exactly the same time stamp.

On days with clear sky conditions however, the interpolated values provide a better representation of the monitored system efficiency. An example of such a day can be found in Figure 2.8, the 29th of May, 2020. On this day, the monitored efficiency can be compared to the efficiency simulated with the Power Conversion model. For this simulation, only the efficiencies of the optimizers and the inverter are included, so no losses in the cables or other components are added. A confidence interval of 2% is added below the graph of the simulated efficiency to account for potential cable losses. Table 2.1 shows the root-mean-square error of each of the validations with and without cable losses included.

Table 2.1: Root-Mean-Square Error (RMSE) of the validation results.

	14-11-2019	**17-03-2020**	**29-05-2020**	**13-07-2020**
RMSE	7.52	9.33	7.08	5.60
RMSE (2% cable losses)	7.14	9.18	6.47	4.86

The RMSE is slightly lower for the validations which include 2% cable losses. However, more precise measurements are needed to validate the tool in more detail.

2.7. Chapter Conclusions

This chapter aimed to answer two of the secondary research questions of this research. The first sub-question that was discussed concerns the development of an input model for power optimizers, needed to simulate the INNOZOWA system in the PVMD modeling toolbox. A power optimizer is a device which combines a DC-DC converter with an MPP tracker and is used to maximize the energy yield of a PV module. This optimizer has some internal consumption which needs to be considered in the energy yield simulation of a PV system. To simulate these internal losses, a MATLAB based model was created in which manufacturer provided efficiency curves of power optimizers are utilized. On top of the power optimizer efficiency, the tool can also perform a string size check for SolarEdge optimizers. Lastly, a compatible inverter can be added to the system.

The model for power optimizers is integrated in the PVMD modeling toolbox and placed in a new 'main' script: Power Conversion. The second sub-question that is answered in the chapter relates to this new Power Conversion script. To make the new script functional and convenient for future users, other models are added as well. The models that are integrated in the new Power Conversion script are a model for inverters and a model for cable losses. The inverter model is based on the industry standard SNL model. The losses in the cables can be simulated using a fixed loss percentage or a detailed cable calculation. With the detailed calculation, the user can specify cable characteristics of multiple cable sections.

The Power Conversion model is provided with many user interfaces which enables user-friendly operation of the tool. The user does not have to adjust lines of code in order to make the simulations, which make the tool convenient to use. Moreover, all simulations should be possible with just basic project information and manufacturer data sheets. Furthermore, a manual is created which explains in detail all the steps needed to make a simulation in one of the models. This manual can be found in Appendix B. It should be noted that the Power Conversion tool is mainly intended as a simulation tool for existing systems. Although multiple warnings are included in the models, the models lack the design capacity of other, established tools, such as PVsyst.

Although the Power Conversion tool is thoroughly tested and evaluated during its development, it turned out that it is not needed in future simulations for this project. The main goal of the development of a power optimizer input model was to use the model to simulate the power optimizers of the INNOZOWA system. However, the monitoring system that is used in the project provides an option to directly assess the module output power. This means that the power conversion model is not needed in subsequent simulations of this project.

Finally, the Power Conversion tool was thoroughly validated using INNOZOWA input data. However, this input data proved to be insufficiently detailed resulting in unrealistic values for the efficiency for days with changing weather conditions. For days with clear sky conditions the simulated efficiency seems to represent the monitored efficiency closely provided that some additional losses are added to account for the losses in the cables. More precise measurements are needed to validate the tool in more detail.

2.8. Chapter Recommendations

Although the Power Conversion tool is mainly finished, there are parts that should be added to improve the tool. This section recommends the following action on the tool:

- When simulating a system with the new Power conversion tool, several losses are taken into account (e.g. cable losses and losses in the power optimizer). There are however, several other losses associated with PV systems. Some of these losses include: module mismatch, maximum power point tracking losses, losses in diodes and connections, soiling losses, and module aging. These loss factors are not taken into account in this version of the Power Conversion tool and should be added as an option in a later version. These could be simple fixed percentages or detailed models.

- At this moment, the Power Conversion tool uses a single database for the SNL model constants of all the inverters. However, in the tool several inverter types are available. The tool currently has some very basic filter options to only show the inverter type that the user selects. Ideally, separate databases are needed for the different inverter types.
- In the detailed cable calculation script of the new Power Conversion tool, the user has to input the cable properties manually. An option could be added which enables an automatic cable property calculation, based on user inputs and standards.

3

Simulating the INNOZOWA PV Pilot system in the PVMD Toolbox

Energy yield simulations of PV systems can be used for many applications, such as designing or refining a new PV system or the development of new PV technologies. The reason for making energy yield simulations of the INNOZOWA PV system is threefold. First, it provides the opportunity to test the PVMD modeling toolbox to its limits. The subsystems of the INNOZOWA project are uncommon PV systems, which makes the simulation process challenging. Hence, the simulation process is expected to yield noteworthy feedback and recommendations for the toolbox and the simulation procedure. Second, this project provides the opportunity to verify the simulation results with monitored data. Comparing the recorded energy yield with the simulated energy yield can provide useful information about the accuracy and precision of the toolbox and its models. A previous study showed that the toolbox can reach a ±15% accuracy for energy yield simulation of bifacial modules, when using local hourly irradiance data and a setting of 50,000 rays in the module part of the simulation [21]. This project can validate this number and asses the uncertainties that underlie this accuracy. Furthermore, considering the aforementioned accuracy for simulating bifacial modules, the simulations can provide some insight in the performance of the modules.

The aforementioned reasons for simulating the INNOZOWA PV pilot system in the PVMD modeling toolbox are formalized in the two following research question:

3. *Which parameters should be used to accurately simulate the energy yield of the INNOZOWA PV Pilot system in the PVMD modeling toolbox?*
4. *Which parts of the PVMD modeling toolbox can be improved based on the experience of simulating the INNOZOWA PV pilot system?*

This chapter contains eight sections. First the INNOZOWA system is described, detailing all the relevant characteristics of the system. Second, the meteorological input data-sets that are used to make the energy yield simulations are provided. The third section contains the simulation procedure. Sections four and five present the results of the energy yield simulations. Section six discusses these results in more detail. Section seven provides suggestions for improving the PVMD modeling toolbox based on the experience of simulating the INNOZOWA system. lastly, the chapter closes with the chapter conclusions and recommendations.

3.1. System Overview

This section gives an overview of the system that is being tested for the INNOZOWA pilot project. The goal of this section is to describe the scope of the system and to list the most important system characteristics which are used as inputs in the simulation. First, the two modules that are used in the pilot set-up are introduced. Second, a description is provided for each of the three distinct subsystems: the Ground-based System, the Retractable System, and the Tracker System. Finally, the balance of system is discussed, which includes the power optimizers, the inverter and reflector.

3.1.1. PV Modules

Within the three PV pilot subsystems that are being tested for the INNOZOWA project, two distinct PV modules are used:

1. The first module is a monocrystalline, monofacial module from LG, the LG330N1K-V5. The technical specifications of this module can be found in Table 3.1. This module is referred to as the monofacial module in subsequent writing.
2. The second module that is used in testing is a monocrystalline, bifacial module from LG, the LG400N2T-J5. The technical specifications of this module can be found in Table 3.1. This module is referred to as the bifacial module in subsequent writing.

Table 3.1: Technical specifications of the bifacial and monofacial modules [33, 34].

	Parameter	**LG330N1K-V5**	**LG400N2T-J5**
Electrical Properties	Maximum Power (Pmax) [Wp]	330	400
	MPP Voltage (Vmpp) [V]	34.1	42.2
	MPP Current (Impp) [A]	9.69	9.49
	Open Circuit Voltage (Voc) [V]	41	49.4
	Short Circuit Current (Isc) [A]	10.27	10.23
Mechanical Properties	Number of Cells	6 x 10	6 x 12
	Module Dimensions [mm]	1,686 x 1,016 x 40	2,024 x 1,024 x 40
	Cell Dimensions [mm]	16.17 x 16.17	16.17 x 16.17
Temperature Coefficients	Voc [%/°C]	-0.27	-0.26
	Isc [%/°C]	0.03	0.03

3.1.2. Ground Based System

In total, three distinct subsystems are tested during the INNOZOWA pilot phase. These three system are described in some detail in this and the next two subsections. The first subsystem that is described is the Ground-based System. The reason this system is included in this pilot is to asses the differences and similarities between a land-based PV system and the two floating PV systems. The Ground-based System consists of two mounting racks of four modules each. The front mounting rack consists of four monofacial modules. These modules are installed under a tilt angle of 15 degrees. The back mounting rack consists of four bifacial modules. These modules are installed under a tilt angle of 15 degrees and are equipped with a reflector, which is installed on surface-level. This reflector is used to reflect a larger fraction of light on the back-side of the bifacial module.

Figure 3.1: On-site photograph of the Ground-based System, installed for the INNOZOWA pilot project.

3.1.3. Retractable System

The second subsystem is the Retractable System, which is one of the two floating PV systems. The system has a fixed southward azimuth and consists of 26 modules divided over six rows. Each row is mounted on two floaters and is connected with cables to four poles which are secured in the waterbed. These cables can be used to retract modules and floaters to the front or backside of the construction. This operation is needed when maintenance needs to be carried out on the lake. The front row of the subsystem consists of six monofacial modules while the other panels consist of five bifacial modules. All modules are installed under a tilt angle of 15 degrees. The last two rows are equipped with a reflector which is installed just above the water surface. An isometric drawing of the Retractable System is shown in Figure 3.2.

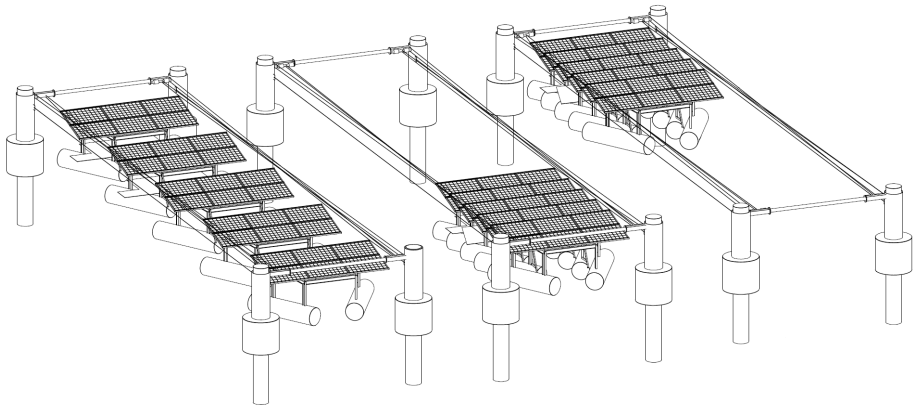

Figure 3.2: Isometric drawing of the Retractable System. The drawing shows the system during normal operation (left) and during the retracted states.

3.1.4. Tracker System

The Tracker System is the second of the two floating PV subsystems that are being tested for the INNOZOWA project. The system consists of four rows of four modules each. The first and second row contain four monofacial modules which are installed at an angle of zero and 15 degrees respectively. The third and fourth row contain bifacial modules, installed at an angle of zero and 15 degrees respectively. The last two rows are also equipped with a reflector. The system has a southward azimuth and has the capability to act as a single-axis tracking system. The tracking is facilitated by a pump which pumps water in and out the hollow chambers of the floating structure. By filling these chambers with water, the structure is able to tilt in east and westward direction. An isometric drawing of the floating structure is shown in Figure 3.3. A tabular overview of the (in total) nine study cases is given in Table 3.2.

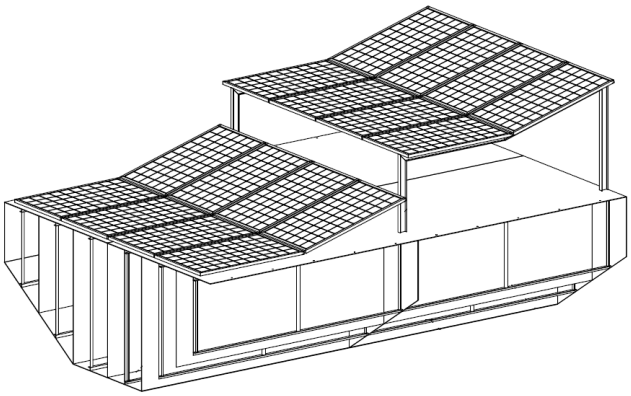

Figure 3.3: Isometric drawing of the Tracker System.

Table 3.2: Overview of the subsystems that are being tested within the INNOZOWA pilot project.

Study Case	Subsystem	Type	Tilt Angle [deg]	Azimuth [deg]	Reflector	Number of Modules
#1	Ground-based	Monofacial	15	180	NA	4
#2	Ground-based	Bifacial	15	180	Yes	4
#3	Retractable	Bifacial	15	180	Yes	10
#4	Retractable	Bifacial	15	180	No	10
#5	Retractable	Monofacial	15	180	NA	6
#6	Tracker	Bifacial	15	Variable	Yes	4
#7	Tracker	Bifacial	0	Variable	Yes	4
#8	Tracker	Monofacial	15	Variable	NA	4
#9	Tracker	Monofacial	0	Variable	NA	4

3.1.5. Balance of System

This subsection briefly discusses other relevant equipment of the INNOZOWA PV pilot system: the power optimizer, the inverter, the reflector, the pump of the tracker System and the environmental sensors.

Power Optimizer
Each module is connected to an individual power optimizer. The concept of a power optimizer was introduced in Section 2.1 of Chapter 2. The main reason to install power optimizers in this PV pilot system is their ability to monitor the energy production of each individual module. The optimizer type that is installed at each module is the *SolarEdge P505*.

Inverter
The three subsystems are connected to a single, central inverter. The inverter that is used in this project is the *SolarEdge SE17K*, which operates at a fixed input voltage. The subsystems are connected to this inverter by two parallel strings. String 1 contains the modules from the Retractable System and String 2 contains the modules from the Tracker System and the Ground-based System.

Reflector
As mentioned in the three previous subsections, most bifacial modules are equipped with a reflector. This reflector is made of an orange reflective material. An important characteristic for such a reflector is the albedo of the material. The effective albedo for monocrystalline silicon modules was found to be 0.6849 [35].

Pump
The Tracker System is equipped with a pump. This pump is used to move water between the compartments of the floating structure. This enables the floating structure to act as a single-axis tracking system. The maximum tracking angle of the system is 27°. Although this is not the ideal angle, the angle cannot be increased due to wind load. The pump that is used is the *DAB EVOPLUS 80/180 M*. The internal consumption of this pump is an important parameter when comparing the different INNOZOWA subsystems. A detailed calculation of this internal consumption can be found in Subsection 5.3 of Chapter 5.

Sensors
To monitor the ambient conditions at the INNOZOWA pilot site, several sensors are installed: one temperature sensor and three irradiance sensors. The first irradiance sensor is located on the top of the container which houses the inverter. The second sensor is placed under the battery container of the Retractable System. This sensor faces down towards the water. The final irradiance sensors is placed on the backside of the bifacial modules of floater four of the Retractable System. The irradiance sensor that is installed is the *SolarEdge 1-IRR-SEN-SE1000*, which has an accuracy of ±5% [36]. The sensors became operational on the May 14, 2020.

3.2. Meteorological Input Data

In the previous section, the technical details of the modules, subsystems and the balance of system were described. These are important input parameters for the 'CELL', 'MODULE' and 'ELECTRIC' parts of the PVMD modeling toolbox when simulating the INNOZOWA PV pilot system. In this section, the meteorological data that is needed in the 'WEATHER' part of the simulation is formulated. To research the effects of different meteorological data-sets, four data-sets are created: A data-set based on climate data, a data-set based on interpolated weather data and finally two data-sets based on on-site irradiance measurements with a 60 and 15 minute resolution. The following subsections detail the creation of these data-sets. The data that is needed in each data-set is listed below:

- Date (year/month/day/hour)
- Solar Altitude [degrees]
- Solar Azimuth [degrees]
- Direct Normal Irradiance (DNI) [W/m^2]
- Diffuse Horizontal Irradiance (DHI) [W/m^2]
- Global Horizontal Irradiance (GHI) [W/m^2]
- Ambient Temperature [°C]
- Wind Speed [m/s]

3.2.1. Climate Data-set

The energy yield simulations that are made for the INNOZOWA system feature four data-sets with increasing gradations of accuracy. The data-set with the lowest expected accuracy is the climate data-set, which is described in this subsection.

The climate data that will be used in the energy yield simulations is downloaded from the Dutch PV Portal 2.0. This is a website/data-portal created by a collaboration between the PVMD group and the Royal Netherlands Meteorological Institute (KNMI). From this website, meteorological data of 46 weather station throughout the Netherlands can be downloaded [37]. The data that is provided through this portal is weather data averaged over a period of 25 to 30 years. Relevant meteorological data that can be gathered from this website for the use in the PVMD modeling toolbox is: the wind speed, ambient temperature and the Global Horizontal Irradiance (GHI). Additional relevant parameters which are automatically calculated when downloading data from the Dutch PV Portal are: the sun azimuth and altitude and the diffuse and direct fractions of the GHI. This data-set is downloaded for the five closest KNMI measurement locations with respect to the INNOZOWA pilot site: Deelen, Hupsel, Arcen, Volkel and Herwijnen. Figure 3.4 shows these locations on a map.

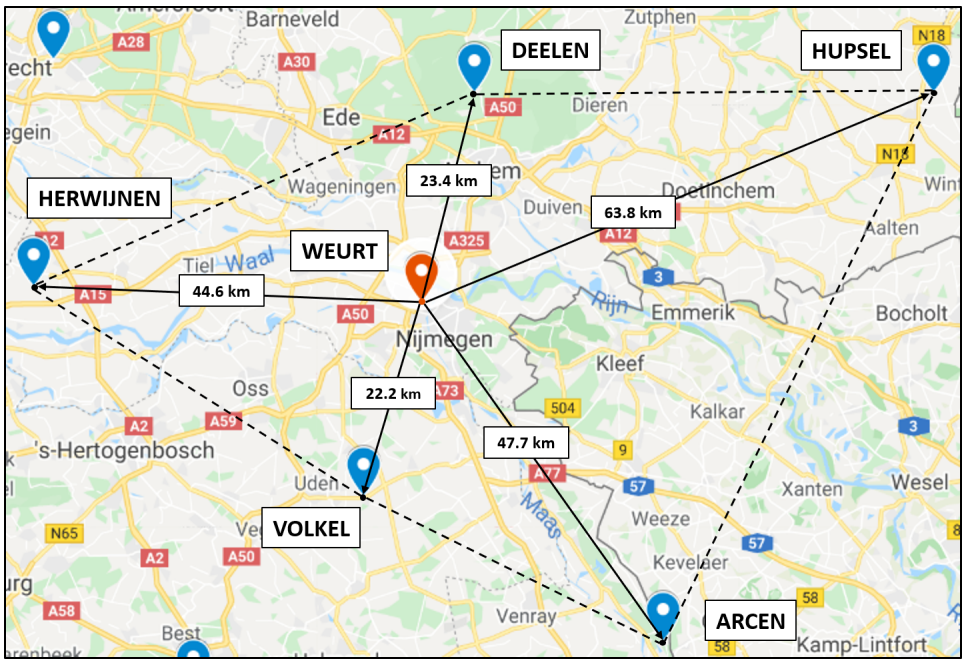

Figure 3.4: Map of the INNOZOWA pilot site (in the center) and the surrounding KNMI measurement stations.

After downloading the data-set, it needs to be interpolated to determine the respective values at the INNOZOWA pilot site. There are many interpolation techniques that can be used to interpolate climate and/or weather data. The selection of such a technique is mainly based on the required accuracy and the topology of the landscape. Previous research showed that the Inverse Distance Weighted method (IDW) is a suitable interpolation technique for the Netherlands. The method is fast, accurate and is suitable for plains [38]. The IDW method can be mathematically expressed as:

$$L_{IDW} = \frac{\sum_{n=1}^{m} L_n/D_n}{\sum_{n=1}^{m} 1/D_n} \tag{3.1}$$

In this equation, L_n is the meteorological parameter measured at location n and D_n is the distance from the measurement location to the pilot site in Weurt. This distance is calculated with the Haversine formula. This formula can be mathematically expressed as:

$$D_n = 2r * arcsin\left(\sqrt{sin^2 * \frac{lat_n - lat_0}{2} + cos(lat_0) * cos(lat_n) * sin^2 * \frac{long_n - long_0}{2}}\right) \tag{3.2}$$

In this equation, lat_n and $long_n$ are the latitude and longitude of the KNMI measurement locations. lat_0 and $long_0$ are the latitude and longitude of the INNOZOWA pilot site. r is the radius of the earth. The distances of each measurement station to the pilot site are indicated in Figure 3.4.

After interpolating the climate data-set, the irradiance parameters are processed in Meteonorm 7.3 to apply the location specific Sky View Factor (SVF). The SVF for several points were retrieved by TU Delft, using horicather equipment [39]. In total, five measurement spots were selected at the INNOZOWA pilot site. A map of these spots is shown in Figure 3.5.

Figure 3.5: Map of the five SVF measurement points at the INNOZOWA pilot site. Reproduced from [39].

Location B is selected as the most relevant measurement spot, as most systems are in close proximity of this location. For the height, 1m is selected, as most systems have a height larger than 1m. The Sky View Factor at this location was determined to be 98.84% [39].

Finally, the last two input parameters are calculated: the solar altitude (as) and azimuth (As) at the pilot location. Both azimuth and altitude are calculated based on an algorithm described in Appendix E of Solar Energy by Smets et al [23]. Inputs for this algorithm are the time and the location of the INNOZOWA pilot site. Since the retrieved GHI is an hourly average, the solar altitude and azimuth are calculated at an half hour offset. The calculation of these parameters concludes the accumulation of data for the climate data-set.

3.2.2. Interpolated Weather Data-set

When creating a data-set for simulating the energy yield of a PV module in the PVMD modeling toolbox, in the best case on-site weather measurements are used, as these are expected to yield the most accurate results. However, for a large part of this thesis project, the on-site irradiance sensors were not operational. Moreover, no ambient temperature or wind speed measurement sensors are installed on-site. Considering this lack of on-site data, a data-set is created based on weather data from the KNMI. This data-set is to be interpolated to determine the weather characteristics at the INNOZOWA pilot site in Weurt. The weather data is downloaded from the KNMI data-portal 'Hourly data of the weather in the Netherlands' [40]. The KNMI data-set consists of the hourly average wind speed [m/s], the ambient temperature [$^{\circ}C$], and the Global Horizontal Irradiance [W/cm^2].

The data is then interpolated using the same method described in the previous subsection, the IDW method. Since the KNMI data-portal does not provide the Diffuse Horizontal Irradiance (DHI) and the Direct Normal Irradiance (DNI), they need to be calculated. The Direct Normal Irradiance can be deduced with Equation 3.3.

$$GHI = DHI + DNI * cos(90 - as) \tag{3.3}$$

In this equation, GHI is the interpolated irradiance parameter and as is the solar altitude. The DHI can be calculated with a model. There are multiple models that can be used to predict the diffuse fraction of the light. Previous research showed that the BRL model, named after its authors, is the most suitable decomposition model to use for The Netherlands [38]. The BRL model is a multiple variable logistics model. The final result of the model is the ratio between the diffuse fraction and the GHI:

$$d = \frac{I_{diffuse}}{I_{global}} \tag{3.4}$$

This ratio is calculated based on multiple 'predictors'. These predictors are: the hourly clearness index, daily clearness index, solar altitude, apparent solar time and a measure of persistence of global radiation level. These predictors can be calculated with readily available input parameters such as the time, time zone, longitude and latitude, and the GHI [41].

The values of DHI and DNI are calculated with Meteonorm, while simultaneously applying the local sky view factor. For this factor, again location B was selected. Finally, the solar altitude and azimuth are calculated for the INNOZOWA pilot site.

3.2.3. On-site Irradiance Data-set

The two final data-sets are created from the on-site irradiance measurements that are made at the INNOZOWA pilot site. At this site, an irradiance senor is installed of which the data can be retrieved via the monitoring platform. The sensor became operational at the 14th of May, 2020. Data up to the 15th of July is included in the data-set.

The data with the smallest common interval that can be gathered from the monitoring website is first, data with a 15 minute interval, and second, data with a 60 minute interval. Although using data with a 15 minute interval is expected to increase the accuracy of the simulations, data with a resolution lower than 60 minutes cannot be processed in Meteonorm 7.3. Since Meteonorm is used to apply the local SVF and to calculate the DHI and DNI from the irradiance, this step cannot be left out. To mitigate this issue, two solutions are presented. First, a data-set is created based on a 60-minute interval. This data-set can then be processed in Meteonorm and used for subsequent simulations. Finally, a second

data-set is created based on a 15-minute time interval. To calculate the diffuse and direct fractions of the light from the on-site irradiance measurement without the use of Meteonorm, a conversion factor is used. This conversion factor is calculated for every interval by using Equation 3.5.

$$C_1(t) = \frac{DNI_{60min}(t)}{GHI_{60min}(t)}, \quad C_2(t) = \frac{DHI_{60min}(t)}{GHI_{60min}(t)} \tag{3.5}$$

These conversion factors are then interpolated to four values for every hour, matching the 15-minute interval. Using Equation 3.6 the interpolated conversion factors are used to calculate a DNI and DHI value for each time interval.

$$DNI_{15min}(t) = C_1(t) * GHI_{15min}(t), \quad DHI_{15min}(t) = C_2(t) * GHI_{15min}(t) \tag{3.6}$$

This method provides a way to create an input file for the toolbox while bypassing Meteonorm. Section 3.4 provides the simulation results for each data-set described in this section. However, first the simulation procedure is described in some more detail.

3.3. Simulation Procedure

This section describes in detail how the PVMD modeling toolbox is used to make energy yield simulations of the INNOZOWA subsystems. This toolbox was already briefly introduced in the Section 1.3. This section details the choices that were made in each step of the simulation process.

3.3.1. Cell Simulation

The first step in the simulation process is the 'Cell simulation'. In this part the user has the option to choose between several solar cell technologies. These technologies are defined by their layers. For the INNOZOWA project, two module types are used: a bifacial module and a monofacial module. This means that in total, two cell simulations are made, one for the monofacial module and one for the bifacial module. Since the exact properties of the layers are unknown, the predefined cell structures are selected.

3.3.2. Module Simulation

The second step in the simulation procedure is the 'Module Simulation' part. In this part the properties of the module are defined. The properties of the modules can be easily retrieved from their respective data-sheets. Some parameters are however not available, such as the cell spacing and the edge spacing. For these values an approximation is made. The dimensions of the structures are obtained from the installer's technical drawings as well as from measurements taken during an inspection of the system. Apart from the module properties and dimensions, some other parameters need to be specified as well in this part of the simulation: the number of rays and the properties of the surface area.

The number of rays has been a heavily discussed topic in previous thesis projects. Elias Garcia Goma concluded in his thesis that 100 rays in the optimum trade-off in terms of computational time and accuracy [19]. Julen Extebarria concluded that this number of rays was not accurate enough and suggested to use 1000 rays as the optimum amount [20]. Finally, Ignacio Narváez Alavez concluded in his thesis that even 1000 rays would be too inaccurate, and showed that 50,000 rays were needed to approximate the energy yield of the reference case that was used to validate the tool [21]. Based on this final research, 50,000 rays are used in the simulations of this research.

A second important set of properties that is defined in the 'Module' part are the properties of the surface area. In total there are three properties that can be set: the surface albedo, the ground haze and the ground diffuse exponent. The albedo values of the different surface materials (grass, water and the reflector) were known at the start of the project and are listen in Table 3.3. The ground haze and ground diffuse exponent determine the surface interaction with the light. Both properties are unknown and therefore set to the default value of 1, representing a surface that scatters incoming light equally in all directions.

Table 3.3: Albedo values used in the 'module part' of the simulation [32].

Material	Albedo
Grass	0.1084
Water	0.0556
Reflector	0.6849

3.3.3. Weather Simulation

In the 'Weather Simulation', which is the third step in the simulation process, the user has to make several decisions. The first decision that has to be made is the choice for what kind of meteorological data to use. For the simulations in this project, four meteorological data-sets are created, which are described in detail in Section 3.2.

The second decision that has to be made by the user in the 'Weather part' of the simulations is the choice for a thermal model. In the version of the toolbox that is used in this research, two thermal models are available: the 'simple thermal model' in which all cells are set to a temperature of 25 degrees Celsius and a 'bifacial thermal model'. Since no specific model for monofacial modules is available, the 'simple thermal model' is chosen for these type of modules. For the bifacial modules, the 'bifacial thermal model' is utilized.

3.3.4. Electrical Simulation

The final step in simulating the energy yield of the INNOZOWA modules is the electrical part. The simulation process of this part is relatively straightforward. The user has to input several important characteristics of the module such as the short circuit current (Isc), the open circuit voltage (Voc), and the voltage and current at maximum power point (Vmpp, Impp). Furthermore, the user has to specify the temperature coefficients of the module and the resistance of the cell. Most of these parameters are retrieved from the respective data-sheets of the module (see Table 3.1). The series and shun resistance of the cell are simulated mathematically based on a single-diode model.

3.3.5. Initial Simulation Results

Initial simulation results showed significant differences between measured and simulated energy yield values. These differences are not in line with the validation results that are shown in earlier research on the PVMD toolbox. Previous research states that a degree of accuracy close to ±15% can be achieved for bifacial modules, using 50,000 rays and weather data with a resolution of one hour [21]. Considering this accuracy is not reached, several choices within the simulation are reconsidered:

- The main factor contributing to the inaccurate results for the bifacial modules is suspected to be the reflector. Since the PVMD modeling toolbox simulates an infinite array of modules, it therefore also simulates an infinite ground area. Furthermore, considering that only one albedo value can be inputted in the tool, this would effectively mean that in the simulations the entire ground is covered with the orange reflective material. To mitigate this issue, a new albedo value is calculated which takes into account the albedo from the reflector as well as from the land. This detailed albedo calculation can be found in Subsection 3.3.6.

- Second, uncertainties can be present on the PV installation side. Two main uncertainties can be identified: 1) soiled, damaged, or broken modules, leading to a lower overall output of the sub-system. 2) dissimilarities between the installation on paper (on which the simulations are largely based) and the actual system installation. To determine if these problems are present in one of the INNOZOWA subsystems, an on-site inspection is conducted. During this inspection, aided by thermographic imaging and a thorough visual inspection survey, several installation faults were brought to light. These faults included: modules installed at wrong tilt angles, misaligned module azimuths, moderately and heavily fouled modules and several other small particularities. These findings are described in detail in the next chapter, Chapter 4. The parameters that influence the outcome of the energy yield simulations, such as the tilt and azimuth are changed in subsequent simulations based on the findings of this inspection.

- The final main uncertainty that is likely to contribute to deviations between simulation results and the monitored data is the thermal models that are used. For monofacial modules there is currently no thermal model available, hence the cell temperature was set to a fixed value of 25 degrees Celsius. To mitigate this issue a new simple but effective thermal model was implemented in the toolbox: the Duffie-Beckman model [42]. This model takes into account the ambient temperature and the wind speed. From these factors the cell temperature is calculated by Equation 3.7.

$$T_M = T_a + \left(\frac{T_{NOCT} - 20^\circ}{800}\right) * G_m \left(\frac{9.5}{5.7 + 3.8 * w}\right)\left(\frac{\eta_{cell}}{0.9}\right) \tag{3.7}$$

  In this equation, η_{cell} is the efficiency of the cell and T_{NOCT} is the cell nominal operating cell temperature, which can both by inputted by the user through a user interface.

3.3.6. Recalculating the Reflector Albedo

As stated in the previous section, the infinite ground combined with a single albedo value presents a high degree of uncertainty for the bifacial modules with reflector. To mitigate this uncertainty a new albedo value is calculated using view factors. This factor is defined as the fraction of the radiation leaving surface A that is intercepted by surface B [43]. Using these view factors for both the reflector and the surrounding grass, a new albedo value can be calculated using Equation 3.8.

$$Albedo = Albedo_{reflector} * VF_{reflector} + Albedo_{grass} * VF_{grass} \tag{3.8}$$

As for the albedo values, it is very important to select the proper value. Research showed that surface areas have a significant effect on the spectral distribution of the light. Since the PV module is depended on the spectrum of light it receives from the reflective area, it is key to include this in the calculation of the albedo. The spectral dependant albedo for monocrystalline silicon for the orange reflector was calculated in an earlier stage and was found to be 0.6849 [35]. To calculate the spectrally responsive albedo for grass to crystalline silicon modules, Equation 3.9 can be used in combination with experimental data. [44]

$$a_{grass_{c-si}} = \frac{\int A(\lambda) SR(\lambda) G_{tot}(\lambda)}{\int A(\lambda) G_{tot}(\lambda)} \tag{3.9}$$

In this equation, $A(\lambda)$ is the spectrally distributed reflectivity of the material, $SR(\lambda)$ is the spectral response of the module, and $Gtot(\lambda)$ is the total irradiation on the surface of the module. The data that is used to calculate the albedo originates from an experiment conducted on a piece of grass in Delft. The calculation yields an effective albedo of 0.298 for monocrystalline silicon, which is comparable to values found in literature [44]. It should be noted that the properties of the grass change throughout the year, e.g. in periods with less rain grass get dry which would also change the albedo. To keep the simulations relatively straightforward, the albedo of the grass is assumed to be the same value throughout the year.

Although the spectrally responsive albedo's are known for both grass and the orange reflector, the two view factors of Equation 3.8 are still missing. Using geometrical parameters of both the module and the reflector, the view factor of the reflector can be calculated using Equation 3.10, where A_1 is the surface area of the module and x, y, η, and ξ are the geometrical parameters of the module and the reflector. Figure 3.6 shows a schematic overview of these geometrical parameters. Within Equation 3.10, function $g(x, y, \eta, \xi)$ is defined by Equation 3.11, where α is the tilt angle of the module. [45]

$$VF_{reflector} = \frac{1}{A_1} \int_{\xi_1}^{\xi_2} \int_{\eta_1}^{\eta_2} \int_{y_1}^{y_2} \int_{x_1}^{x_2} g(x, y, \eta, \xi)\, dx\, dy\, d\eta\, d\xi \tag{3.10}$$

$$g(x, y, \eta, \xi) = \frac{sin^2(\alpha)}{\pi} * \frac{x\xi}{\left[x^2 - 2x\xi cos(\alpha) + \xi^2 + (y - \eta)^2\right]^2} \tag{3.11}$$

Finally, the view factor of the grass can be calculated using the relation shown in Equation 3.12.

$$VF_{grass} = 1 - VF_{reflector} \tag{3.12}$$

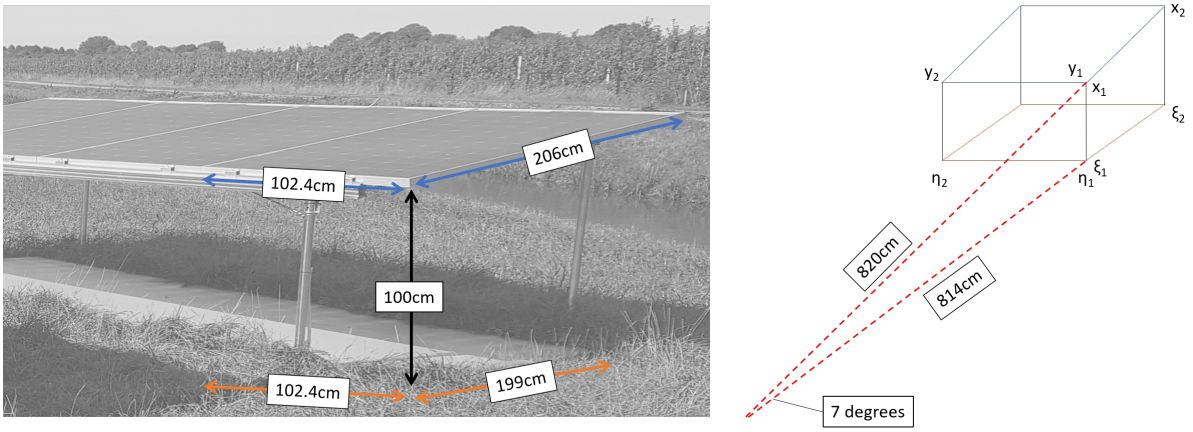

Figure 3.6: Schematic overview of the geometrical parameters used for the recalculation of the albedo. The left picture shows an example of the Ground-based System with its dimensions. On the right side a schematic overview of this system is shown with the parameters that are used for calculating the view factor.

The results of the spectrally responsive albedo, corrected with the view factors, for each system are shown in Table 3.4.

Table 3.4: Recalculated albedo values based on installation specific view factors.

Subsystem	Albedo
Ground-based	0.4784
Retractable	0.2643
Tracker	0.3543

3.4. Simulation Results - Meteorological Input Validation

The previous sections showed the technical details of the INNOZOWA subsystems as well as the formulation of the different meteorological input files and the simulation procedure. This section and the next present and discuss the simulation results. In this section, energy yield simulations are shown for the Ground-based System, based on the four data-sets that are prepared for this study: the climate data-set, the interpolated weather data-set, and the on-site weather data-set with a 60 and 15 minute interval. The goal of this section is therefore to analyse the simulation results in detail and to establish the limitations and advantages of using each of the meteorological input files. Based on this analysis, one of the input-files is selected which is then used in the subsequent section to simulate the energy yield of the floating systems. For the simulations in this section the monofacial and bifacial modules of the Ground-based System are used, as these subsystems are expected to yield the most accurate simulation results. This simulation process took several months and many iterations were needed. The results that are presented in this section are based on the latest insights and input parameters.

3.4.1. Simulations Based on Climate Data

The first batch of simulations that are shown are the energy yield simulations based on climate data. Figure 3.7 shows the results of these simulations. The results of the monofacial module and the bifacial module are shown in the top and bottom graphs, respectively. The red bars represent the simulated energy yield, while the blue bars represent the average measured energy yield of the respective modules in the system. A second graph is added to show the percentual difference between the measured and the simulated energy yields.

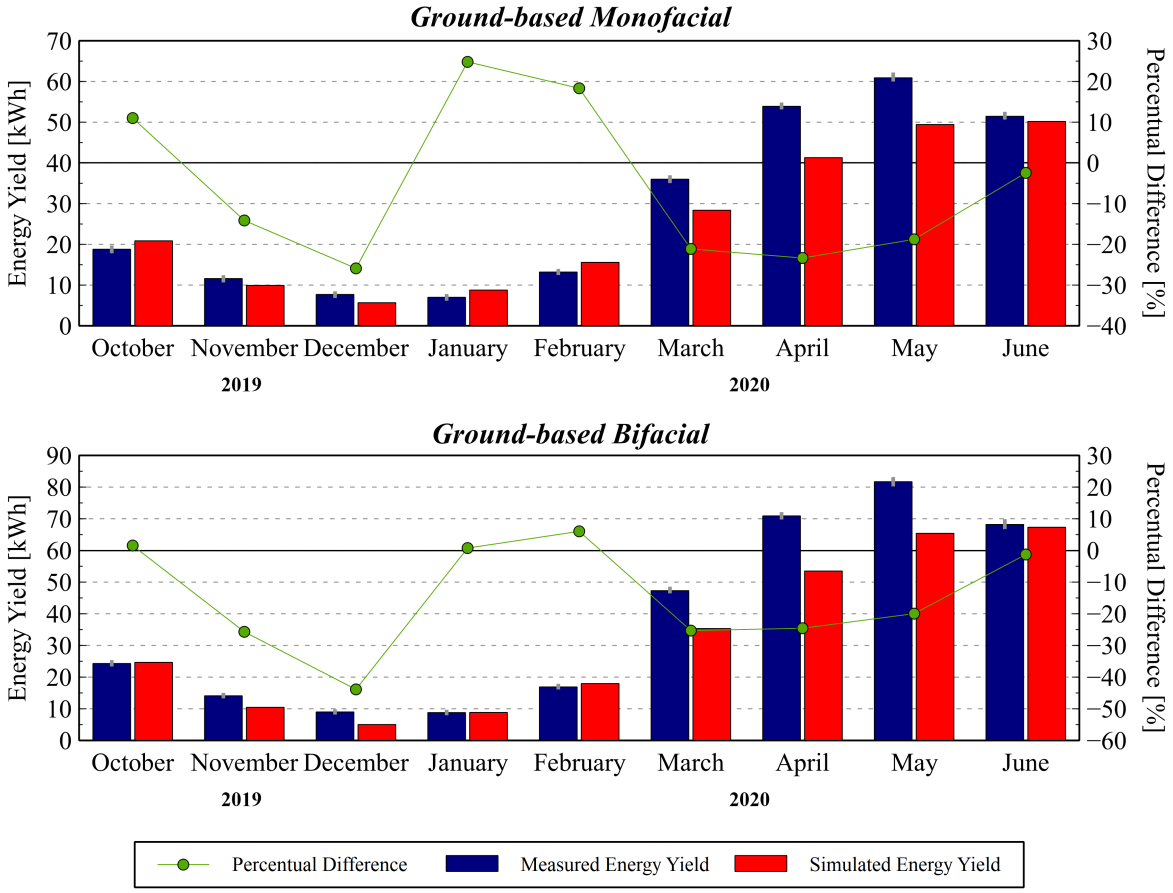

Figure 3.7: Energy yield simulation results of the Ground-based System, using climate data. The top graph shows the results for the monofacial modules, while the bottom graph shows the results for the bifacial modules. The green line represents the percentual difference between the two bars.

As can be concluded from Figure 3.7, there are several months at which the simulated energy yield value closely represents the actual measured value, such as in June. In this month the total irradiance as represented by the climate data was within 5% of the actual on-site measured irradiance. The energy yield simulations for most of the other months are however highly inaccurate if compared to the measured data. This is because during these months the climate data is not well correlated with the actual weather data. This is especially apparent in the months March, April and May, as these were the sunniest spring months ever measured since the start of the KNMI records [46]. This explains why the simulations vastly underestimate the energy yield during these months. Furthermore, according to the KNMI, December 2019 took the fourth place as sunniest December ever recorded (since 1906), which explains the significant deviation during this month [47].

It can be concluded that energy yield simulations based on climate data can be usefull if the actual irradiance is closely represented by the climate data-set. However, during the monitoring period of the INNOZOWA project, several records are broken with regards to the hours of sunshine. This data-set, therefore, won't be used in subsequent simulations.

3.4.2. Simulations Based on Interpolated Weather Data

Figure 3.8 shows the results of the energy yield simulations of the Ground-based System, based on interpolated weather data. The graphs show the measured and simulated energy yields, and the percentual difference between them.

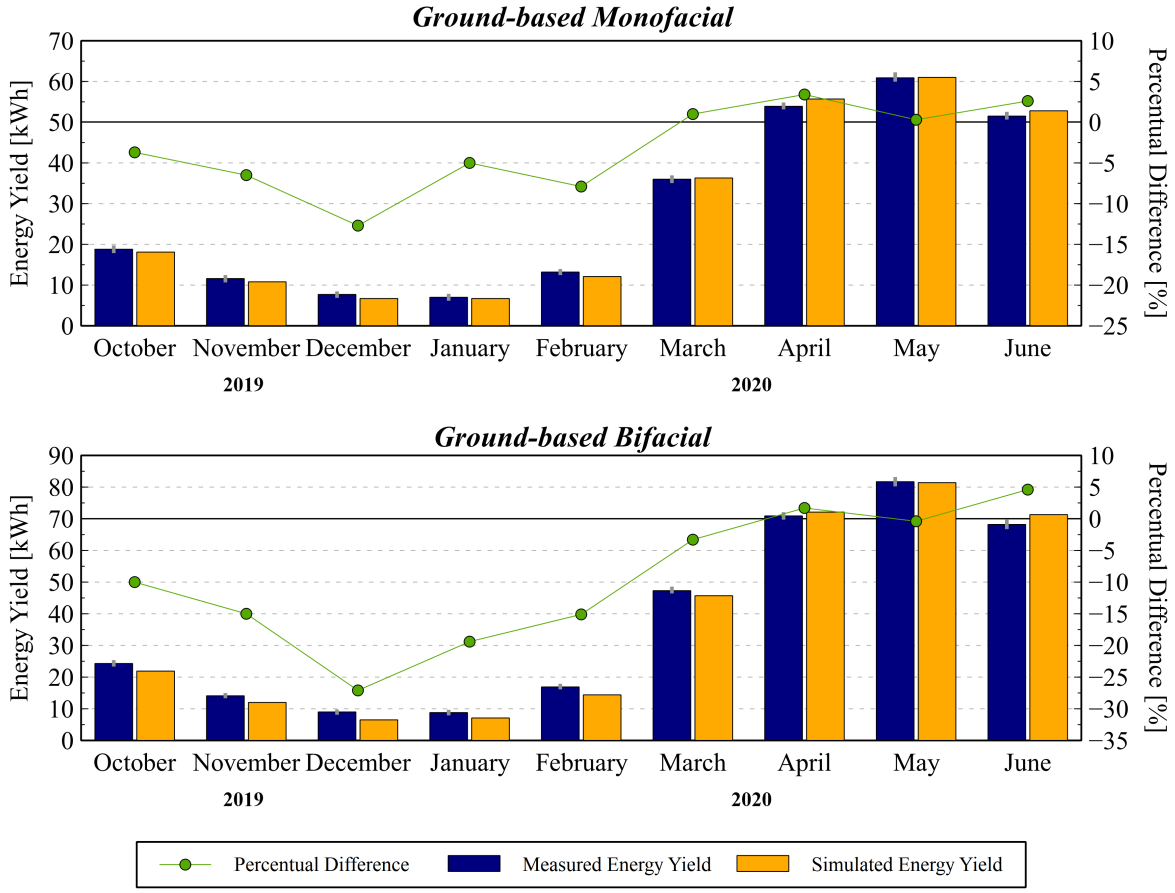

Figure 3.8: Simulation results of the Ground-based System, using interpolated weather data. The top graph shows the results for the monofacial modules, while the bottom graph shows the results for the bifacial modules.

The accuracy of the simulations of the Ground-based monofacial module is within the range of 5% to -15%, which makes it far more accurate than the simulations based on climate data. This is especially notable in the spring months. The accuracy during the winter months is however still relatively low, with a 15% difference in December as the low-point. For the bifacial module, the percentual difference between the measured and the simulated energy yields falls within the range of 5% to -30%. This is a significant difference from the accuracy (±15%) that was reached with a previous validation study using comparable inputs [21]. However, winter months were not included in that study. Several issues could underlie this lack of accuracy in the results, such as the ability of the models in the toolbox to deal with low irradiance situations or the representation of the actual weather data by the interpolated weather data. A detailed analysis of the main uncertainties in the simulations can be found in Section 3.6.

Even though the monthly accuracy is quite high for some months, like May, the daily and hourly differences are relatively high. From an analysis between daily energy yields it can be concluded that on a daily basis the energy yield simulations are significantly less accurate than on a monthly basis. This makes the interpolated weather data-set a non-ideal data-set to use in the subsequent calculations. Section 3.6 provides more details on the daily differences between simulated and measured energy yield for this data-set.

3.4.3. Simulations Based on On-site Irradiance Data

Figure 3.9 shows the results of the energy yield simulations based on on-site irradiance data with a 60-minute resolution.

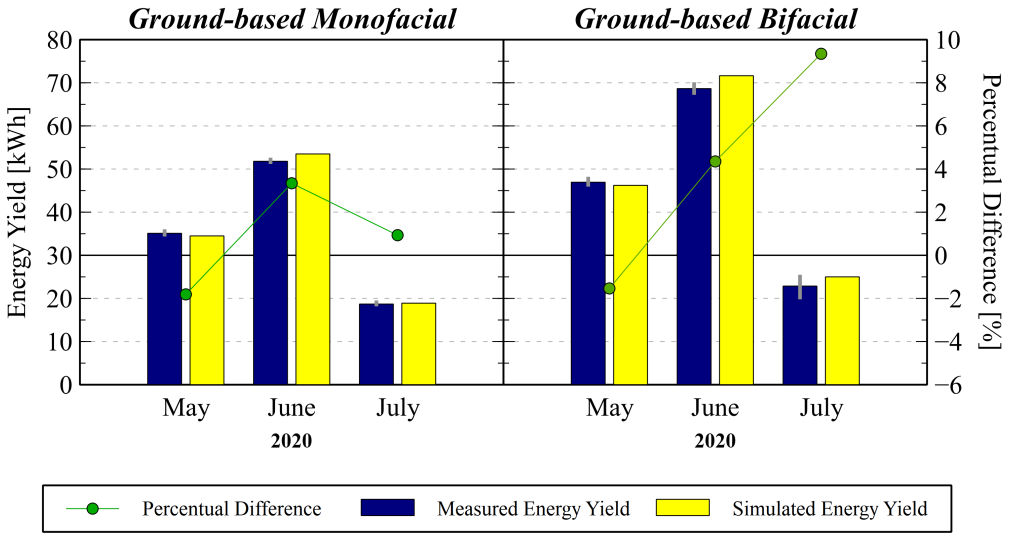

Figure 3.9: Simulation results of the Ground-based System, using on-site weather data with a resolution of 60 minutes.

The graphs only shows the data from the 15th of May up until the 14th of July, as this was the available data at the moment of simulating. As can be noted from the graph, the percentual difference between the measured and simulated energy yields is within the range of -2% to 4% for the monofacial module and -2% and 10% for the bifacial module. Although the monthly differences between the simulated and the measured yields are comparable with the differences calculated for the simulations based on interpolated weather data, the daily and the hourly variations have decreased.

Figure 3.10 shows the results of the energy yield simulations bases on on-site irradiance measurements with a 15-minute resolution.

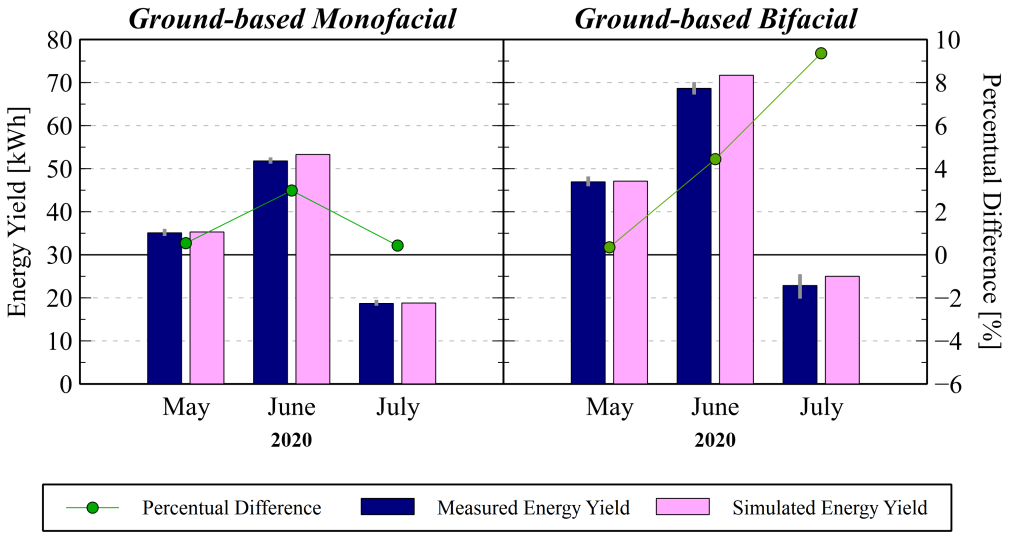

Figure 3.10: Simulation results of the Ground-based System, using on-site weather data with a resolution 15 minutes.

The percentual difference between the measured and simulated energy yields only slightly improves for both systems in May. However the accuracy increase is negligible in June and July. From a comparison between the daily simulated and monitored energy yield it can be concluded that decreasing the time interval from 60 minutes to 15 minutes slightly flattens the peaks. However, decreasing the resolution from 60 minutes to 15 minutes quadruples the computing time of the simulations. Since the accuracy of the simulations did not significantly improve, the simulations of the floating systems are based on the meteorological data-set with a resolution of 60 minutes. A final comparison between the interpolated data-set, and the weather data-set with a resolution of 15 and 60 minutes is provided in Section 3.6.

3.5. Simulation Results - Floating Systems

This section contains the results of the energy yield simulations of the floating PV systems. First, the results of the Retractable System are shown. Finally, the simulation of the Tracker System is discussed. The simulations are based on the meteorological data-set with a resolution of 60 minutes.

3.5.1. Retractable System

Figure 3.11 shows the simulation results of the Retractable System.

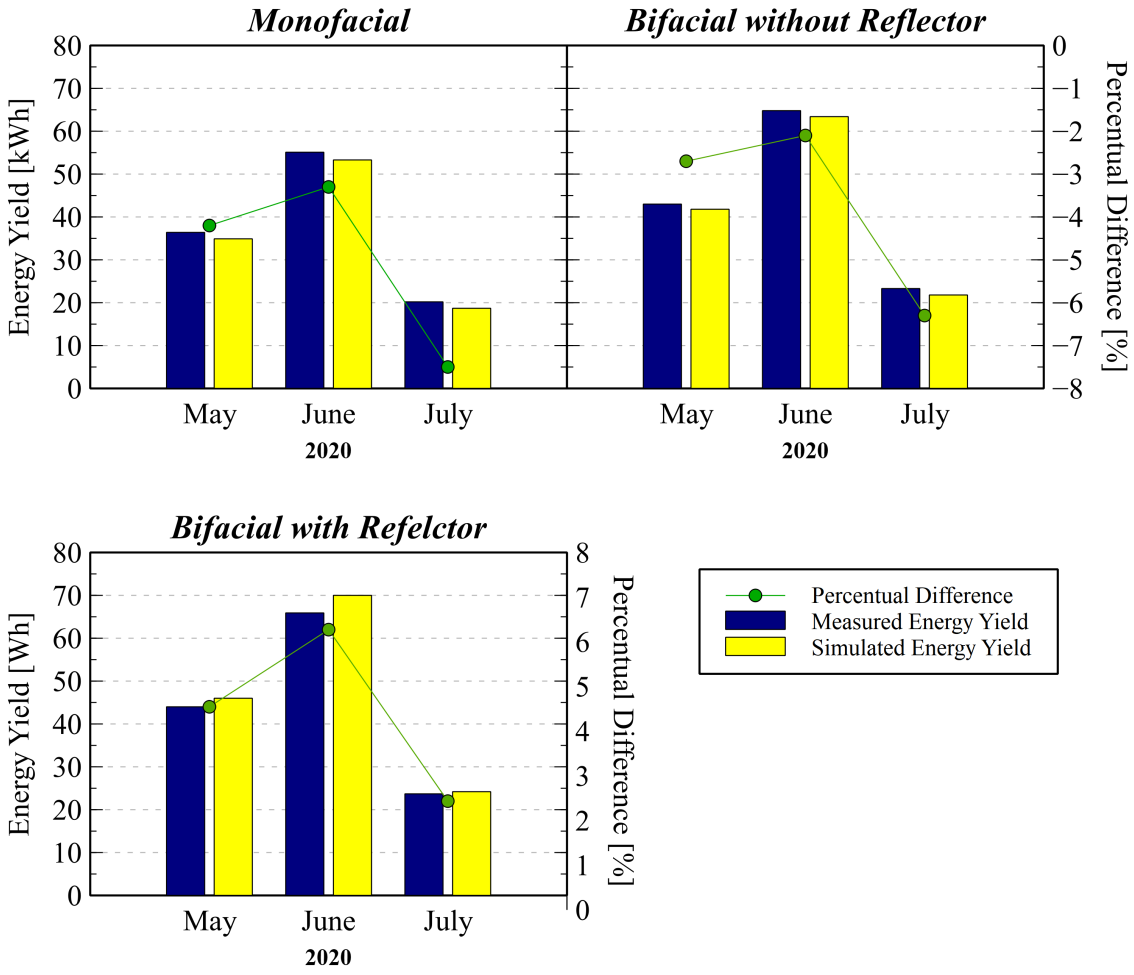

Figure 3.11: Simulation results of the Ground-based System, using on-site weather data.

For both the monofacial panel and the bifacial panel without reflector, the simulations underestimate the energy yield. For the bifacial module with reflector, the simulations overestimate the energy yield.

The percentual differences between the simulated and the monitored energy yields are similar to the differences observed for the simulations of the Ground-based System. Details about the origin of these differences can be found in Section 3.6.

3.5.2. Tracker System

The final system of which the simulations are discussed is the Tracker System. There are however no simulation results to show in this section. The main reason for the absence of these results are the limitation of the PVMD toolbox. The Tracker system tilts in a east-west direction throughout the day. The system therefore has about 100 different tilt angles throughout the year. For a simulation in the PVMD modeling toolbox this would effectively mean that for each tilt angle a new simulation has to be made in the 'MODULE' part of the toolbox, where the tilt angle of the module is set. Considering that the simulations can take several hours when using hourly data, 50,000 rays and only a single tilt angle, the simulations time would increase a hundredfold when introducing the variable tilt angles of the Tracker System. Furthermore, even if an infinite amount of time was available for these simulation, the current set-up of the code does not allow for varying the tilt angle in time in the 'ELECTRICAL' part of the simulations. This would mean that the simulations have to be made for each tilt angle individually after which the simulations of all tilt angles can be combined.

To mitigate this issue, several solutions can be applied. The first option is to use another software package, such as SAM, to simulate the energy yield of a system with and without tracking capabilities. Based on these results, a conversion factor can be calculated for each simulated point in time. This factor represents the gain of adding tracking to the system. The gain factor can then be applied to the simulation results of the PVMD modelling toolbox to get energy yield including the tracking. There are however several problems with this method. The options in SAM are limited and eventually this method does not provide a sustainable solution for the PVMD modeling toolbox. A technically more challenging option is to write new code for the toolbox which allows for the addition of tracker capabilities. An absolute necessity of this code is that it would need to significantly reduce the simulation time described above. Although it is outside of the scope of this project to create this new code, a suggestion is presented, which can be implemented in next iterations of the toolbox.

To make simulation of systems with tracking capabilities possible in the PVMD toolbox, first an option needs to be added to the 'MODULE' part of the simulation where the user can select the type of tracking. One option could be to load in an Excel file with tracking angles at certain time stamps. To cut the simulation time, the toolbox should only calculate the outputs that are relevant for each respective tilt angle. For example, a westward tilt angle of 4 degrees is only relevant for 10 instances in the year for the Tracker System of the INNOZOWA project. This means that its not needed to calculate the output of the module for *every* conceivable solar zenith and azimuth for this particular tilt angle. The results of these simulations can then be combined and further processed in the toolbox. The feasibility of such a code could be topic of further research.

3.6. Simulation Uncertainties

Throughout the two previous sections, the simulated energy yield based on different meteorological data-sets is compared to the measured energy yield. The differences between the simulated yield and the measured yield are already briefly explained for some of the simulations. However, to understand these differences in more detail, a closer look is needed. This section, therefore, aims to answer two important questions about the simulation results:

1. Which factors contribute to the overall uncertainty of the simulations?
2. Is it possible to determine which factors specifically influence the accuracy of the simulations on a daily or hourly basis?

Starting with the first question regarding the overall underlying uncertainties of the simulations. These uncertainties can be divided into two main categories: 1) uncertainties on the model side and 2) uncertainties in model inputs. It is difficult to make a quantitative statement about the uncertainties in the models used in the PVMD toolbox. It is however not inconceivable that there are at least some

uncertainties concerned with the modeling of the cell parameters, the module parameters and the electrical parameters. A more direct example of models which contain uncertainties are the thermal models which are selected in the electrical part of the simulation. For the monofacial modules, the Duffie-Beckman model is used which tends to underestimate the module temperature at higher wind speeds if compared to a more complex fluid-dynamics model [23]. Furthermore, new thermal models are currently in development as the current models were found to be inaccurate [48].The final example for uncertainties on the model side are the uncertainties in the BRL model, which is used to calculate the direct and diffuse fraction of the light from the measured GHI.

The second set of uncertainties concerns the inputs used in the different PVMD toolbox models for the energy yield simulations. The list below provides a comprehensive overview:

- **Cell Parameters.** Default cell characteristics are used of a typical crystalline silicon solar cell, since the characteristics of the cells of the LG modules are unknown. There could be discrepancies between the characteristics of these cells which could contribute to uncertainties in the simulations.
- **Unknown module parameters**. There are several module parameters which remained unknown, such as the cell and edge spacing. A conservative assumption was made for these parameters.
- **Fouling of the modules.** As will become apparent in the next chapter, some of the modules and reflectors are moderately to heavily fouled by bird droppings. This results in a lower energy yield of the fouled modules. The simulations do not account for this fouling.
- **Azimuth change of the floating structures.** The floating structures can move slightly out of position resulting in a changing azimuth. This effect was observed several times on the Tracker System during an inspection of the INNOZOWA system, which is described in Chapter 4. Since the floating systems are turning away from their optimal azimuth, this effect would result in a lower energy yield of the modules.
- **Accuracy of the irradiance sensor.** According to the datasheet of the irradiance sensor, the sensor has an error margin of ±5%. Furthermore, the irradiance sensor provides a value every four to five minutes. The resolution of these measurements are not entirely adequate to capture the faster changing weather conditions, like clouds passing before the sun.

Finally, there is one uncertainty that fall outside of both of the aforementioned categories, which is the uncertainty of the measurements to which the simulated values are compared. The uncertainty of these measurements do not necessarily concern the actual measuring of the module outputs but the time interval at which these outputs are measured. This problem was found during the validation of the Power Conversion tool and is described in detail in Section 2.6 of Chapter 2. To summarize: the module outputs are measured at irregular time intervals; approximately every 5 to 10 minutes. From these outputs the hourly energy yield is calculated, which lacks the accuracy of an energy yield calculated based on data measured at a more regular time interval. It is difficult to estimate the magnitude of this inaccuracy. As a conservative estimate, an error margin of ±1% to ±5% could be estimated. In other words, the current method of monitoring the output of the modules is not adequate for detailed analysis. A final note on the function of the optimizers as measuring devices can be found in Chapter 5.

Now the overall uncertainties that underlay the simulations are known, a detailed analysis can be made of the simulations to determine which factors specifically influence the accuracy on a daily or even hourly basis. This analysis mainly focuses on meteorological parameters such as the irradiance and cloud coverage since these values change on an hourly basis and can therefore possibly show a correlation with the hourly accuracy of the simulations. Figure 3.12 shows the daily accuracy of the simulations for the monitoring period 15-05-2020 to 14-07-2020. Three graphs are plotted, showing the accuracy of the simulations based on interpolated weather data and on-site irradiance with a 60 and 15 minute interval.

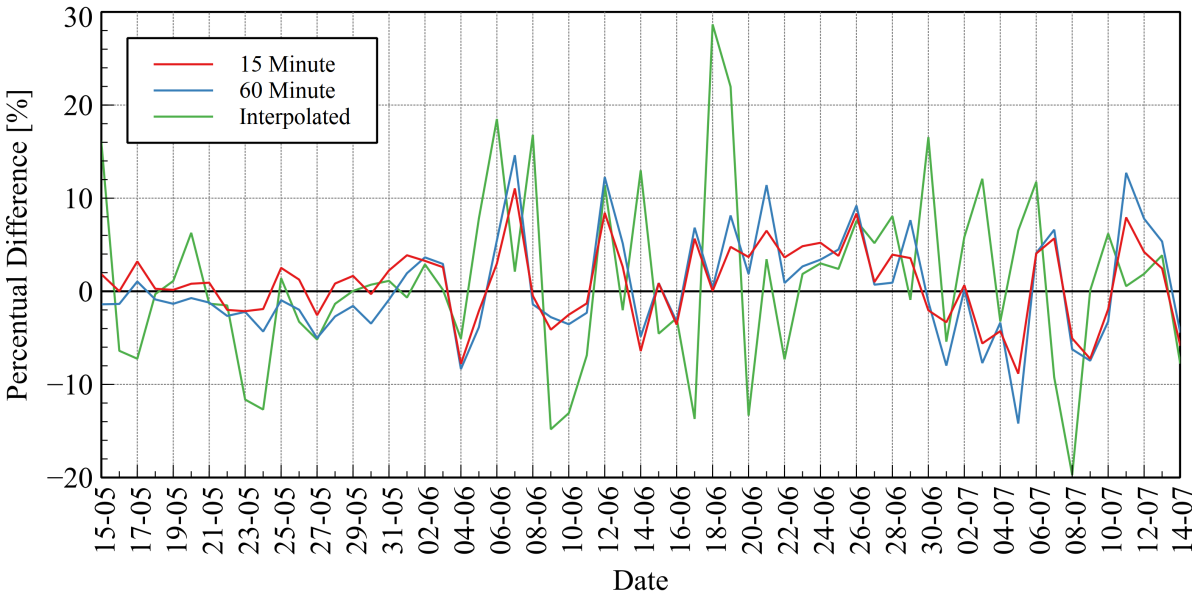

Figure 3.12: Comparison of the percentual difference between the energy yield simulations using interpolated weather data and weather data with 15 and 60 minute resolutions. The results that are shown in this graph are for the Ground-based monofacial module.

The graph provides insight into the accuracy of the simulations on a daily basis. Although the energy yield simulations for May and June based on interpolated weather data are relatively accurate on a monthly basis, Figure 3.12 shows significant deviations if daily energy yield simulation results are considered. Furthermore, slight differences can be observed between the peaks of the simulation results based on 15 and 60 minute data. The main question that arises from this graph is why for some days the simulations are more accurate than for other days. The main hypothesis at the start of this analysis is that due to the irregular measurements of both the irradiance sensor as well as the output measurement of the modules, the percentual difference between the simulations and the monitored data is larger on days with changing weather conditions while on clear sky days, the percentual differences are small.

To check this hypothesis, several meteorological parameters are compared to the daily percentual difference of the simulations based on on-site weather data with a 60 minute interval. These parameters include the total sun hours, the cloud coverage, and the (maximum) temperature which are downloaded from the KNMI database [49].

From the analysis it can be concluded that the total number of sun hours only show a weak correlation with the percentual difference. For the 12 sunniest days (days with over 13 hours of sun), the percentual differences are relatively low (±5%). There are however days with a relatively high amount of sunshine and low accuracy and days with a low amount of sunshine and high accuracy. Furthermore, other parameters such as cloud coverage and temperature showed no correlation with the accuracy of daily simulation results. The next step is to evaluate hourly data.

Figure 3.13 shows the average hourly accuracy of the simulations of the monofacial modules of the Ground-based System, based on on-site irradiance data with a resolution of 15 minutes. The error bars in the graph show the spread of the values by the standard deviation. As can be concluded from the graph, the percentual differences are high for early morning and late evening. The absolute differences are however small at these times, as early morning and late evening energy yields are typically relatively low. For most parts of the day the accuracy is on average ~5%. The spread in values is significant, ±10% throughout the day. However, in the studied time period no clear correlation can be found between meteorological parameters such as cloud coverage, or sun hours and the accuracy of the simulations.

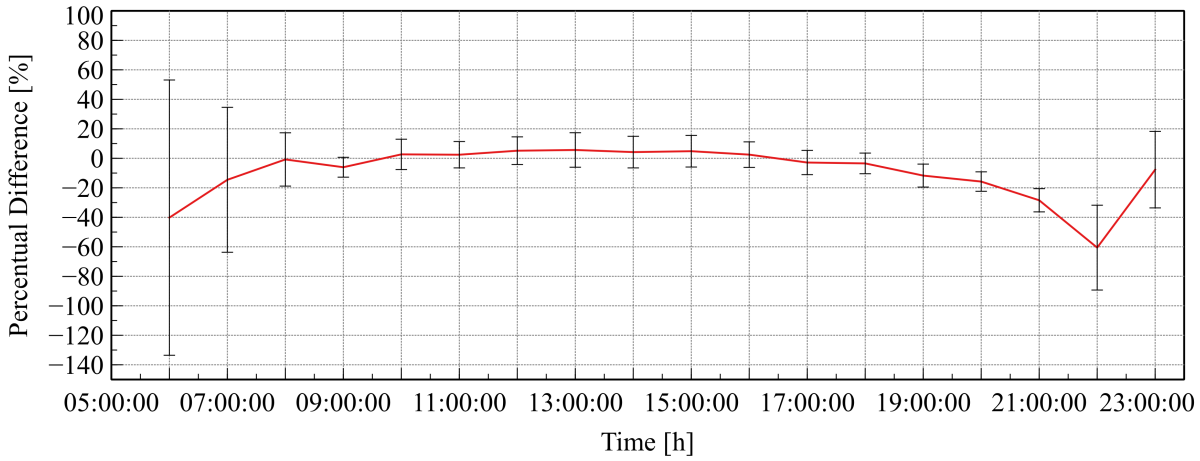

Figure 3.13: Average hourly accuracy of the simulations based on on-site irradiance data with a resolution of 15 minutes.

The differences between the simulated energy yield and the monitored values arise from a set of multiple factors, including: models (such as the thermal model and BRL model), the model inputs (such as the irradiance and the module characteristics), and the energy yield data from the monitoring tool. The hypothesis mentioned earlier in this section cannot be proven. Higher resolution irradiance and energy yield data is needed to assess the accuracy of the toolbox more closely. Furthermore, a better controllable testing set-up should be used if a more detailed analysis is required of the PVMD modeling toolbox.

3.7. PVMD Toolbox Suggestions for Improvement

The previous section described some of the uncertainties that are related to the energy yield simulations that are made for this thesis project. Several of these uncertainties are related to the PVMD Modeling Toolbox. Some uncertainties can be mitigated by modifications to the toolbox. Furthermore, the experience from using the toolbox for an extended period of time resulted in some suggestions for improvement. Since one of the main questions stated at the beginning of this chapter concerns the improvement of the toolbox, this section aims to provide a list of suggestions for its improvement. First, general comments and recommendations are provided. Finally, suggestions on specific scripts of the toolbox are made.

3.7.1. General Comments and Recommendations

- The first main critique on the toolbox is the lack of any documentation for most parts of the tool. For the solar cell simulations software, GenPro4, a PDF file is available which contains some theoretical background. Besides this document there is no supporting material that can be used to guide the user through the tool. This makes the PVMD toolbox currently very hard to use for a new user. I would suggest to create a 'User Manual' similar to the one that was made for the Power Conversion tool (see Appendix B). Furthermore, some kind of change log should be kept to track all the changes that are made on the toolbox.

- The second reason why the PVMD modeling toolbox is hard to use at times is because the code is quite 'messy' in some scripts, which makes it a lot harder to figure out what the code actually does. Some examples of this are: to-do comments, redundant legacy code, large sections of code that are in comments, the lack of comments in some scripts, not using code sections. The toolbox would greatly improve by cleaning up redundant code while simultaneously keeping to a stricter coding etiquette.

- The final main point concerns the development of the toolbox. Currently several students are working independently on several parts of the toolbox. The development of the tool would benefit greatly from a more integrated approach where students are work together more closely on the development of the tool (support, testing and troubleshooting are some concrete examples of

this.) Furthermore, it would be very useful if there was some overarching development plan to stir the development of the tool in the right direction.

3.7.2. Comments and Recommendations on Specific Scripts

- **CELL.** Although simulations of a solar cell based on its layer structure provides great flexibility for cells of which the cell structure is known in detail, it presents uncertainty for cell of which the layer structure is unknown. For most commercial PV modules, companies want to keep their cell structure confidential as this is their key intellectual property. Generally one can figure out the layers of a typical solar cell based the main technology that is used. However, detailed information is mostly unknown. This presents an uncertainty already at the start of the simulation process. The significance of this uncertainty is however hard to quantify and could be topic of future research.
- **MODULE.** The toolbox has one pre-defined module type: the four-legged frame. There are several obscure parameters which need to be changed manually in the code, such as the frame width and margin between the cell and module. These parameters should be added to the main input form. Furthermore, from the form it is not clear whether the module is placed in landscape or portrait mode. A option could be added to the input form to switch between these two modes.
- **MODULE.** The user has the ability to change several optical behaviour properties of the surface in the 'four legged frame' code. These inputs determine the characteristics of an infinite surface area. This makes it relatively difficult to add reflective surfaces to the module, which is why in this project view factor algebra was used to calculate the albedo of the surface. Another option would be to create a new module type which has the option to include a stand-alone reflector, based on user inputs. Julen Garro Etxebarria implemented such an module in his thesis, so it already has proven its feasibility [20].
- **MODULE.** Some of the parameters that are required to reconstruct the PV module are for some modules not available on the data sheets of the manufacturer. These parameters include: the cell spacing, the edge spacing, the frame width and the cell margin. A guideline or rule of thumb should be provided to guide the user through these inputs. These guidelines can be added to the aforementioned manual.
- **MODULE.** Currently no option is included to add tracking capabilities of the toolbox. Subsection 3.5.2 describes how such an option can be added to the tool.
- **MODULE.** The current version of the toolbox does not allow for the implementation of secondary objects, such as trees, chimneys, or poles. For the simulations of this project it means that the support poles of the Retractable System, which shade the monofacial modules, cannot be included in the simulation. Comparable software packages, like PVsyst, have this option to include these objects. The feasibility of such an addition could be a topic for further research.
- **WEATHER.** At the 'weather' part of the simulation, the user has to submit an Excel file with meteorological input data. This file has to include the altitude and azimuth of the sun as well. Currently, the user has to calculate these solar position parameters with a secondary tool. It would be a significant workflow improvement if such a tool is directly included in the PVMD toolbox. Furthermore, this addition should be able to warn the user for wrong inputs. This solar position tool can easily be implemented in the current infrastructure of the PVMD toolbox, and can be based on inputs such as the latitude, longitude, starting date and time interval. The same suggestion can be made for the direct and diffuse parts of the irradiance that the user has to specify. It would be a great workflow improvement if the PVMD toolbox has the ability to calculate the direct and diffuse fractions from the specified global horizontal irradiance (GHI). This can be achieved by adding a model, such as the BRL model [41] or any other comparable model, to the toolbox. The user would then be able to select a model from a library which is then used to decompose the inputted GHI. Again this input model can be based upon accessible input parameters such as the location latitude, longitude, starting date, and time interval.
- **ELECTRIC.** In the current ELECTRIC script, the total energy yield is calculated based on a setting which has to be manually changed. First of all, this process should be automated, based on the

timestamps uploaded in the 'WEATHER' part. Furthermore, an option should be added to allow for the processing of variable time intervals as well. The tool should easily be able to calculate simple but useful outputs, such as the hourly/daily/total energy yield. This would cause a significant workflow improvement and would allow the user to analyse the outputs of the simulations a lot faster.

3.8. Chapter Conclusions

The INNOZOWA project provides the opportunity to test the PVMD modeling toolbox in detail. This Chapter therefore aimed to simulate the INNOZOWA systems as accurately as possible while establishing the required input parameters to do so. The experience of making energy yield simulations of the INNOZOWA systems provided several suggestions for improvement of the PVMD modeling toolbox.

Four different meteorological data-sets were created as inputs for the simulations: a data-set based on climate data, a data-set based on interpolated weather data, and two data-sets based on on-site irradiance data with 60 and 15 minute resolutions. To create these data-sets, a variety of tools and models were used, such as: the Inverse Distance Weighted interpolation technique to interpolate the meteorological parameters, the BRL model to get the direct and diffuse fractions of the light from the Global Horizontal Irradiance, and Meteonorm to apply the local Sky-View Factor of the systems.

Initial simulations with the toolbox showed significant difference between measured and simulated energy yield values. Several issues were identified and mitigated. Among the solutions are: using view factor algebra to calculate a new albedo value of the surface, carrying out an on-site inspection which helped to identify several installation errors and small particularities in the system, and the implementation of a new, simple, thermal model, the Duffie-Beckman model.

Using the meteorological input data-sets and taking into account the adaptations to models as well as inputs, numerous energy yield simulations were made. This simulation process took many iterations over a period of several months. The simulations based on climate data proved to be highly inaccurate, especially in months of which the irradiance data did not correlate with the actual irradiance data. Simulations based on on-site irradiance data drastically decreased the percentual difference between the simulated and measured energy yields. The differences between the yields in the winter months showed however significant differences, especially for the bifacial simulations. This could either mean that the models used in the PVMD toolbox have trouble processing these low irradiance periods, or that the model inputs, such as the irradiance are not accurate enough during these months. Simulations based on on-site irradiance data proved to be the most accurate. Monthly as well as daily energy yield showed a percentual difference of about ±10%.

The reasons for these differences between the monitored energy yield and the simulated energy yield were investigated thoroughly. However, in the end, no clear correlation was found between meteorological inputs and the accuracy of the simulations. It is assumed that the differences arise from a set of many uncertainties that still underlie the simulations, including: unknown cell and module parameters, fouling of the modules, variable azimuths of the floating structures, accuracy of the on-site irradiance sensor, accuracy and resolution of the module output parameters, and uncertainties on the model side, such as the BRL model and the thermal models.

The simulations resulted in several recommendations for improvement for the toolbox and its models. These recommendations mainly concern additions or adjustments to make the toolbox easier to use, especially for new users. Furthermore, a detailed proposal is provided to include tracking capabilities in the PVMD modeling toolbox. Feature research could show the feasibility of such a model.

Overall it can be concluded that making energy yield simulations in the PVMD modeling toolbox is a hard and long process which requires deep understanding of every aspect of the toolbox. Due to the many uncertainties that still underlie the simulations of the INNOZOWA systems, it is hard to quantify the overall accuracy of the toolbox or its individual parts. A better controllable environment in combination with higher resolution input data could provide more insight in the overall accuracy of the toolbox.

3.9. Chapter Recommendations

- Several recommendations are made in Section 3.7 to improve the PVMD modeling toolbox. General recommendations include: the creation of a manual and/or change log, cleaning up /refactoring (old) code, and the creation of an overarching development plan. Specific recommendations include: addition of several input parameters to the user form of the module, the addition of tracking capabilities, automatic calculation of meteorological parameters, such as the altitude and azimuth, from time and location, and the extension of the electrical part to allow for variable time intervals.
- Simulations based on interpolated weather data resulted in highly inaccurate results for the winter months. On-site irradiance data could provide more insight into uncertainties that underlie these simulations during the winter months.

4

On-Site PV Module & System Inspection

During the energy yield simulation procedure, described in detail in Section 3.3 of Chapter 3, the initial simulation results of the INNOZOWA subsystems showed at first significant differences with the actual measured energy yield data. This difference resulted from several problems found in the models used to make the energy yield simulations. An effort was made to mitigate several of these problems to get the simulations to the required level of accuracy and precision. Next to the models, some uncertainties were expected on the installation side, i.e. deviations in the system installation. The two most likely uncertainties that could be present in the PV system itself are:

- The modules can be soiled, damaged or broken, which lowers their energy yield.
- There are deviations between the actual PV installation and the PV installation on paper.

To find out if these uncertainties indeed present itself in the INNOZOWA PV system, an on-site PV module and system inspection was conducted. The research question that is associated with this inspections is:

6. *Are there any defects or deviations present in the system that could contribute to model and data uncertainties and how can these defects or deviations be found during an on-site inspection?*

An important boundary condition associated with this research question is to thoroughly inspect the modules of the Tracker System. As will be apparent in the next chapter, concerning the monitoring of the different systems, several modules of this system show atypical behaviour. The inspection of these modules is therefore of additional importance.

This chapter is divided into four main parts. First a description is given of the methods that were used during the inspection of the modules. Second, the findings for each of the three INNOZOWA systems are described in detail. Third, these findings are discussed in the chapter conclusion. Finally, several recommendations are provided at the end of the chapter.

4.1. Inspection Methods

Due to the growth of the PV industry, inspection of PV systems has become increasingly important. Early recognition of defects in PV systems and modules can contribute to a higher system efficiency and a longer lifetime of the system. Research shows that there are a number of problems that can be detected in old as well as in new PV plants [50]. Common faults typically detected in PV modules are:

- Damage to the glass and/or frame.
- Hot spots, caused by a cell or a group of cells dissipating power drained from the neighbouring cells. These hot spots can be caused by a number of reasons such as module fouling and mechanical damage of the cell.

- Faults in the electrical installation, such as loose contacts and wiring or defect bypass diodes.
- Soiling of the modules.

Several methods can be utilized to check for these kind of faults in a PV module and its balance of system. The most notable methods are: IV-curve tracing, electroluminescence (EL), photoluminescence (PL), infrared (IR) imaging and visual inspection. For the inspection of the INNOZOWA pilot system, two methods are selected: IR imaging and visual inspection, which are both industry standard methods. The two next subsection will introduce both of these inspection methods in some more detail.

4.1.1. Visual Inspection

Visual inspection is typically the first step that is taken in PV module inspection. It is a relatively easy and fast way of detecting some common failures in PV modules. During a visual inspection, cracks, yellowing, misalignment, delamination, bubbles, snail trails and burnt cells can be observed [50]. It is important however, to know how and where to look during such an inspection. To aid the visual inspection of the INNOZOWA modules, the 'Tool for Evaluation of Fielded PV Module Conditions', created by NREL, is used [51]. This tool, which is in the form of a questionnaire, is specifically developed to make a comprehensive evaluation of visual defects in PV modules. The form consists of 14 sections, each containing specific questions about individual module components. An example of a completely filled-out form can be found in Appendix C. Other experiments that were conducted during the visual part of the inspection are: measurement of the module tilt angles and module azimuths, and measuring the dimensions of the subsystems.

4.1.2. Thermographic Imaging

Visual inspection is a powerful method to quickly inspect PV modules. However, not all defects and issues in a PV module can be detected with the naked eye. Thermographic imaging is one of the methods that can fill this gap. It is a non-contact, non-destructive technique, able to detect and diagnose defects in PV modules under operating conditions [52]. A thermal camera receives infrared radiation from an object and creates a thermal image from this information. According to Planck's law of black body radiation, the infrared radiation of an object is proportional to the temperature of the object. Creating thermal images from this radiation thus results in images with a colour gradient based on the temperatures of the objects in the image. These images can be analyzed with special software to determine local temperatures and identify possible faults. This techniques is already widely used in the industry. Typically, handheld thermal camera's are used during these inspections while for large-scale PV plants, light unmanned aerial vehicles (UAV's), or drones are utilized. A thermal camera is attached to this drone, which allows for fast and accurate inspection of large-scale plants [53].

Although thermographic imaging is relatively easy to perform, it should be compliant to several standards to the get the best results. First, the inspection must be carried out in closed circuit conditions, since the faults are only observable under electric load [50]. Second, camera angle and distance are of importance as well. The images should not be taken perpendicular, but at angles of 5 to 60 degrees [54]. Additionally, measurements at different angles and distance could contribute to increased fault detection. Finally, back side measurements should be made as well to combine the advantages of both front side and rear side measurements. Other important guidelines concern the ambient conditions, which are briefly explained in the next subsection.

4.1.3. Ambient Conditions

Proper ambient conditions are important when conducting an inspection of PV modules by thermal imaging. Thermal images should be taken when the modules work at full capacity. It is therefore important to carry out the inspection on a day when the modules operate (close to) their maximum power point. Minimum required standards with respect to ambient conditions are described in both literature and manufacturer guidelines. Irradiance should be in the range of 500 - 700 W/m^2 with clear sky conditions to avoid shading by clouds. Furthermore, both ambient temperature and wind speed should be relatively low to decrease ambient effects on the temperature [50, 54]. To be as transparent as possible, a graph containing the ambient temperature and the global horizontal irradiance is shown in Figure 4.1 [40].

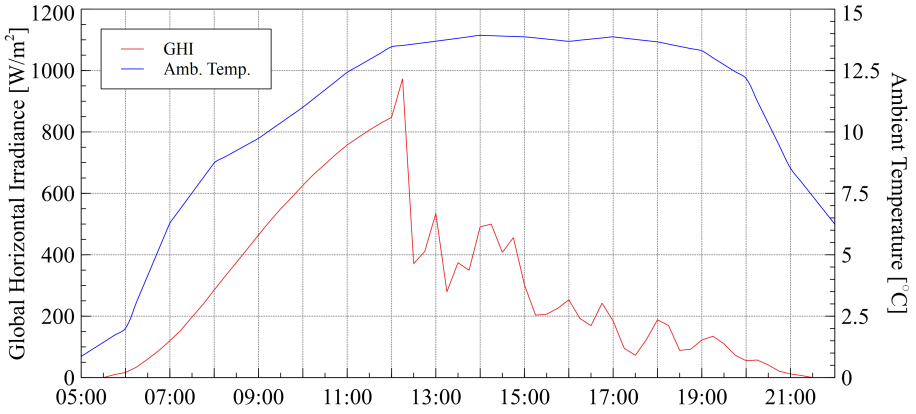

Figure 4.1: Global Horizontal Irradiance [W/m^2] and ambient temperature [$°C$] during the on-site inspection on 15/05/2020 [40].

4.2. Inspection Findings

The following sections contain the findings from the inspection. The findings are categorized per system. For each system, first the findings from the visual inspection are discussed. Second, if applicable, thermal images are shown. Finally, the influence of these findings on the energy yield simulations and on the monitored data is discussed.

4.2.1. Ground-Based System

Several important anomalies were discovered during the visual part of the inspection of the Ground-based System. At several points, the system deviated from the intended design.

Both the monofacial panel as well as the bifacial panel are installed at an incorrect tilt angle. The measured tilt angle of the monofacial panel was found to be 12.7°. The right hand picture of Figure 4.2 shows the tilt angle of the bifacial panel, which was found to be 7°. The intended tilt angle of the panels is 15°. This means an 8° difference for the bifacial modules, which significantly influences the energy yield of the modules.

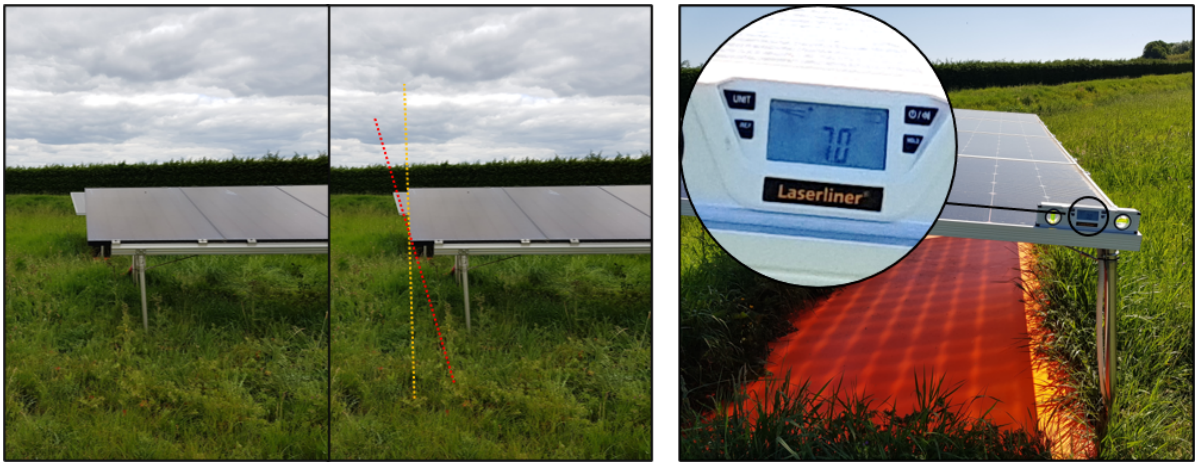

Figure 4.2: The two figures on the left show the misalignment of the module azimuth, indicated by the dotted lines. The figure on the right shows the module tilt angle of the bifacial Ground-based Module.

Not only are the modules installed at a wrong tilt angle, the azimuth of the modules was found to be misaligned as well. As can be seen in the left hand picture of Figure 4.2, the monofacial panel and the bifacial panel are not aligned. A compass was used to measure the azimuth of the panels but the

results of this measurement were found to be unreliable, as the compass was heavily distorted by the metal of the frame. To estimate the azimuth, drone footage was overlaid with a schematic overview of the pilot site. From this comparison, it was found that the azimuth deviates about 15° in a westward direction from the intended azimuth of 180°. Details of this estimation can be found in Appendix D

The SolarEdge monitoring website lists the two module types that are used at the INNOZOWA PV pilot system: the LG330N1C-V5 and the LG400N2T-J. The initial simulations are therefore based on these module types. However, upon inspection, the nameplates of the modules did not correspond with the module types listed on the monitoring website. The monofacial module type is actually the LG330N1**K**-V5. The bifacial module type could not be retrieved as this information was hidden by the frame. Other module information, such as the Vmpp, Impp, Voc, and Isc was visible however. These parameters did, unfortunately, not correspond to any existing module type.

During the inspection, some minor anomalies were found as well. Grass and weeds are growing close to the reflector, blocking incoming sunlight. At some places, weeds grow over parts of the reflector. If not properly maintained, this vegetation jeopardizes the function of the reflector. An easy solution would be to lay some pavement or gravel around the reflector.

Most of the modules of the Ground-based System are lightly to moderately fouled, mostly by bird droppings. An example of such a soiled module is shown on the left hand picture in Figure 4.3. On the right side of this figure, a close-up, thermal image is shown of one of these bird droppings. As can be observed in this image, the bird droppings cause local hot-spots, resulting in lower energy yield of the module. Although these bird droppings are typically washed away by rain after some time, dirt builds up at the bottom of the frame. At the moment of inspection, this layer of dirt almost reached the bottom row of cells, possibly shading them even further.

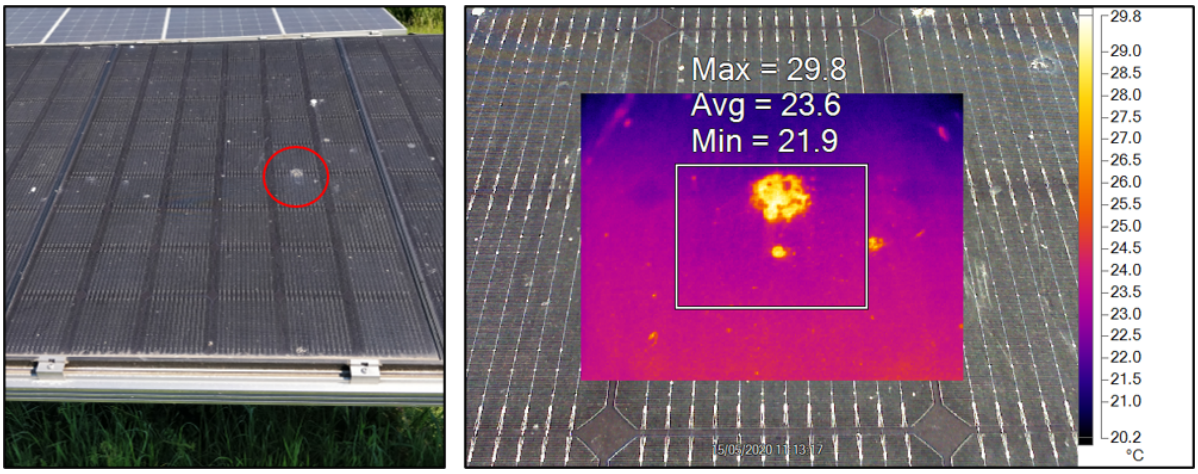

Figure 4.3: The figure of the left shows one of the monofacial modules of the Ground-based System. The image on the right shows a thermal close-up of one of the fouled spots on the module.

Although many modules have hot-spots due to bird-droppings, no defects were noticed to the cells. Furthermore, no damage was detected on the glass, frame, cables or junction box. However, due to the significant amount of dirt and bird-droppings it was hard to distinguish between dirtiness and defects. It would therefore be interesting to analyze some of the modules in detail, after the project, with e.g. electroluminescence.

The aforementioned findings are important for making accurate energy yield simulations of the system. The new module azimuth and tilt angles are used in the final energy yield simulations, of which the results are described in Section 3.4 of Chapter 3. Other findings, such as the fouling of the modules lowers the overall energy production of the module. It is, however, hard to quantify the energy losses due to this fouling.

4.2.2. Tracker System

The second system that was thoroughly inspected is the Tracker System. As already briefly described in the introduction of this chapter, some modules in the Tracker System showed atypical behaviour in terms of energy output. It is therefore important to inspect these modules with extra attention for damage or other particularities.

First, the tilt angles of the modules were measured and the azimuth of the Tracker System was determined. The tilt angles are all within ±0.5° of their intended design values. The azimuth however deviates slightly from the intended azimuth of 180°. The azimuth of the system is determined at 180° ±20°. Due to wind and current, the azimuth of the system can shift about 20 degrees east and west at times. This shifting was observed multiple times during the inspection. The reason for the shift in azimuth are the anchoring points of the system, one of which is shown in Figure 4.4. These anchoring points are not capable of keeping the system in the same spot.

Figure 4.4: The picture on the left shows the Tracker System with in the foreground one of the anchor points. The picture on the right shows a close-up of this anchor point.

A second important observation made of the Tracker System was the heavy fouling of the modules due to bird droppings. Especially the front row of the system was heavily soiled, which causes severe hot-spots. An example of this fouling is shown on the left side in Figure 4.5. On the right side of this figure, a thermal close-up image is shown, which shows a temperature of 49.0 degrees Celsius. Other rows were found the be moderately fouled as well.

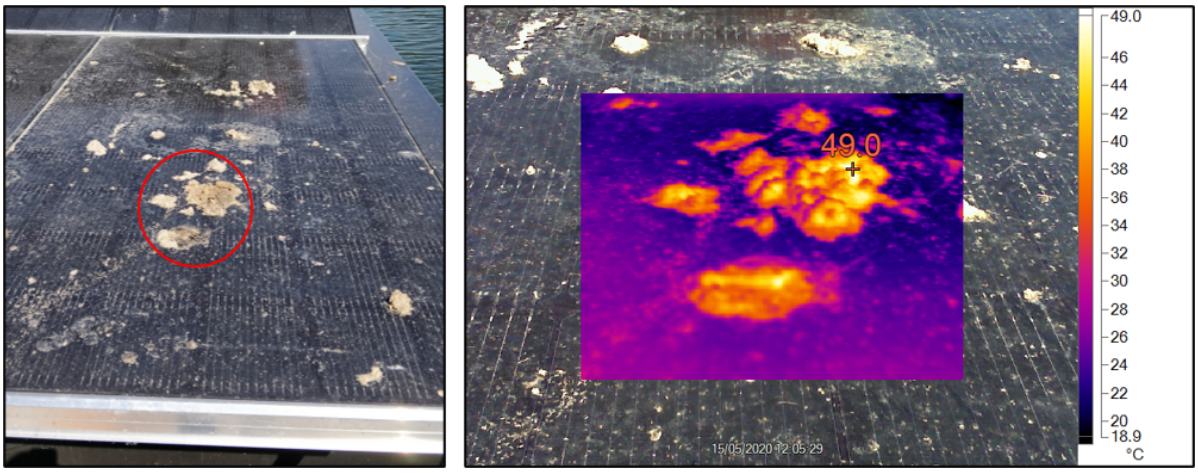

Figure 4.5: The picture on the left shows one of the monofacial modules of the Tracker System, installed at a 0 degree tilt angle. The image on the right shows a thermal close-up of the fouled spots on the module.

Although most of the modules in the system are heavily fouled, no serious damage could be detected visually or with thermal imaging. However, it seemed that the monofacial modules of the two front rows were slightly discoloured. This was however hard to confirm due to the heavy fouling of the modules. Overall, the system was very hard to inspect. The proper angles and distances for the thermal imaging could hardly be maintained, resulting in thermal images of low quality.

4.2.3. Retractable System

The final system that was inspected is the Retractable System. At the moment of inspecting this system, the sky was completely cloudy and almost no direct irradiance was present. Due to this change in weather, no precise thermal images could be made of the modules. However, several important findings were made visually.

First, as with the two other systems, the tilt angles of the modules were determined as well as the system azimuth. The tilt angles of the modules were found to be 16°. The azimuth of the system was determined at 180° ±20°. This is, again, a slight deviation from the intended azimuth of 180°. The misalignment of the azimuths of the different rows of the Retractable System can be observed in Figure 4.6.

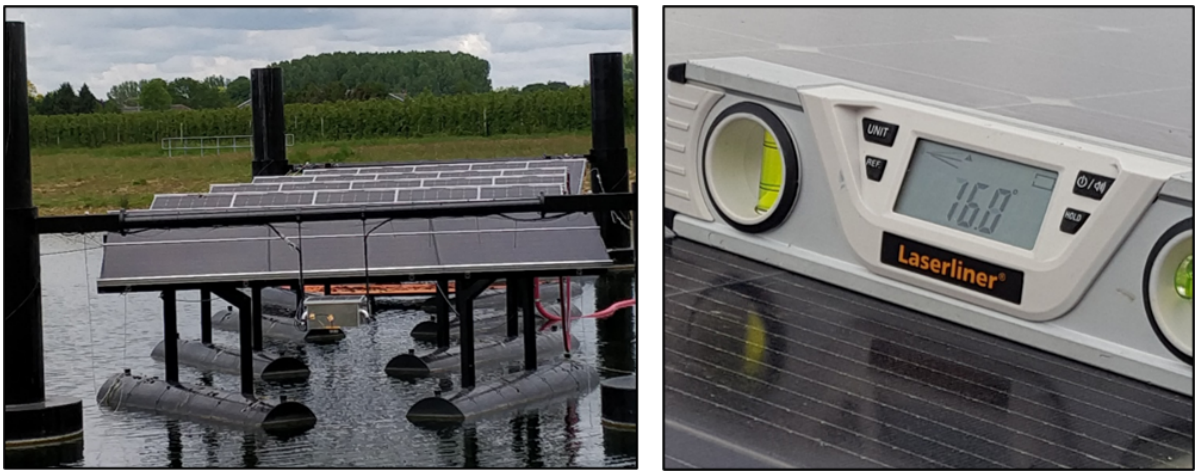

Figure 4.6: The figure on the left shows the five rows of the Retractable System, each at a slightly different azimuth. The figure on the right shows the tilt angle of the last row of the Retractable System.

The second important finding for the Retractable System concerns the fouling of the two reflectors of the last two rows of the system. As can be observed in Figure 4.7, the two reflectors are heavily fouled by bird droppings and even a birds nest. This greatly affects the reflective capacity of the reflectors. This fouling should be taken into account when assessing the energy yield of the modules of these two rows.

The damage that was detected on this system was limited to some bird droppings and the heavy fouling of the reflectors. As mentioned before, thermal imaging was not possible due to a negative change in ambient condition. Again, the system was hard to inspect due to the relative highly mounted and unstable modules.

Figure 4.7: The two heavily soiled reflectors of the Retractable System.

4.3. Chapter Conclusions

An on-site PV module and system inspection was conducted on May 15, 2020, to find defects and/or deviations in the INNOZOWA system installation. During this inspection, each INNOZOWA subsystem was thoroughly investigated using several methods. The inspection methods that were used are visual inspection aided by an NREL developed questionnaire and thermographic imaging. Many abnormalities were found during the inspection: panels installed at wrong tilt angles, the misalignment of the module azimuth of several subsystems, and most notably light to heavy fouling of the modules and reflectors by bird droppings. These droppings, resulted in local hot-spots, which in turn result in a lower energy yield of the modules. Furthermore, these hot spots could potentially damage the cell and module. Apart from the hot spots caused by bird droppings, no other damage is detected in the system. The modules of the Tracker System, which were of special interest to this inspection, also showed no significant damage. The two front rows of the Tracker System seemed slightly discoloured, but due to the fouling of the modules this was hard to confirm.

The results from this inspection are used in the final energy yield simulations of Chapter 3. Furthermore, lessons can be learned for future floating PV system installation and inspection. Several recommendations are provided in the next section.

4.4. Chapter Recommendations

- Several installation faults are detected during the on-site inspection. These faults could have been detected by a post-installation inspection. It is therefore recommended to carry out such a post-installation inspection for future INNOZOWA (pilot) systems, especially if scientific research is important.
- The location of the floating systems conflicts with an area where a significant number of birds live/breed. This causes a significant number of bird droppings on both the modules and reflectors. These bird droppings cause hot spots which decrease the energy yield of the modules. Moreover, these hot-spots can damage the modules over-time. It is therefore important to minimize the amount of bird droppings. There are several commercially available options to keep birds away from the systems, such as: sound, spikes, netting or lasers [55].
- Reflectors are an important asset for the bifacial modules. They should be kept free from any potential blocking of light by e.g. grass. An easy solution would be to lay some pavement or gravel around the reflector of the bifacial modules of the Ground-based System.
- The inspection of the floating systems is time consuming and at times not practically possible. Some places are impassible, such as the bifacial modules of the Tracker System. Visual and thermal inspection of the ground-based modules took about 30 minutes while the inspection of both

floating systems took several hours. If these systems are scaled up, other techniques should be used to carry out inspections. A promising technique, which was already mentioned in Subsection 4.1.2 is the use of drones.

- The azimuth of the Tracker System and the azimuth of the Retractable System can deviate from their intended azimuth of 180 degrees due to wind and currents. This could be a deliberate design choice to allow the tracking/retracting capabilities of the respective systems. The deviation from the ideal azimuth results in a lower overall energy yield of the PV modules. It is recommended to study the possibility of fixing the azimuth in a more robust way for both floating systems.
- No damage was found on any of the 16 modules of the Tracker System with the thermal camera or the visual inspection. Research in the lab, by means of, e.g. electroluminescence or IV-curve tracing, could completely exclude any damage to the modules. Furthermore, it could be interesting to study the short term effects of the heavy fouling on the modules.

5

Monitoring of the INNOZOWA PV Pilot System

Throughout this report, the performance of the INNOZOWA PV pilot system was briefly discussed on several occasions. In chapter 2, Section 2.6, the efficiency of the system was calculated and used to validate the new Power Conversion tool. In Chapter 3, sections 3.4 and 3.5, the energy yield of the system was compared to a simulated energy yield. This chapter will provide a complete and detailed analysis of the performance of the INNOZOWA system. This analysis is important because it can uncover some of the weak spots of the different pilot systems that are being tested. Through a thorough examination of the relevant data, anomalies can be found which could lead to improvements of the systems. This chapter aims to answer two of the secondary questions of this report:

6. *Based on a thorough data analysis of the different subsystems, are there any anomalies in the data and where do these anomalies come from?*

7. *How can the INNOZOWA PV pilot subsystems potentially be improved and which subsystem is the most likely to be used for subsequent projects and up-scaling?*

As mentioned before in this report, each module in the INNOZOWA system is continuously monitored by a SolarEdge power optimizer. The monitored data is stored on a server which can be accessed through the SolarEdge monitoring website. This website is very user unfriendly as it does not allow for the data to be downloaded with a high resolution for longer periods of time. A second method of retrieving the data is the SolarEdge Monitoring API which allows the user to get inverter data automatically from the servers. However, this option does not allow to get data from the power optimizers. All the relevant data is therefore downloaded manually, with a one hour resolution, from the monitoring website and stored locally in an interactive Excel file for further analysis.

This chapter is structured as follows. First an overview of the energy yield of each of the systems is provided. From this overview, the performance of each of the systems is analyzed. The second section concerns problems encountered with the monofacial modules of the Retractable System. Section three discusses the internal consumption of the Tracker System. Fourth, the anomalies in the energy yield of the Tracker System are discussed. Section five evaluates the results of the irradiance sensors which are installed for the INNOZOWA pilot project. Section six discusses the effects of wind on the INNOZOWA subsystems. Finally, the conclusions and recommendations are provided.

5.1. Module Energy Yield

This section details the results of monitoring the energy yield of the INNOZOWA PV pilot system. The monitoring period started on the 11th of September 2019 and will continue at least until the end of September 2020. For the analysis in this thesis project, the data from October 2019 to July 2020 is included. Figure 5.1 shows the total average energy yield of each of the nine study cases of the

INNOZOWA PV pilot system. Before analyzing this data in more detail, several comments should be made about the process of gathering the data:

- On several occasions throughout the monitoring period, the hourly energy yield of a module in the system showed an implausibly high value of two to five times the installed capacity. At these instances the energy yield of each module is set to a value of zero. In total, there were about ten of these instances throughout the monitoring period. These values can be attributed to miscalculations in the SolarEdge monitoring tool.
- In October and November of 2019, several modules of the Retractable Systems were drifting away from their intended position. This happened only to five of the ten modules, while the remaining five stayed in position. Because of this drifting, the energy yield of these modules was greatly reduced. It is therefore decided not to include the energy yield data of these modules during these months.
- The following analysis consists of the monitoring results of a 10 month monitoring period. The months August and September of 2020 are not included in the analysis. This means that the analysis is not representative for a full year of monitoring and that the overall results can slightly change.

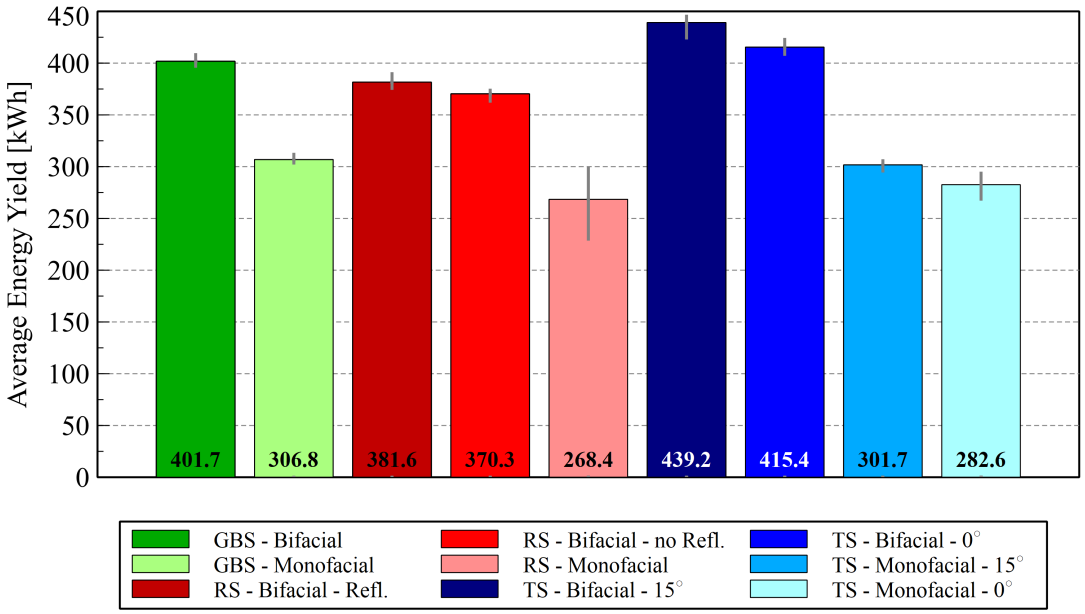

Figure 5.1: Total average energy yield per subsystem. The grey error bars indicate the minimum and maximum energy yield of a module in the respective subsystem (GBS = Ground-based System, RS = Retractable System, TS = Tracker System).

Figure 5.1 shows the total average energy yield per study case in kilowatt-hours. The error bars in this graph depict the minimum and maximum energy yield of a module of the respective study case. Several conclusions can be drawn from this graph. First of all, the size of the error bar of the monofacial modules of the Retractable System suggests a large spread in values. The main reason for this spread in energy yield is the shadows that are casted by the poles of the support structure of the Retractable System. More information on this phenomenon can be found in the next section. Secondly, it can be concluded that the bifacial modules of the Tracker System, installed at a tilt angle of 15°, have the highest average energy yield of all the study cases. It should be noted however that the Tracker System has some internal consumption from operating the pumps which enable the tracking. A detailed calculation of this internal consumption can be found in Section 5.3. Finally, it can be concluded that all the bifacial modules outperform the monofacial modules. This is however not unexpected as the capacity of the bifacial modules is 70Wp higher. To make an equitable comparison between the monofacial and bifacial modules, a graph is plotted in Figure 5.2, showing the average energy yield per installed capacity (i.e. the specific energy yield).

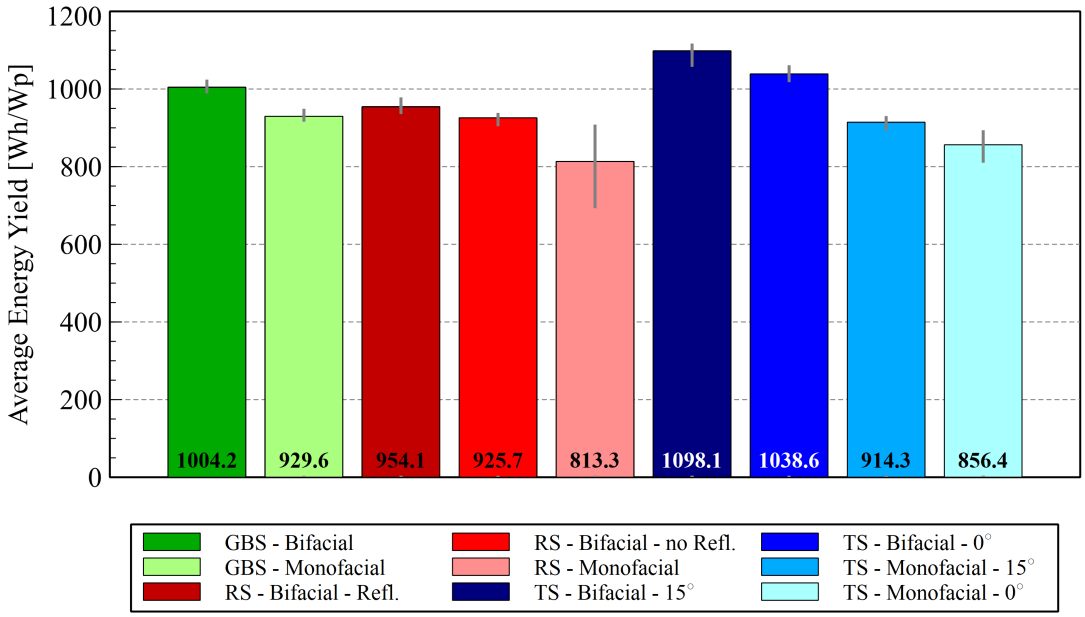

Figure 5.2: Total average energy yield per subsystem per installed capacity. The grey error bars indicate the minimum and maximum energy yields per installed capacity of a module in the respective subsystem (GBS = Ground-based System, RS = Retractable System, TS = Tracker System).

For the calculation of the average energy yield per installed capacity, the Standard Test Conditions (STC) values of the modules are used. For the bifacial modules, the contribution of the backside is not included for one main reason. The contribution on the backside heavily depends on the albedo of the surface area and the surroundings. These are different for each of the study cases, which means that not one single value can be selected for the rear side contribution.

From Figure 5.2, it can be concluded that the energy yield of the monofacial modules is now closer to the bifacial modules. There are however still significant differences between, for example, the bifacial modules of the Tracker System, installed at a tilt angle of 15 degrees and the monofacial modules of the Tracker System, installed at a tilt angle of 0 degrees. To get into more detail, the monthly energy yield per installed capacity is plotted in Figure 5.3 for the entire monitoring period. This provides the opportunity to analyse each of the study cases in some more detail. From these figures, several conclusions can be drawn about each of three subsystems:

- **Ground-based System**. The monofacial and bifacial modules of the Ground-based System produce a steady energy yield throughout the 10 month monitoring period. Over the entire monitoring period, the bifacial modules produced about 25% more energy than their monofacial counterparts. Furthermore, as can be observed from the error bars, the difference between the minimum and maximum energy yields of the individual modules is relatively low. These results make the ground-based modules an ideal reference case.
- **Retractable System**. When analyzing the energy yield data of the modules of the Retractable System, several conclusions can be drawn. The first thing to note is the energy yield of the bifacial modules with reflectors. These modules yield about 5% percent less energy than the bifacial modules of the reference case even though they are installed at a more optimal tilt angle. This is noteworthy, since in Section 1.1.1 of the Introduction several positive effects of PV on water were described. These effects, such as the cooling effect of water and less fouling, should have increased the energy yield of the floating bifacial modules. The inspection of the modules, described in detail in Chapter 4, showed that the reflectors of the bifacial modules were heavily fouled. This mainly explains the difference in energy yield between the floating bifacial modules with reflectors and the ground-based reference case.

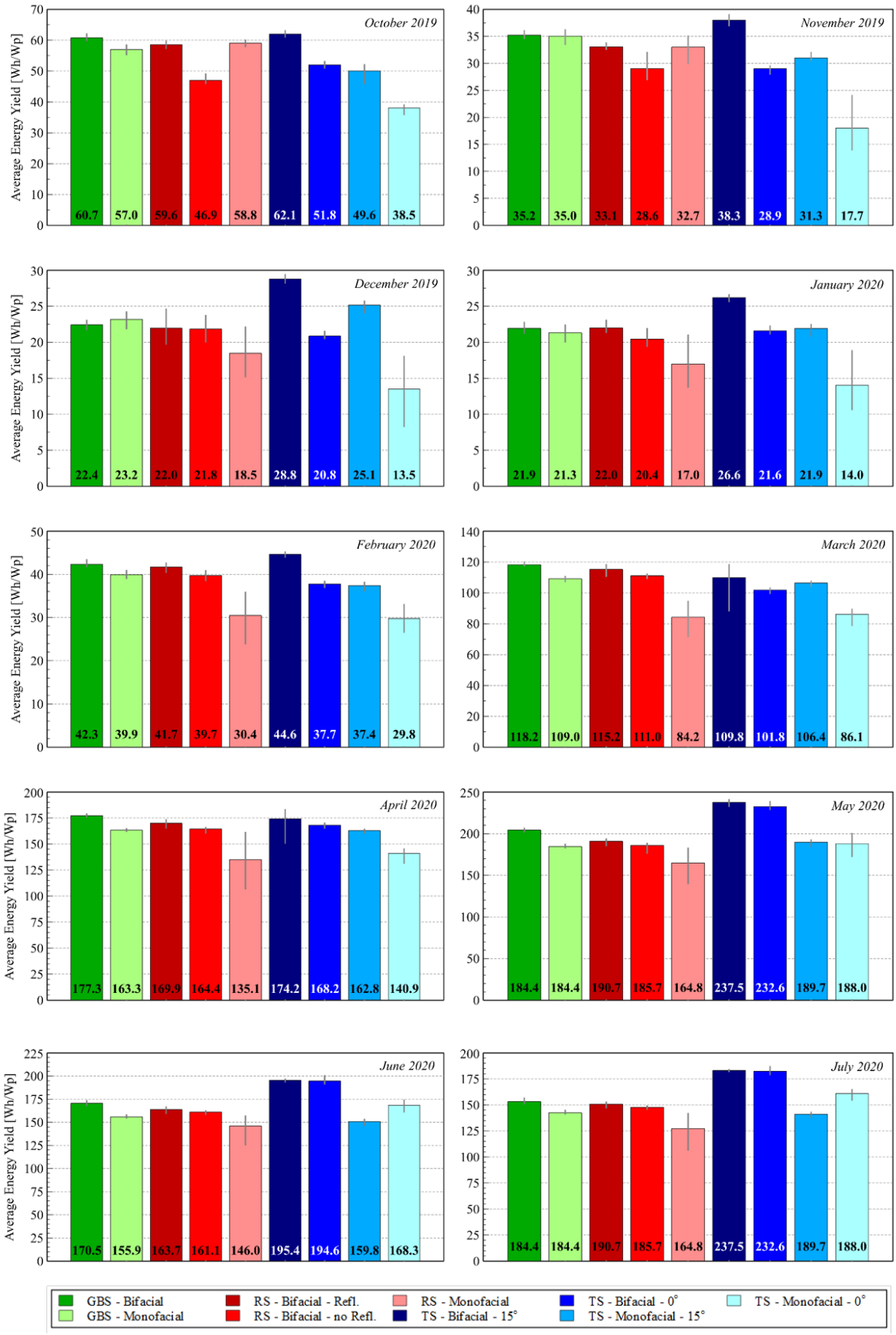

Figure 5.3: Total average energy yields per subsystem. The grey error bars indicate the minimum and maximum energy yield of a module in the respective subsystem (GBS = Ground-based System, RS = Retractable System, TS = Tracker System).

The second observation that can be made is the relatively small difference between the energy yields of the bifacial modules with reflector and the bifacial modules without a reflector. Over the course of the entire monitoring period, the modules with a reflector produced only about 3% more energy. This can be mainly explained by the heavy fouling of the reflectors, which significantly lowers the rear side illumination of the bifacial modules.

The final observation concerns the error bars of the monofacial modules of the Retractable System. These bars are significantly longer than the error bars of the bifacial modules of the Retractable System or those of the reference case. A detailed explanation of this phenomenon is provided in the next section.

- **Tracker System**. The Tracker System has both the highest yielding modules and lowest yielding modules of the nine study cases. The bifacial modules, installed at a tilt angle of 15°, produced about 9% more energy than the bifacial reference case. To make a proper comparison of this system with the reference case, the internal consumption of the Tracker System should be included. From a detailed calculation in Section 5.3 it follows that this consumption is relatively low; less than 1% of the yearly energy production per module in the Tracker System.

  The effects of the tracking on the modules with different tilt angles can visually be observed in Figure 5.3. From November until March, the monofacial modules with a 15 degree tilt angle produced more energy than the bifacial module with a tilt angle of 0 degrees. This can be explained by the lower altitudes of the sun during these months, which creates more favorable conditions for modules installed at steeper tilt angles. The opposite effect can be noticed in June and July, where the monofacial modules installed at a tilt angle of zero degrees, produced a higher yield than the monofacial modules installed at 15 degrees. Considering all the results it can be concluded that when using the tracking angles calculated for this pilot project, 15 degrees is the most favorable tilt angle.

  The final remark on the performance of the Tracker System concerns the large error bars at the energy yield of the monofacial modules, installed at a zero degree tilt angle. These large error bars are mostly present from November to January. These error bars depict a large difference between the highest yielding module and the lowest yielding module. In December of 2019, the highest yielding module of this study case produced 50% more energy than the lowest yielding module. There are multiple hypotheses to explain this phenomenon. These are explored in detail in Section 5.4.

5.2. Shading by the Poles of the Retractable System

In the previous section it was established that some of the monofacial modules of the Retractable System seemed to produce significantly less energy than others. From the data it can be concluded that during the monitoring period the difference between the highest yielding module and the lowest yielding module was about 25%. The total amount of energy that is not produced, considering the highest producing module as the reference case, is about 181kWh. This is a significant amount of energy and it is therefore essential to locate the source of this energy loss and to come up with possible solutions. It is found that a major part of the losses can be contributed to the shadows that are casted on the modules by the poles of the support structure of the Retractable System. To illustrate this, Figure 5.4 shows several graphs on the next page.

The graphs in this figure show the energy yield of the modules on a day in March with clear-sky conditions. In the top-left corner of this figure, the lay-out of the six monofacial modules is shown. The black dots represent the poles of the support structure. When the sun is in the east, modules 1.1.12 and 1.1.15 are shadowed by the east pole, as can be clearly noticed in the top-right graph. When the sun is in the west, modules 1.1.24 and 1.1.16 are affected by the west pole. The modules located in the middle, 1.1.3 and 1.1.23 are only partly influenced by the shadows from both poles. Considering the losses that are caused by the poles, it could be worthwhile to investigate the feasibility of lowering them.

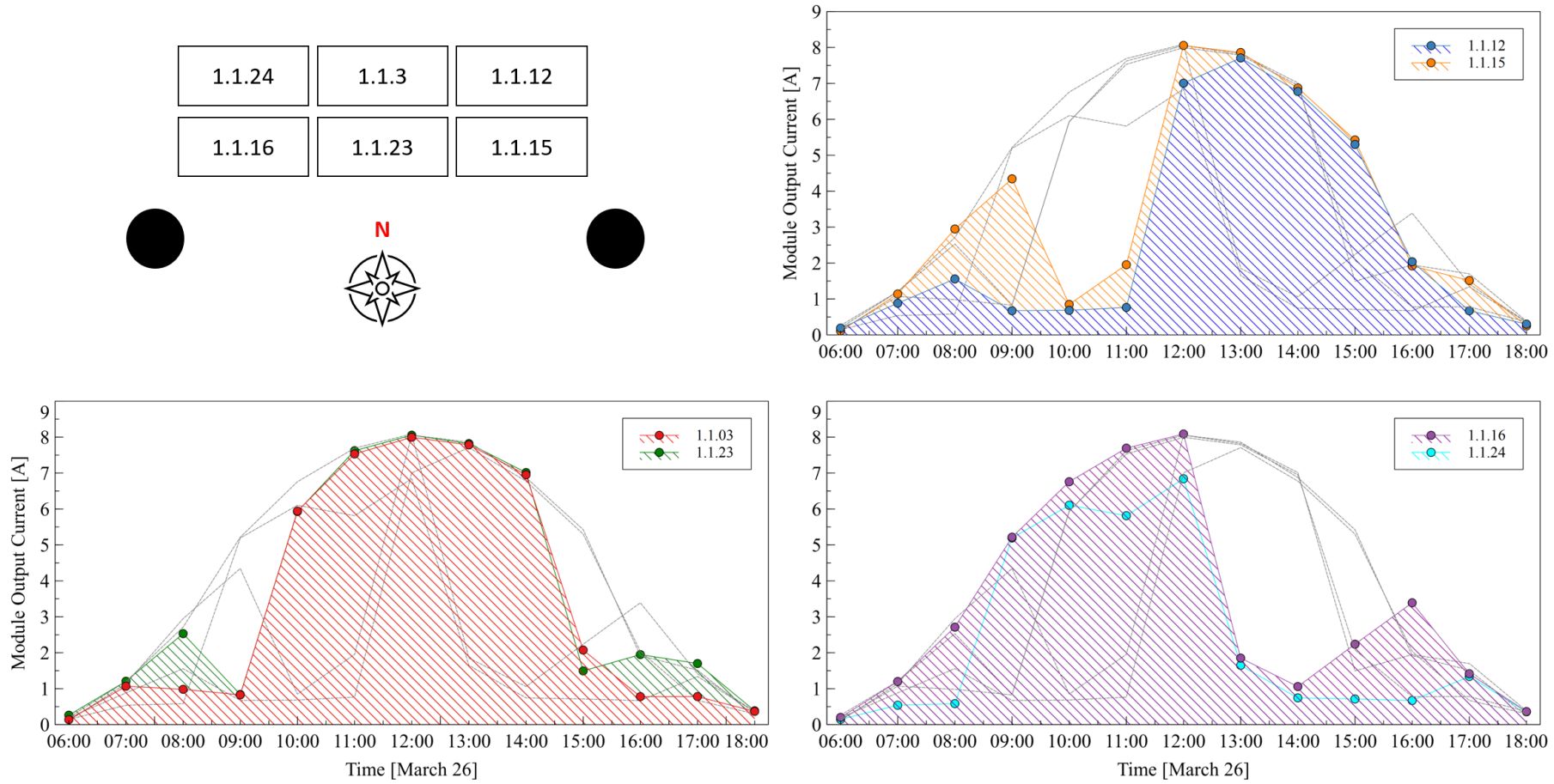

Figure 5.4: The effect of the shadow from the support structure of the Retractable System on the monofacial modules. Top left: lay-out of the six front row modules. The black dots represent the poles of the support structure that cause the shadow.

5.3. Internal Consumption of the Tracker System

The internal consumption of the Tracker System is an important parameter when analyzing the performance of the Tracker System. Therefore, the consumption is calculated in detail in this subsection.

No power consumption measurements are taken during the monitoring period. Therefore, a theoretical consumption is calculated based on the technical details of the pumps and of the tracker unit. The information that is available for this calculation is limited since the set-points of the pump are unknown, so the calculation results should be interpreted as an estimation.

The Tracker System consists of several hollow compartments on each side. Filling these compartments with water by the pumps enables the tracking capabilities of the system. The size of each compartment is about 1.3m^2 and there are 2 compartments on each side of the floating structure. The time in which the compartments need to be filled to achieve a certain tilt angle determines the capacity of the pumps. To calculate this filling time, the tracking angles of the system are used. A list of tracking angles with a resolution of 15 minutes for an entire year was created in an earlier stage by the PVMD group. These tracking angles are converted to a percentage. This percentage represents the amount of water in the compartment. A 27° eastward tilt angle means that the 'eastward compartments' are filled for 100%, while a 0° angle would mean that the both westward and eastward compartments are filled for 50%. These percentages are calculated for each of the tilt angles in eastward and westward direction. From these percentages the filling time between the different angles can be calculated, assuming one pump is available. The maximum capacity needed is 2.6 m^3/h. For subsequent calculations a capacity of 3 m^3/h is assumed. The pump head can be relatively low, so the minimum value of about 3m is selected. From the pump curves, shown in Figure 5.5, it follows that the pump needs about 50W of power to facilitate the flow and head.

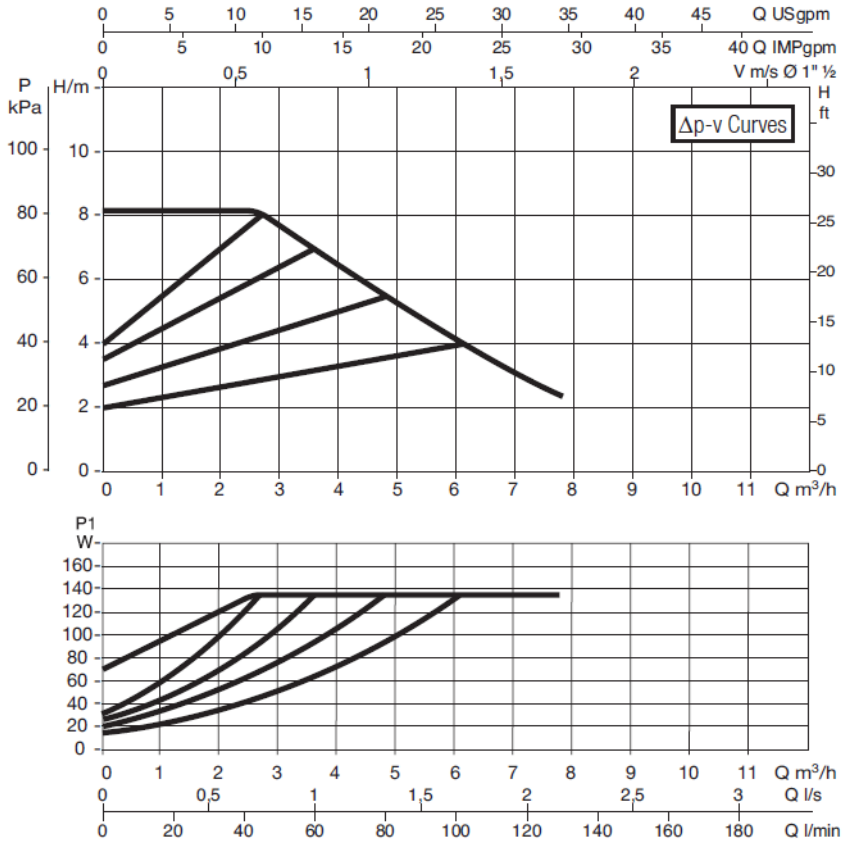

Figure 5.5: Pump curve of the DAB EVOPLUS 80/180 M. Reproduced From [56].

Multiplying the power and filling time, the energy consumption at each of the tilt angles can be

calculated. On a yearly basis this means that the pump consumes about 15817 Wh/year. However, the systems needs to tilt back from a westward position to an eastward position during the night. Assuming the night consumption to be equal as the day consumption, about 31633 Wh/ year is consumed by the pumps. Considering there are 16 modules on the Tracker System, this is about 1.97kWh/year/module. For the highest yielding modules on the Tracker System this means that the pump consumes about 0.45% of its own energy yield (assuming the energy yield of the monitoring period), while for the lowest yielding modules this percentage is about 0.7%. This number will decrease when using a full year of energy yield data, instead of the 10 month monitoring period. Detailed set-point data, such as the flow and head for every change in tilt angle could contribute to a more detailed estimation of the internal consumption of the Tracker System.

5.4. Anomalies in the Energy Yield Data of the Tracker System

In the first section of this chapter, the energy yield of each of the nine study cases was analyzed in detail. One of the findings from this analysis was the major difference between the highest and lowest yielding module of study case #9, the monofacial modules of the Tracker System, installed at a 0 degree tilt angle. From Figure 5.3 it can be concluded this discrepancy mainly presents itself during the winter months, from approximately November until February. This section aims to find the root cause of this phenomenon. Three hypotheses are explored:

1. The modules are not connected correctly, are damaged, broken, or heavily fouled.
2. The PV system is not designed properly (e.g. to many modules in a string).
3. The internal control of the system cannot handle the variety of modules in the string.

5.4.1. Hypothesis 1 - Problems with the Module

Before exploring this hypothesis in more detail, the differences between the modules of this particular system are shown. Figure 5.6 shows the energy yield of the four modules of study case #9. From this figure it can be concluded that the energy production seems to be cascading; Module 1.2.7 produces slightly more than module 1.2.11, which in turn produces slightly more than 1.2.16, etc. The order seems to be equal for all month and module 1.2.1 systematically produces the lowest yield. The biggest difference can be found in December, where module 1.2.1 produces over 50% less energy with respect to module 1.2.7.

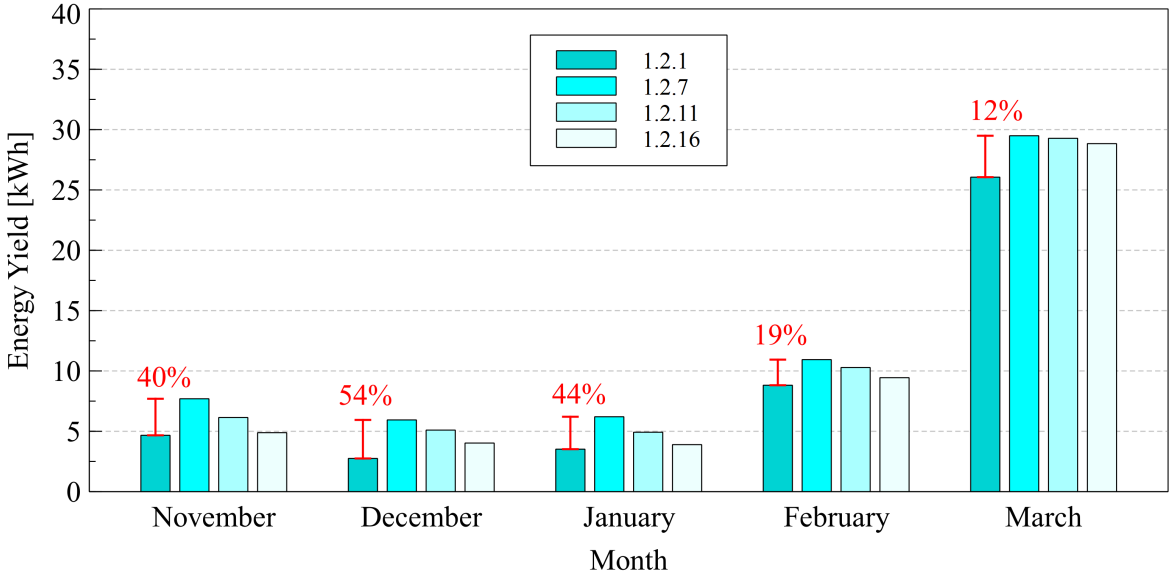

Figure 5.6: Energy yield of the monofacial modules of the Tracker System installed at a tilt angle of zero degrees and the difference between the highest and lowest yielding module.

Several problems could underlie this phenomenon. This subsection explores the possibility of the modules being broken, damaged or fouled. From the on-site inspection, conducted on the 15th of May, 2020, it followed that no significant damage was found on these modules. It was found however that the modules are slightly discolored which could explain the reduced performance of some of the modules. But since all modules were evenly discoloured, this effect would be visible for all four modules. Furthermore, given the fact the differences in energy yield are only observed in the winter months, while in the months thereafter the differences are comparable to those of the reference case, it can be concluded that damage to the modules seems highly unlikely.

A second observation from the inspection was that the modules were found to be heavily fouled by bird droppings. This fouling could explain the difference in energy yield as it would lower the module output current. However, given the amount of rainfall during the winter months it seems unlikely that the modules were heavily fouled for a period of over half a year. Furthermore, when looking at the hourly yield figures of the inspection date, only small differences in energy yield are observed.

5.4.2. Hypothesis 2 - Design Issues

The second hypothesis that is explored is the possibility of a design flaw. There are strict regulations when it comes to the design of a PV system and in particular a system which uses power optimizers. It could for example be possible that there are not enough optimizers in the string, or that the inverter is not adequately sized. This could results in the curtailment of some of the modules. In order to determine if the system is properly designed, the data sheets of the optimizer and inverter are thoroughly examined. Table 5.1 lists all important design parameters of the power optimizer.

Table 5.1: Power optimizer design specifications [57].

Nominal DC input power	505 W
Absolute maximum input voltage	83 Vdc
Maximum short circuit current	14 Adc
Maximum installed power per string	11,250 Wp
Minimum optimizers in string	14
Maximum optimizers in string	50
Parallel strings with uneven length or orientation	yes
Minimum DC power SE15K and above	11KW (total)

From these parameters it can be concluded that the output values of the modules that are connected to the optimizers are far below the limits of the optimizer. Furthermore, the maximum installed power per string, detailed in Table 5.2, is below the maximum allowed limit of 11,250Wp as well.

Table 5.2: Maximum installed string and system power based on STC values and additional bifacial conditions.

	STC	**BiFi100**	**BiFi200**
Installed power in string 1	9980 Wp	10,480 Wp	10,980 Wp
Installed power in string 2	8760 Wp	9060 Wp	9360 Wp
Total installed power	18,740 Wp	19,540 Wp	20,340 Wp

Based on the inverter design specifications from the datasheet, shown in Table 5.3, it can be concluded that the maximum DC power from the modules is within the limits of the inverter.

Table 5.3: Inverter design specification [28].

[Maximum DC power	22,950 W
Maximum DC voltage	1,000 Vdc
Nominal DC voltage	750 Vdc
Maximum DC current	23 Adc

Finally, it can be concluded that nominal input voltage of the inverter is exceeded by the maximum

voltage in both strings, shown in Table 5.4. This voltage is however regulated by the power optimizers to be at a constant value of 750V.

Table 5.4: Installed voltage based on STC values.

Installed voltage in string 1	1032.2 V
Installed voltage in string 2	902.4 V

Based on an analysis of important system design parameters such as the input voltage, current and power of the power optimizer and inverter, it can be concluded that there are no design flaws in the system. To further analyse the system design, access was requested to *Designer*, which is special SolarEdge Design software. This access was however rejected by the installer of the INNOZOWA PV pilot system.

5.4.3. Hypothesis 3 - Failing Internal Control

This subsection explores the possibility of the internal control system deliberately decreasing the energy production of some of the modules of the Tracker System. In order to understand the implications of this hypothesis, first the working principles of a SolarEdge PV system are reiterated.

The INNOZOWA system consists of two parallel strings, string 1 and string 2, which consist of 26 and 24 modules respectively. Both strings are connected to the same inverter, the SolarEdge SE17K. This inverter operates with a fixed voltage of 750V. This means that the voltage of both strings, at all times, is kept at approximately 750V by a separate feedback loop. The inverter input current is dictated by the total power production and can be calculated by dividing this power by the fixed input voltage. Each module in both strings is connected to a SolarEdge power optimizer, the P505. This power optimizer ensures the maximum power output by an input control loop. This loop dictates the input voltage and current to the power optimizer. [25]

This hypotheses states that the output of some of the modules is deliberately decreased to comply to the string voltage of 750V. The reason why this might be needed is the variety of module types in the string. This variety causes a wide range of module power outputs. Together these power outputs determine the string current. The string current is then used to determine the output voltage of each individual optimizer. For a module with a high power output, this might mean the voltage needs to be boosted in order to comply to the string current while modules with a relatively low power output need to decrease their voltage level. Since some of the optimizers work in boost mode, the fixed inverter input voltage of 750 volts is reached at an earlier stage. In other words, some of the modules need to decrease their production in order to facilitate a lower voltage contribution to the string. From this hypothesis it follows that this would not have occurred given an inverter with a higher fixed input voltage of, e.g. 850V. The reason why this might happen to the modules study case #9, is because they produce the least amount of energy in the string. The main reason this effects might occur more frequently in the winter months is that the differences in module output current seem larger during these months. This leads to more instances where the voltages are boosted.

Paradoxically, if the operating point of the modules is not set at a lower level, more power would be available at the inverter which in turn would increase the string current. An increased string current would result in a lower optimizer output voltage across the entire string, which would enable the front row modules to maintain their energy production (or at least at a higher level).

The Dutch SolarEdge support team was asked for help on this matter, but there was no response from their side. To resolve this issues, the problem might need to be escalated to the technical team of SolarEdge as they would probably know in some more detail why this phenomenon occurs. Furthermore, it would be interesting to see if this phenomenon occurs in the same capacity in the coming winter months. Finally, the modules could be analyzed in more detail after the pilot project, using for example electroluminescence, to see if damage to the modules can be completely excluded.

5.5. Evaluation of the Irradiance Sensor Measurements

The reflectors installed at several of the bifacial modules of the INNOZOWA PV system are an important asset for these modules. To research the effects of these reflectors, several irradiance sensors are installed at the INNOZOWA pilot site. One sensor is installed on top of the container of the inverter, a second is installed below the battery box of the Retractable system (facing the water), and a third sensor is installed on the backside of one of the bifacial modules of the Retractable System. The first and the second sensor can be used to calculate the albedo of the water, while the third sensor can be used to evaluate the reflectance of the reflector. The aim of this subsection is to evaluate the albedo and reflectance measurements of these sensors and to analyse their performance in the INNOZOWA system. Figure 5.7 shows the average hourly albedo of the water in the top graph and the average hourly reflectance of the reflector in the bottom graph.

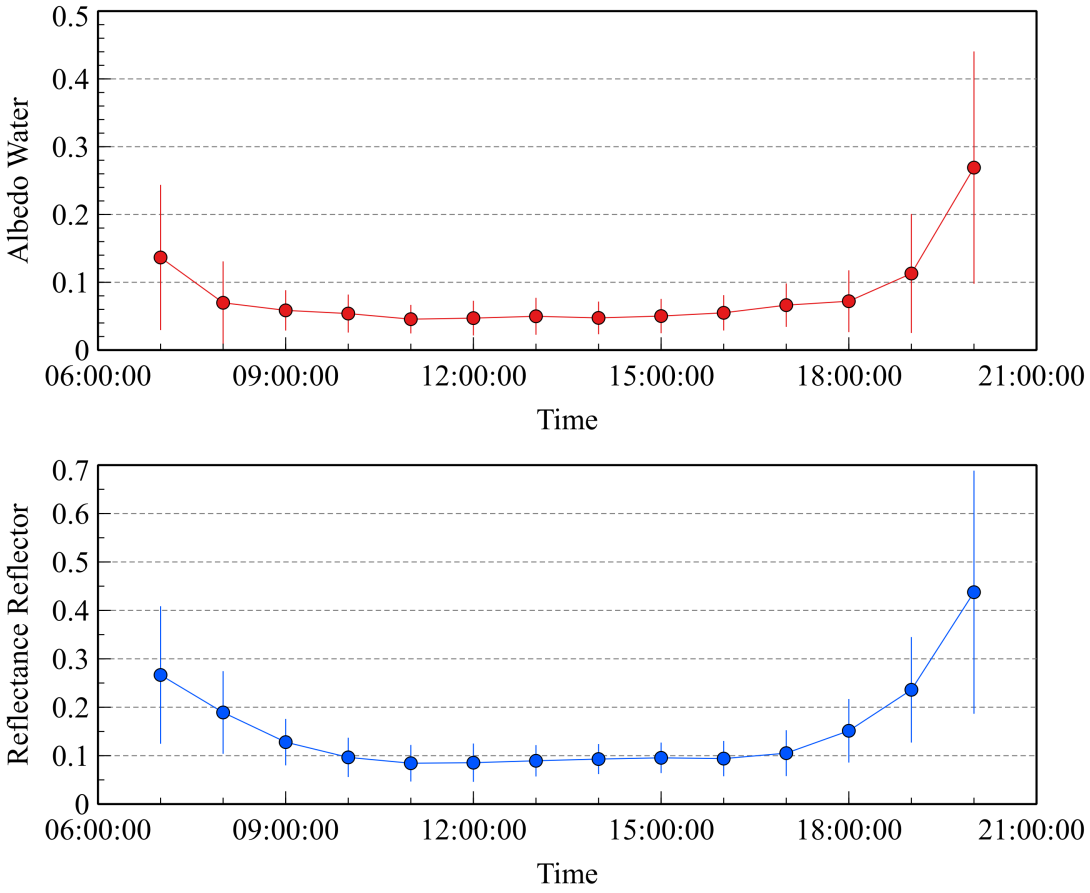

Figure 5.7: Average hourly albedo of the water at the INNOZOWA site and the average hourly reflectance of the reflector installed at one of the bifacial modules of the Tracker System.

The graphs show the average hourly albedo and reflectance for a period of about 80 days. Furthermore, the standard deviation is plotted to show the spread of the values. The albedo value of the water is on average about 0.05 during the day. Both the value and the spread of the albedo increase during the early morning and late evening. An albedo value of 0.05 is relatively low as this would mean that only 5% of the incident light is reflected back to a bifacial module in the case no reflector is present. This partly explains the difference in energy yield between the bifacial modules of the Retractable System without reflector installed and the bifacial reference case.

The reflectance of the reflector is about 0.095 throughout the monitoring period. Again, the value and spread increase during early morning and late evening. A reflectance of 0.095 means that about 10% of the incoming light is reflected during the day time. From the LG datasheet of the bifacial module it follows that a contribution of about 10% means a 25W increase in maximum power when STC values

are considered [34]. It should be noted however that during the on-site inspection of the INNOZOWA PV pilot system, the two reflectors of the Retractable System were heavily fouled. This significantly influences the reflectance of these reflectors.

5.6. Effects of Storms on the INNOZOWA PV System

Floating structures are prone to wind and waves resulting from this wind. These natural phenomena could cause the structure to move out of place which can significantly affect the power output of the system and in a worse-case scenario it could damage the system. It is therefore important to investigate the effects of wind and gusts on the floating structures of INNOZOWA. An opportunity to carry out such a research presented itself in February 2020. During this month two European winter storms passed over the country: storm Ciara and storm Dennis. In this section, first the characteristics of these storms are specified and second the effects of these storm are briefly described.

On Sunday 9 February the storm named Ciara passed over the Netherlands. Interpolated hourly average wind speed values show wind speeds of 40 to 50 km/h from 10:00 until 24:00. The highest gust measured at the two closest KNMI measurement points 'Deelen' and 'Volkel' was 86.4 km/h and 97.2 km/h respectively [49]. Based on historical KNMI data, the system had not experienced these kind of wind speeds and gusts before during the pilot. Approximately a week later, on the 16th of February, storm Dennis passed over the country. Again, high wind speeds and gusts were measured. See Figure 5.8 for a comparison of the on-site wind speed during both storm days.

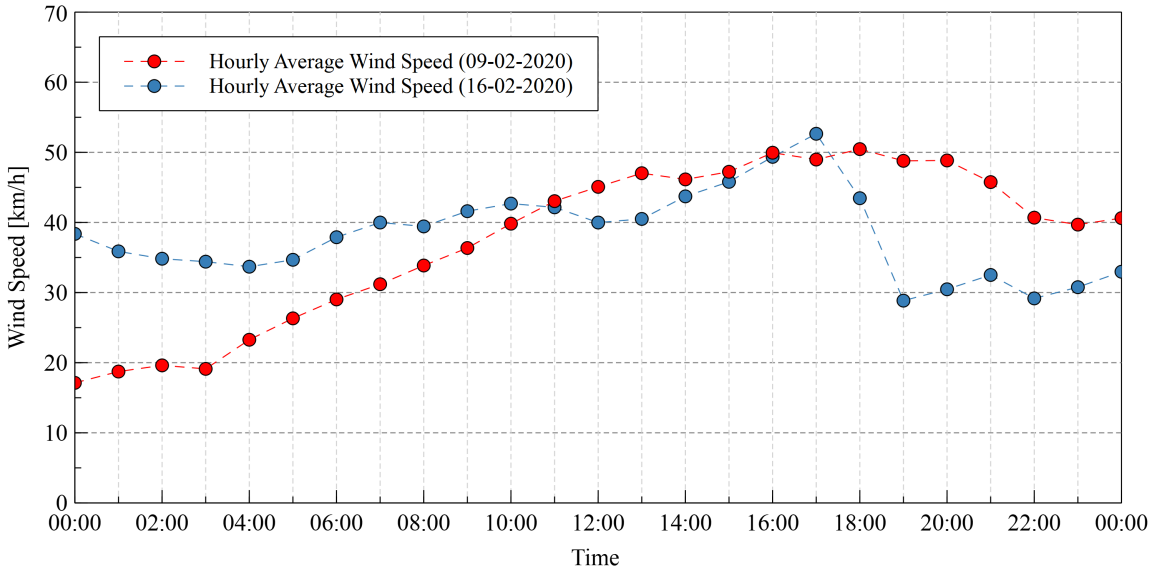

Figure 5.8: KNMI interpolated hourly average wind speeds on the 9th and 16th of February 2020 [40].

To check if any damage was inflicted on the system by the two storms, two steps were taken. First, an on-site inspection was conducted to check if the systems were still in place and if any damage to the system could be visually observed. The conclusion from this inspection was that all modules were still in place and that no damage was visually detected. The second step was to check the energy production of each module individually, to see if the power output of one of the modules significantly decreased compared to the output before the storm. Again, the observations made showed no damage caused by the storms. Not all floating systems in the surrounding area survived the storms however. A floating PV park only 10km away from the INNOZOWA pilot site was severely damaged by storm Dennis [58].

5.7. Chapter Conclusions

Throughout a period of over 10 months, multiple key performance indicators of the INNOZOWA system were sharply monitored. The goal of this monitoring was to check for any anomalies or particularities and to determine some of the important parameters such as the internal consumption of the Tracking System and the water albedo.

From the analysis of the energy yield of the modules it can be concluded that the bifacial modules outperform the monofacial modules based on performance per installed capacity. Furthermore, it can be concluded that the bifacial modules of the Tracker System, installed at a tilt angle of 15 degrees, outperform the ground-based reference case by about 9%. Furthermore, it should be noted that the influence of the reflector seems relatively low, based on the difference between the bifacial modules of the Retractable System. Finally, it can be concluded that the increase in module efficiency due to placing the modules on water is negligible in the case of INNOZOWA. This effect is widely described in literature [6] [7] but could not be validated in this research.

The internal consumption of the pump was calculated. The total consumption is estimated to be around 31633 Wh/year, which is less than 1% of the total yearly energy production per module of the Tracker System. This calculation is based on several estimations and assumptions. The INNOZOWA project team was asked to provide more detailed information about the pump operating schedule (set-points of head and flow at certain time stamps), but was unable to do so in time. When this information is available, a detailed calculation should be made.

Three hypothesis were explored regarding the lower energy yield of several of the modules of the Tracker System. It can be concluded that it is unlikely that the modules are damaged or broken, or heavily affected by fouling. Furthermore, it can be concluded that the system is designed according to the SolarEdge specified regulations and standards. The final hypothesis, which states that the module output of some modules is deliberately decreased to comply to the fixed inverter input voltage, seems at this moment the most plausible. Further research and consultation with the SolarEdge technical team could provide more insight.

The albedo of the water was analyzed for a period of over two months. It can be concluded that this value is on average about 0.05 during the most relevant operating hours. This supports the claim that a relatively small percentage of light is reflected from the water and a reflector is needed for floating bifacial modules. The relfectance of such a reflector was monitored as well. Although the reflector was heavily fouled for most of the monitoring period, the reflectance was found to be about 0.095 during day hours. This translates to a 25W gain for the bifacial modules of the INNOZOWA PV pilot project if STC values are considered.

Finally, the effects of storms were monitored during two major Europeans winter storms: storm Ciara and storm Dennis. It was found, through visual observation and yield monitoring, that no damage was inflicted by these storms. This gives the INNOZOWA system an edge over 'traditional' floating systems which are more prone to storms.

5.8. Chapter Recommendations

- If the project team decides to carry on with this selection of module types and set-ups, it is recommended to select the bifacial modules installed at a tilt angle of 15 degrees for the Tracker System and the bifacial modules with reflector for the Retractable System as these produced the most energy in their respective system. It should be noted however that this analysis is based on a ten month period and that the results can slightly change after the remaining two months of monitoring.

- It was found that due to the poles of the support structure of the Retractable Systems, about 181kWh was lost during the 10 month monitoring period. This is a significant amount of energy. Further research could examine the feasibility of lowering these poles.

- The additional gain by adding reflectors is relatively low (3%), as can concluded from the energy yield of the bifacial modules of the Retractable System. The two most likely reasons for this relatively low gain are the fouling of the reflectors and its relatively small size compared to the size of the panel. It is recommended to increase the size of the reflector and to keep the reflector clean from bird droppings. Relevant recommendations on the control of birds were provided in the previous chapter.
- It is recommended to calculate the consumption of the pump is more detail. The current calculations is based on several assumptions. If the set-points of the flow and head are provided by Hakkers, a detailed calculation can be made.

6

Conclusions and Recommendations

Each of the main chapters of this thesis report closed with chapter specific conclusions and recommendations. In this chapter of the report the chapter conclusions and recommendations are summarised and an overarching conclusion is presented based on the main question and secondary questions presented in the Introduction. Finally, the most important recommendations of this report are provided

6.1. Conclusions

Floating photovoltaics is a relatively new technique of generating a sustainable form of electricity using solar PV on bodies of water. The technique has several advantages over conventional ground and roof-based systems. There are still several challenges left for floating PV but its potential seems immense. To accelerate the development of floating PV, several projects are initiated throughout the Netherlands. One of these projects is called INNOZOWA (innovative sun on water). This projects aims to accelerate the development of floating PV on bodies of inland water. The INNOZOWA project provides an opportunity to test the current version of the PVMD modeling toolbox in detail. This toolbox is developed to make detailed energy yield simulations of PV modules. Considering the opportunities that the INNOZOWA pilot project provides for improving the PVMD modeling toolbox and the knowledge that can be gained about floating PV systems in general, this master thesis project was initiated. The main question that this research aimed to answer is:

How does the energy production of the INNOZOWA PV Pilot system compare to energy yield simulations made with an improved version of the PVMD modeling toolbox?

To answer this main question, seven secondary questions were answered throughout this report:

1. *How to model the efficiency of a power optimizer and include it as an input model in the new Power Conversion script of the PVMD modeling toolbox?*

   A power Conversion tool is developed for the PVMD modeling toolbox. This tool is capable of simulating the efficiency of power optimizers, inverters and cable sections. The tool consists of 17 independent script files containing over 800 lines of code. It is fully integrated in the current version of the PVMD modeling toolbox. The tool is easily expandable thanks to the included Excel templates. In this tool, the efficiency of power optimizers is calculated based on the efficiency curves specified by the optimizer manufacturers.

   Two important steps in the development of such a tool are validation and documentation. A comprehensive manual is created to support the user in operating the tool. Furthermore, the Power Conversion tool was thoroughly tested and validated using INNOZOWA input data for days with different weather conditions. Since no input *and* output data was available for both the optimizers and the inverter, the overall system efficiency was validated. The simulation results of the overall system efficiency showed reasonable and predictable values. However, the efficiency

calculated from measured data proved to be insufficiently detailed to make a comprehensive comparison with the simulated efficiency. Detailed data is needed to make a proper validation of the Power Conversion tool.

2. *Which components are needed to build a functional and convenient power conversion tool for the PVMD modeling toolbox, how are these components modeled, and how can they be included in the PVMD modeling toolbox?*

   After consultation with several stakeholders it was decided to include a model for inverters as well as for cables to the new Power Conversion script of the PVMD modeling toolbox. The inverter efficiency is calculated by the widely used SNL performance model for inverters [30]. An input-model for cable losses is added as well to account for the heat that is dissipated in the wiring of the system. The user can select a fixed loss percentage or make a detailed cable calculation based cable characteristics. Furthermore, the tool has several build-in warnings and checks to prevent the user from putting in wrong data.

3. *Which parameters should be used to accurately simulate the energy yield of the INNOZOWA PV Pilot system in the PVMD modeling toolbox?*

   Energy yield simulations were made based on module data-sheet specifications and several meteorological data-sets. Initial simulations showed significant deviations with measured data. To mitigate this issue the albedo value of the reflectors of the bifacial modules was recalculated and a new thermal model was applied. Simulations based on-site irradiance data with a resolution of 15 minutes yielded the most accurate results. The percentual difference between measured and simulated values was found to be ±10% on monthly as well as on daily basis. No clear correlation could be found between hourly meteorological parameters and the percentual difference between simulated values and measured values. There are still multiple uncertainties that underlie the simulations. The accuracy of the monitoring tool and the irradiance sensors, fouling of the modules, and uncertainties on the model side are expected to have the most significant contribution to the percentual difference between measured and simulated energy yields.

4. *Which parts of the PVMD modeling toolbox can be improved based on the experience of simulating the INNOZOWA PV pilot system?*

   The simulation process yielded several recommendations for improvement on the toolbox. These recommendations are divided into general comments and comments on specific scripts. A comprehensive list can be found in the next section.

5. *Are there any defects or deviations present in the system that could contribute to model and data uncertainties and how can these defects or deviations be found during an on-site inspection?*

   An on-site inspection of the INNOZOWA PV pilot system and modules was conducted on May 15, 2020. This inspection was aided by an NREL questionnaire and thermographic imaging. The main findings of this inspection were: heavy fouling of the monofacial modules of the Tracker System, heavy fouling of the reflectors of the Retractable System, and significant deviations in module tilt angle and azimuth of the Ground-based System. No significant damage was found on any of the modules or system components. The results from this inspection were used as inputs for the energy yield simulations. Furthermore, the inspection provided context for the analysis of the monitored energy yield data.

6. *Based on a thorough data analysis of the different subsystems, are there any anomalies in the data and where do these anomalies come from?*

   Through a meticulous data analysis, major anomalies were found in the energy yield data of the monofacial modules of the Retractable and of the monofacial modules of the Tracker System, installed at a tilt angle of 0°. In the first case, these anomalies resulted from the shadows that are casted by the supporting poles of the Retractable System, resulting in an energy loss of 181kWh throughout the monitoring period. In the second case the anomalies arised from a yet unknown source. Three hypotheses were explored to explain this phenomenon. Damaged modules or soiling seem unlikely as the root cause of the problem. Although paradoxical, it seems that the internal control of the power optimizers deliberately decreases the output of some of the modules to comply to the fixed string voltage.

7. *How can the INNOZOWA PV pilot subsystems potentially be improved and which subsystem is the most likely to be used for subsequent projects and/or up scaling?*

   To answer this question, the energy yield of each of the nine study cases of INNOZOWA was monitored for a period of ten months (October 2019 - July 2020). From the monitored values it can be concluded that only the bifacial modules of the Tracker System outperform the bifacial ground-based reference case. An important parameter to consider in this comparison is the internal consumption of the Tracker system. This consumption was calculated based on several assumptions and was found to be less than 1% of the average yearly energy yield per module in the Tracker System. Furthermore, it can be concluded that a module tilt angle of 15 degrees is the most favorable tilt angle when considering the floater tilt angles that are currently programmed.

   Several features of the floating systems can be improved based on the findings from this report. The main improvement concerns the reflectors of the Retractable System. Energy yield analysis of the INNOZOWA systems showed that the difference between the bifacial modules with and without reflector is only about 3%. The main reason for this relatively small difference could be the heavy fouling of the reflectors, which results is a lower albedo. Furthermore, from the view factor calculations in Chapter 3 it can be concluded that the albedo resulting from this reflector is significantly lower than the albedo of the reflectors of the other two systems, which is mainly due to the reflector size. If the size of the reflector is increased and its surface is kept clean, the rear side contribution of the bifacial modules is expected to increase. Finally, it was found through analysis of the albedo of the water that a reflector is essential for the operation of bifacial modules on water as the albedo of the water is very low (0.05) during daylight hours.

6.2. Recommendations

The work from this thesis report yielded several recommendations. In this section the major recommendations on the PVMD Modeling Toolbox and the INNOZOWA system are provided.

Recommendations on the PVMD Modeling Toolbox

- If the development of the new Power Conversion tool is continued, it is recommended to add several additional features, such as: loss factors for common losses in PV systems, separate databases for the different inverter types, and an automatic cable sizing tool.
- It is recommended to create documentation (like the manual created for the Power Conversion tool) for the PVMD modeling toolbox, to improve usability for new users. Other general recommendations include: refactoring (old) code and the creation of an overall development plan for the toolbox.
- The current version of the toolbox has no way of simulating the tracking capabilities of a PV system. It is recommended to research the feasibility of such an implementation. One of the main goals of the development this tracking script would be keep the simulation time as short as possible.
- Other recommendations on specific parts of the toolbox include: addition of other module types to the toolbox (different orientation or including a reflector), including the ability to simulate objects in the surround area (like the poles from the support structure of the Retractable System), implementation of altitude and azimuth calculations to improve the workflow of the tool, and the addition of the ability to process irradiance data with irregular time intervals. A full list of recommendation is found in Section 3.7 of Chapter 3.

Recommendations on the INNOZOWA System

- If the INNOZOWA project team decides to progress with the development of the Retractable System it is recommended to increase the size of the reflectors (if the design allows). Furthermore it is recommended to investigate the feasibility of lowering the two front poles of the support structure as they cast shadows on the front row panel, resulting in a significant energy loss.

- If the INNOZOWA project team decides to progress with the development of the Tracker System it is recommended to select the bifacial modules with a tilt angle of 15 degrees as this system has the highest overall energy yield based on the ten month monitoring period. Furthermore, it is recommended to calculate the pump consumption in more detail as the current calculation is based on several assumptions.
- It is recommended to implement more rigorous measures against the birds that heavily soil the reflectors and modules of the INNOZOWA PV pilot system. Several industry proven techniques are available on the market.

Bibliography

[1] International Renewable Energy Agency (IRENA), “Renewable Capacity Highlights,” Tech. Rep., March 2019. [Online]. Available: www.irena.org/publications.

[2] United Nations, “Summary of the Paris Agreement,” December 2015. [Online]. Available: https://treaties.un.org/pages/ViewDetails.aspx?src=TREATY&mtdsg_no=XXVII-7-d&chapter=27&clang=_en

[3] A. Sahu, N. Yadav, and K. Sudhakar, “Floating photovoltaic power plant: A review,” *Renewable and Sustainable Energy Reviews*, vol. 66, pp. 815–824, 2016.

[4] International Renewable Energy Agency (IRENA). Trends in Renewable Energy. [Online]. Available: http://resourceirena.irena.org/gateway/ (Accessed: Jan 2020).

[5] E. Skoplaki and J. A. Palyvos, “On the temperature dependence of photovoltaic module electrical performance: A review of efficiency/power correlations,” *Solar Energy*, vol. 83, no. 5, pp. 614–624, 2009.

[6] L. Liu, Q. Wang, H. Lin, H. Li, Q. Sun, and R. Wennersten, “Power Generation Efficiency and Prospects of Floating Photovoltaic Systems,” *Energy Procedia*, vol. 105, pp. 1136–1142, 2017.

[7] Y. K. Choi, W. S. Choi, and J. H. Lee, “Empirical research on the efficiency of floating PV systems,” *Science of Advanced Materials*, vol. 8, no. 3, pp. 681–685, 2016.

[8] World Bank Group, ESMAP and SERIS, “Where sun meets water: Floating solar market report—executive summary.” Tech. Rep., 2018. [Online]. Available: http://elibrary.worldbank.org/doi/book/10.1596/32804

[9] R. E. Cabanillas and H. Munguía, “Dust accumulation effect on efficiency of Si photovoltaic modules,” *Journal of Renewable and Sustainable Energy*, vol. 3, no. 4, pp. 1–10, 2011.

[10] W. Folkerts, W. van Sark, C. de Keizer, W. van Hooff, and M. van den Donker, “ROADMAP PV Systemen en Toepassingen,” Rijksdienst voor Ondernemend Nederland (RVO) in collebaration with TKI Urban Energy, Tech. Rep., December 2017. [Online]. Available: https://www.uu.nl/sites/default/files/roadmap-pv-systemen-en-toepassingen-final.pdf

[11] S. D. Loos and R. D. Wortelboer, “Handreiking voor vergunningverlening drijvende zonneparken op water,” Stichting Toegepast Onderzoek Waterbeheer, Amersfoort, Tech. Rep., 2018.

[12] Wood Mackenzie Power & Renewables. (September) Floating solar landscape 2019. [Online]. Available: https://www.woodmac.com/our-expertise/focus/Power--Renewables/floating-solar-2019/ (Accessed: Nov 2019).

[13] T. Kenning. (2017, November) Masdar and Indonesian power giant to build world’s largest floating solar plant. [Online]. Available: https://www.pv-tech.org/news/masdar-and-indonesian-power-giant-to-build-worlds-largest-floating-solar-pl (Accessed: Nov 2019).

[14] A. Lee. (2019, September) India plans world’s largest floating solar power plant at 1GW. [Online]. Available: https://www.rechargenews.com/transition/india-plans-worlds-largest-floating-solar-power-plant-at-1gw/2-1-690729 (Accessed: Nov 2019).

[15] Nationaal Consortium Zon op Water. Zon op Water. [Online]. Available: https://zonopwater.nl/ (Accessed: Nov 2019).

[16] S. Booth, “International Applications for Floating Solar Photovoltaics,” National Renewable Energy Laboratory (NREL), Golden, CO, Tech. Rep., 2019. [Online]. Available: https://www.osti.gov/biblio/1526906

[17] Waterschap Rivierenland, “Model projectplan Hernieuwbare energie 2016,” Tech. Rep., March 2017.

[18] ——. Werkgebied. [Online]. Available: https://www.waterschaprivierenland.nl/ (Accessed: May 2020).

[19] E. G. Goma, “Development of Cell to System Annual Energy Yield Toolbox for Bifacial Modules,” 2018, MSc. thesis, Photovoltaic Materials and Devices Group, TU Delft. [Online]. Available: http://resolver.tudelft.nl/uuid:255ac731-b59b-453a-b899-1ff5dec1add2

[20] J. Garro Etxebarria, “Toolbox for the design and simulation of a floating bifacial PV plant with reflectors,” 2018, MSc. thesis, Photovoltaic Materials and Devices Group, TU Delft. [Online]. Available: http://resolver.tudelft.nl/uuid:a86fd44c-379c-48f8-a737-2c0b01086384

[21] I. N. Alavez, “Monitoring of bifacial floating PV systems and validation of a toolbox for its simulation.” 2019, MSc. thesis, Photovoltaic Materials and Devices Group, TU Delft. [Online]. Available: http://resolver.tudelft.nl/uuid:0bec1518-193d-420c-924e-b21742759800

[22] Google. (2020) RWZI Weurt. [Online]. Available: https://www.google.com/maps (Accessed: May 2020).

[23] A. Smets, K. Jäger, O. Isabella, R. van Swaaij, and M. Zeman, *Solar Energy. The physics and engineering of photovoltaic conversion technologies and systems*. Cambridge, England: UIT Cambridge Ltd, 2016.

[24] L. Hernández-Callejo, S. Gallardo-Saavedra, A. Diez-Cercadillo, and V. Alonso-Gómez, “Analysis of the influence of DC optimizers on photovoltaic production,” *Revista Facultad de Ingenieria*, no. 94, pp. 43–55, 2020.

[25] John Berdner, “Technical White Paper SolarEdge System Design and the National Electrical Code,” SolarEdge Technologies, Inc., Tech. Rep. April, 2011. [Online]. Available: https://www.solaredge.com/sites/default/files/solaredge-system-design-nec.pdf

[26] SolarEdge, “Het rendement van de power optimizers uit de P-serie,” SolarEdge, Tech. Rep., 2018. [Online]. Available: https://www.solaredge.com/nl/downloads{#}/

[27] A. Rohatgi. (2019) WebPlotDigitizer, Version: 4.3. [Online]. Available: https://automeris.io/WebPlotDigitizer (Accessed: Dec 2019).

[28] SolarEdge, “3-fase omvormer SE12.5K - SE27.6K,” Tech. Rep., 2019. [Online]. Available: https://www.solaredge.com/nl/downloads{#}/

[29] SolarEdge, “Application Note SolarEdge String Sizing, EU Regulations,” Tech. Rep. [Online]. Available: https://www.solaredge.com/nl/downloads{#}/

[30] D. L. King, S. Gonzalez, G. M. Galbraith, and W. E. Boyson, “Performance Model for Grid-Connected Photovoltaic Inverters,” Sandia National Laboratories, Tech. Rep. September, 2007. [Online]. Available: https://energy.sandia.gov/

[31] PV Performance Modeling Collaborative. PV_LIB Toolbox. [Online]. Available: https://pvpmc.sandia.gov/applications/pv_lib-toolbox/

[32] H. Ziar, S. Farhangi, and B. Asaei, “Modification to wiring and protection standards of photovoltaic systems,” *IEEE Journal of Photovoltaics*, vol. 4, no. 6, pp. 1603–1609, 2014.

[33] LG, “LG Neon 2 Black.” [Online]. Available: https://www.lg.com/nl/business/solar-download

[34] ——, “LG Neon 2 Bifacial.” [Online]. Available: https://www.lg.com/nl/business/solar-download

[35] H. Ziar, E. G. Goma, F. Sonmez, J. G. Etxebarria, O. Isabella, and M. Zeman, “Albedo in Practice - Spectral and geometrical dependency of albedo,” Bussum, November 2019.

[36] SolarEdge, “Klimaatsensoren - Datasheet,” Tech. Rep. [Online]. Available: https://www.solaredge.com/nl/products/metering-and-sensors/environmental-sensors{#}/

[37] Photovoltaic Photovoltaic Materials and Devices (PVMD) group. The Dutch PV Portal. [Online]. Available: https://pvportal-2.ewi.tudelft.nl/ (Accessed: Feb 2020).

[38] S. Mishra, H. Ziar, O. Isabella, and M. Zeman, “Selection Map for PV Module Installation Based on Shading Tolerability and Temperature Coefficient,” *IEEE Journal of Photovoltaics*, vol. 9, no. 3, pp. 872–880, May 2019.

[39] H. Ziar, O. Isabella, E. G. Goma, F. Sonmez, J. Garro, and M. Zeman, “INNOZOWA - Report on WPs 2.1, 2.2, and 2.3. Horicatching, Albedo Measurements, and Estimation of PV Potential at Test Site Located in Weurt,” Tech. Rep., 2018.

[40] Koninklijk Nederlands Meteorologisch Instituut. ”uurgegevens van het weer in nederland”. [Online]. Available: https://projects.knmi.nl/klimatologie/uurgegevens/selectie.cgi

[41] B. Ridley, J. Boland, and P. Lauret, “Modelling of diffuse solar fraction with multiple predictors,” *Renewable Energy*, vol. 35, no. 2, pp. 478–483, 2010.

[42] D. John A and W. A. Beckman, *Solar Engineering of Thermal Processes Solar Engineering*, 4th ed., John Wiley & Sons Inc, Ed., Hoboken, New Jersey, 2013.

[43] F. P. Incropera, D. P. Dewitt, T. L. Bergman, and A. S. Lavine, *Fundementals of Heat and Mass Transfer*, 6th ed. Hoboken, NJ: John Wiley & Sons, Inc, 2015.

[44] M. Brennan, A. Abramase, R. Andrews, and J. Pearce, “Effects of spectral albedo on solar photovoltaic devices,” *Solar Energy Materials and Solar Cells*, vol. 124, pp. 111 – 116, 2014.

[45] U. Gross, K. Spindler, and E. Hahne, “Shapefactor-equations for radiation heat transfer between plane rectangular surfaces of arbitrary position and size with parallel boundaries,” *Letters in Heat and Mass Transfer*, vol. 8, pp. 219 – 227, 1981.

[46] Koninklijk Nederlands Meteorologisch Instituut. Seizoensextremen lente - Extremen KNMI-station De Bilt vanaf 1901. [Online]. Available: https://www.knmi.nl/nederland-nu/klimatologie/lijsten/seizoensextremen/lente (Accessed: Jun 2020).

[47] ——. December 2019. [Online]. Available: https://www.knmi.nl/nederland-nu/klimatologie/maand-en-seizoensoverzichten/2019/december (Accessed: Jun 2020).

[48] A. N. E. Din, “Improved Electrical Model and Experimental Validation of the PVMD Toolbox,” MSc. thesis, Photovoltaic Materials and Devices Group, TU Delft. [Online]. Available: http://resolver.tudelft.nl/uuid:0cc6ae16-9501-419b-b70a-7a7987c38350

[49] koninklijke nederlandse meteorologisch instituut (KNMI). ”daggegevens van het weer in nederland”. Accessed Feb 2020. [Online]. Available: http://projects.knmi.nl/klimatologie/daggegevens/selectie.cgi

[50] E. Roumpakias, F. Bouroutzikas, and A. Stamatelos, “On-site Inspection of PV Panels, Aided by Infrared Thermography,” *Advances in Applied Sciences*, vol. 1, no. 3, pp. 53–62, 2016.

[51] C. E. Packard, J. H. Wohlgemuth, and S. R. Kurtz, “Development of a Visual Inspection Data Collection Tool for Evaluation of Fielded PV Module Condition,” Tech. Rep. August, 2012. [Online]. Available: https://www.nrel.gov/docs/fy12osti/56154.pdf

[52] J. A. Tsanakas and P. N. Botsaris, “An infrared thermographic approach as a hot-spot detection tool for photovoltaic modules using image histogram and line profile analysis,” *International Journal of Condition Monitoring*, vol. 2, no. 1, pp. 22–30, March 2012.

[53] P. B. Quater, F. Grimaccia, S. Leva, S. Member, M. Mussetta, M. Aghaei, and S. Member, “Light Unmanned Aerial Vehicles (UAVs) for Cooperative Inspection of PV Plants,” *IEEE Journal of Photovoltaics*, vol. 4, no. 4, pp. 1107–1113, July 2014.

[54] Testo, “Practical guide Solar Panel Thermography,” Testo, Sparta, NJ 07871, Tech. Rep. [Online]. Available: http://www.murcal.com/pdf%20folder/15.testo_thermography_guide.pdf

[55] [Online]. Available: https://www.birdcontrolgroup.com/nl/ (Accessed: Jul 2020).

[56] DAB Water Technology, “EVOPLUS SMALL/EVOPLUS SMALL SAN - WET ROTOR ELECTRONIC CIRCULATORS,” Tech. Rep. [Online]. Available: https://www.dabpumps.nl/nl/node/1260

[57] SolarEdge, “Power Optimizer P300 / P370 / P404 / P405 / P485 / P500 / P505,” Tech. Rep. [Online]. Available: https://www.solaredge.com/nl/downloads{#}/

[58] E. van Gastel and E. Stultiens. [Online]. Available: https://bit.ly/31YLGhf (Accessed: Feb 2020).

A

Appendix - Article in Progress in Photovoltaics

This Appendix contains the paper *Innovative Floating Bifacial Photovoltaic Solutions for Inland Water Areas*, which contains all research conducted for the INNOZOWA PV pilot project. This paper has been selected by the *European PV Solar Energy Conference and Exhibition* for possible publication in the journal *Progress in Photovoltaics*. The paper is currently under review and is expected to be published later this year. This master thesis project mainly contributed results from Chapter 4 (Inspection) and Chapter 5 (Monitoring).

Innovative Floating Bifacial Photovoltaic Solutions for Inland Water Areas

Hesan Ziar *[1], Bjorn Prudon [2], Vicky Lin [3], Bart Roeffen [3], Dennis Heijkoop [4], Tim Stark [1], Elias Garcia Goma [1], Julen Garro Extebarria [1], Ignacio Narvaez Alavez [1], Daniel van Tilborg [4], Hein van Laar [4], Rudi Santbergen [1], and Olindo Isabella [1]

***Abstract*— Photovoltaic (PV) technology has the potential to be integrated on many surfaces in various environments, even on water. Modelling, design, and realization of a floating PV system have more challenges than conventional rooftop or free-standing PV system. In this work, we introduce two innovative concepts for floating bifacial PV systems, describing their modelling, design, and performance monitoring. The developed concepts are retractable and enable maximum energy production through tracking the Sun. Various floating PV systems (mono-facial, bifacial with and without reflectors) with different tilts and tracking capabilities are installed on a Dutch pond and are being monitored. Results of the thermal study showed that partially soaking the frame of PV modules into water does not bring a considerable additional yield (+0.17%) and revealed that floating PV modules experience higher temperature special variance compared to land-based systems. Observations showed that the birds' presence has a severe effect on floating PV performance in the short-term. Electrical yield investigation concluded that due to low albedo of inland water areas (~11%), bifacial PV systems must have reflectors. 8-month monitoring showed that a bifacial PV system with reflector and horizontal tracking delivers ~14% more specific yield (up to 29% in a clear-sky month) compared to a mono-facial PV system installed on land.**

Index Terms*— *Photovoltaic (PV) module, PV system, Floating PV (FPV), Tracker, Bifacial PV, Island, Retractable, Partial water soaking, Modeling, Realization, Monitoring, Onshore.

1. Introduction

Bifacial photovoltaic (PV) technology (cells and modules) can absorb light simultaneously from the front and rear sides [1]. This feature brings important advantages concerning mono-facial PV technology: (1) lower land-use for the same Wp installation; (2) lower levelized cost of electricity (LCOE), and (3) smoother daily power profile. Having such advantages and lowering the manufacturing cost have increased the bifacial PV installation rapidly from 97 MWp in 2016 to over 5 GWp in 2019 [2]. The market share of bifacial technology is expected to grow from ~15% in 2019 to ~70% by 2030 [3].

On the other hand, the expected increasing trend for the World population [4] and subsequently the need for food and energy, signifies the importance of the land. In such a situation, floating PV (FPV) systems either on off-shore or on-shore water areas seems like an interesting option to reduce the LCOE and the conflict with other land-user sectors such as agriculture and housing. Installation of PV systems on ocean water brings several challenges such as harsh dynamics,storms and difficult accessibility. Inland water areas could be instead exploited for clean solar energy production in several countries, such as Germany, Finland, and the Netherlands. For the case of the Netherlands, 17% of the land is covered by waterways, lakes, and ponds [5]. Moreover, in countries with high insolation rate and drinkable water scarcity, floating PV can produce electricity and prevent water evaporation as well [6]. For example, in Morocco 3 m^3 of water is evaporated yearly per each m^2 of water surface behind the dams [7]. The market share of the floating PV system is expected to be >10% by 2030 [3].

Combining these two trends in the PV industry, floating and bifacial, could be a promising way forward. However, floating bifacial PV has rather unique requirements, challenges, and opportunities. There is general understanding in the literature that floating PV systems face wave and wind forces with various frequency and domains [8], experience stronger ageing mechanisms caused by moisture and harsh environment [9, 10] while they *might* benefit from the cooler working environment and sunlight reflection from the water [11]. They should also meet the requirement for water ecology, release minimum or zero toxic material to the water, and enable mowing activities. Moreover, as with any novel technology, bifacial and floating PV is still held back by a lack or inaccessibility of long-term field data to demonstrate its real-world performance under various conditions [12]. Therefore, providing that the requirements are met and challenges were overcome, combining bifacial PV and floating systems can bring additional energy yield and keep the land usage rate low.

The aim of this work is to model, design, and monitor floating bifacial PV systems for inland water areas. To realize these research goals, the INNOvative ZOn-pv op Water (INNOZOWA) consortium was formed in 2017 by Delft University of Technology, Waterschap Rivierenland [13], Hakkers BV [14], and Blue21 BV [15]. Main steps were (1) location survey and accurate PV yield modelling, (2) innovative, applicable, and modular design and realization of the floating construction and PV systems, and (3) monitoring for the systems. These three main steps are discussed in detail respectively in Sections 2 to 4 of this paper. In chapter 5, key messages of this research are highlighted. Throughout the study, many myths about floating bifacial PV were debunked that some are in contrast with initial expectation.

2. Location Survey and Modeling

2.1 Location

An artificial pond, developed for water retention purposes and located in Weurt, Eastern Netherlands was selected for this research (see Figure 1). Based on the measurement, the basin has a minimum depth of 0.9 m and up to 1.9 m in the deeper parts. Depending on the season and water retention plans, the basin can occupy an area of 18524 m^2 to 22639 m^2.

[1] Delft University of Technology, Photovoltaic Materials and Devices group, Mekelweg 4, 2628CD Delft, the Netherlands.
[2] Waterschap Rivierenland, De Blomboogerd 1, 4003 BX Tiel, the Netherlands.
[3] Blue21 B.V., Molengraaffsingel 12, 2629 JD Delft, the Netherlands.
[4] Hakkers B.V., Oudsas 11, 4251 AW Werkendam, the Netherlands.
* Corresponding author, email: h.ziar@tudelft.nl; Tel: +316 305 81 907

Figure 1. Panoramic view of the artificial pond located in Weurt, the Netherlands (51.8514 ° N, 5.7950 ° E). The pond is developed as a water retention basin. The pond has a rectangular shape, not perfectly aligned with the South. The longer side of the pond is 42° deviated towards the West (222°).

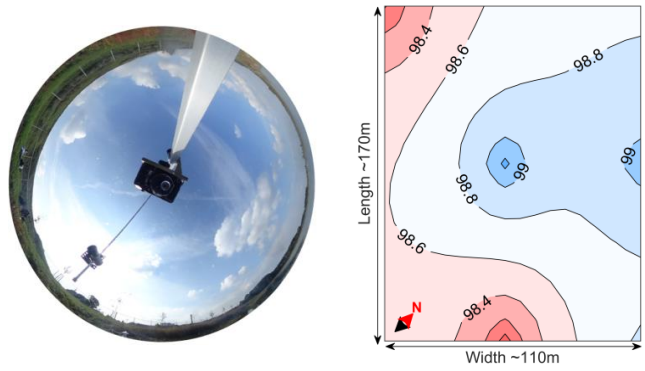

(a) **(b)**

Figure 2. (a) A hori-catcher image at one spot in the pond taken using an upside-down camera and a mirror-like spherical cap. **(b)** Interpolated map of the sky view factor (%) for the pond area. The SVF changes between 97.9% to 99.3%, showing an almost free horizon suitable for photovoltaic installation. One meter above the water surface was considered for SVF calculation as SVF does not significantly dependent on few meters of change in the altitude.

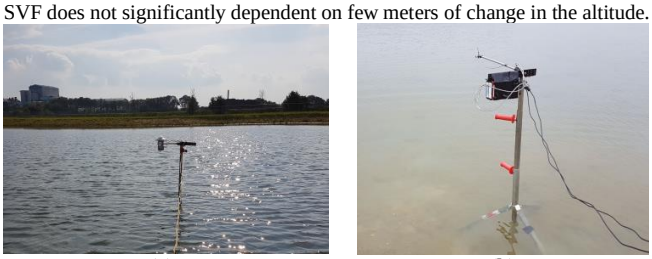

(a) **(b)**

Figure 3. (a) Broadband (285-2800nm), and **(b)** spectrally-resolved (278-1098nm) albedo measurements at two different spots in the pond.

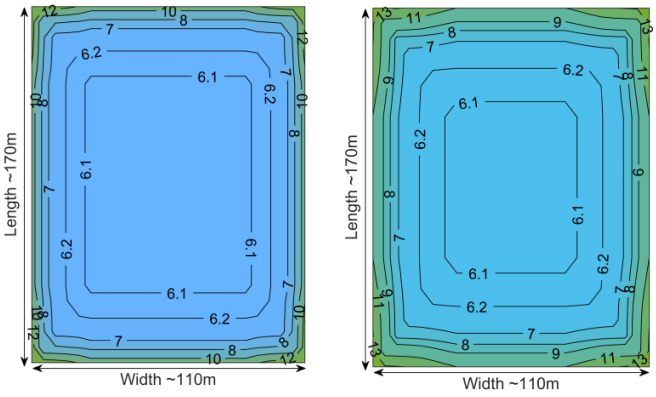

(a) **(b)**

Figure 4. Mapped broadband albedo (%) for the pond area at **(a)** 1 m above water level, and **(b)** 2 m above water level

2.2. Horizon and sky view factor

Skyline-related information is an important input for photovoltaic yield modelling which influences the direct and diffuse components of the sunlight [16]. One key indicator is sky view factor (SVF), which is a unit-less quantity that represents the ratio between the visible sky and a hemisphere centered over the studied location [17, 18]. Skyline information is extracted using a hori-catcher (see Figure 2 (a)) [19] in and around the pond at several spots with different heights. Then, the captured horizon was processed using Meteonorm software package [20] using the approach described in [21, 22]. Further, by applying linear interpolation, a map of SVF was obtained, as can be seen in Figure 2(b).

2.3. Albedo

Albedo is measured by dividing the incoming global radiant fluxes reaching on the down-facing and up-facing parts of a surface. Location, time, geometry, and weather conditions influence the value of albedo [23]. Albedo is spectrally dependent and for photovoltaic applications the effective albedo, which considers the spectral response of the PV cell, should be taken into account [24]. Accurate assessment of albedo becomes more important for bifacial PV installations. Broadband and spectrally resolved albedos were measured both for the water in and the soil around the pond. Figure (3) shows the *Kipp&Zonen* albedometer (sensitive from 285 to 2800nm, measures in W/m^2) and *Avantes* spectrometer (sensitive from 278 to 1098nm, measures in µW/cm^2/nm) which were used respectively to measure the broadband and spectrally-resolved albedos at various spots at the pond. Then, by applying the model described in [23], which bounds the geometrical and spectral features of albedo, maximum value of albedo was calculated for various levels above the water surface at the pond. The mapped albedo of the lake at 1m and 2m above water level are shown in Figure (4). As it can be seen, the closer to the shore and the higher from the water surface the higher the albedo. Figure (5a) shows the spectrally resolved reflected irradiance of the soil and the water at the pond, while figure (5b) shows two sky spectra: measured at the site and standard ASTMG173. Figure (5c) shows the typical response of a mono-crystalline silicon solar cell [25]. Using the information given in Figure (5), the effective albedo of the soil and water are calculated respectively: 15.64% (soil), 7.71% (water 0.5m depth), and 8.11% (water 1m depth). Very low albedo of water predicts a low contribution of the reflected light energy for bifacial PV installation, and therefore, suggests the necessity for using reflectors.

2.4. Yearly irradiation modeling

Mono-facial PV brings the advantage of simplicity and lower costs while bifacial floating PV are expected to yield more [26, 27]. Therefore, in our pre-installation study we considered both mono-facial and bifacial technologies. Mono-facial PV modules can be either placed aligned with the pond orientation for better area usage (higher kWh/m^2) or towards the South for better performance (higher kWh/kWp). For bifacial PV, reflector type and orientation and its distance from the PV module are also become important.

During pre-installation study several design parameters (type and technology of the PV modules, BoS components, etc.) had not been fixed, therefore, the focus was put on the irradiation modelling. Since irradiation is the key component in PV yield analysis [28] the design that receives the highest yearly irradiation will yield higher electrical output.

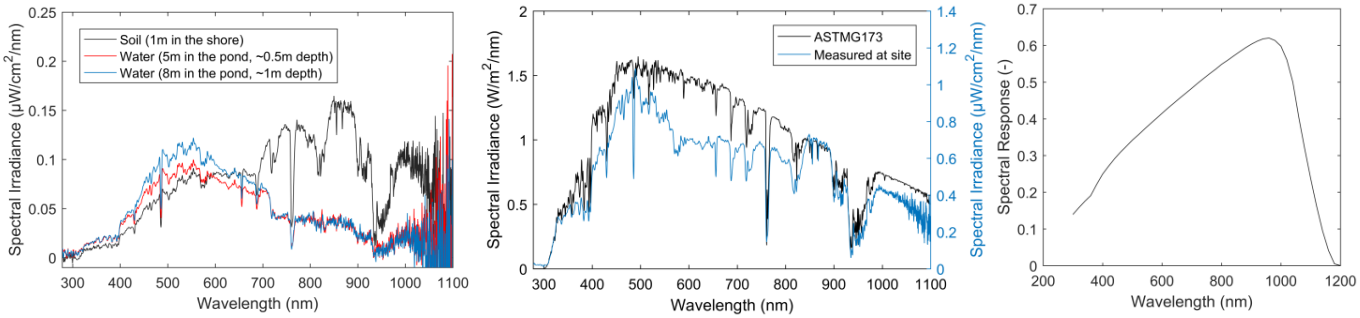

(a) **(b)** **(c)**

Figure 5. Spectrally dependent data for effective albedo calculations. **(a)** Reflected spectrum measured at the pond for the soil and two different depth of water. **(b)** Measured sky spectral irradiance and the ASTM G173 standard global irradiance [29] **(c)** Spectral response of HOQ mono-cSi reference cell reported by Fraunhofer ISE [25]. Measurements were done on 29-Nov-2017 under overcast sky condition, no rain, ambient temperature 2 °C, and the wind speed of 0.5 to 1 m/s. Effective albedo values for the soil, 5m, and 8m in the pond are respectively calculated as 15.64%, 7.71%, and 8.11%. Considering ASTMG173 sky spectrum will changed the values slightly (15.34%, 7.91%, and 8.32%). It is worth noting that for assessing the effective albedo, when the target PV technology is known, relative response of that technology should be used. Note that the front and rear side response of bifacial PV modules are different [30].

Table 1. Comparison of received irradiation on various fixed and tracking mono-facial surfaces at the target location. Since in the Netherlands the PV modules are normally installed at rather a low tilt angle of 12-15° [31], this was considered as a reference case. The optimum fixed tilt was 31° towards the South while the optimum fixed tilt when putting the module aligned with the pond orientation was found to be 27°.

Surface orientation layout	Fixed $\theta_M = 0°$	Std. fixed $\theta_M = 12°$ $A_M = 180°$	2-axis tracking (limited angles) $3 < \theta_M < 15$ $93 < A_M < 267$	1-axis tracking (limited angles) $\theta_M = 3°$ $165 < A_M < 195$	2-axis tracking (no limit) $0 < \theta_M < 90$ $93 < A_M < 267$	Opt. fixed $\theta_M = 31°$ $A_M = 180°$	Opt. fixed (aligned with pond) $\theta_M = 27°$ $A_M = 222°$
Received irradiation (MWh/m²/year)	0.989	1.069	1.143	1.018	1.458	1.112	1.067
Increase (%)	-7.48%	0% (ref.)	6.92%	-4.73%	36.4%	4%	-0.19%

* 0 = North, 90 = East, 180 = South, 270 = West. Opt.: Optimum, Std.: Standard.

Using the location inputs described in Sections 2.1-2.3, several pre-installation yield simulations were done and the result is presented in this section.

The pond is located between five meteorological stations of the KNMI (Koninklijk Nederlands Meteorologisch Instituut) network [32] (see Figure 6). By retrieving the 1-hour resolution global horizontal irradiance (GHI) data from the stations and applying inverse distance weighted (IDW) method [33], the GHI data at Weurt was interpolated, then processed in Meteonorm (horizon was applied), and further broken into direct normal and diffuse horizontal irradiances

Figure 6. Geographical representation of the five meteorological stations around the target area. Inverse distance weighted (IDW) method which is applicable to geographical areas with uniform morphology (such as the Netherlands) was used to interpolate the irradiance data. IDW method assumes that objects that are close to one another are more similar than the ones that are farther apart.

(DNI and DHI) through BRL decomposition model [34], which was shown to be the most accurate irradiation decomposition model for the morphology of the Netherlands [35]. The location receives the irradiation of ~989 kWh/m²/year. Table 1 shows the calculated yearly irradiation for various fixed and tracking mono-facial PV modules. The simulated tracking system was astronomically tracking the Sun position.

Further, to assess the total yearly irradiation on bifacial PV modules, the PVMD toolbox was used [36]. Several cases were studied with various tilt and orientation for the PV module and the reflector, from which a few examples are shown in Figure 7. Simulations showed that putting a reflector very close to the bifacial PV module and relying on the light passing through the cells will not significantly contribute to the total irradiation and should be placed with a distance underneath the bifacial PV module.

The only mono-facial option (See Table 1) that can outperform the tilted bifacial with a horizontal reflector (Figure 7(f)) is when a free-angle dual-axis tracking is done. However, this may not be mechanically feasible that tumbling a floating system might escalate the wind force. Therefore, tracking should be done within a limited range of safe angles. This suggests that maybe a tracking bifacial PV system with limited angles can bring both safe operation, long life-time, high yield, and consequently low LCOE. Therefore, in the design phase, we aimed for a tracking bifacial PV system with reflector, among several other design options, which will give conclusive results about the best solution for floating bifacial PV.

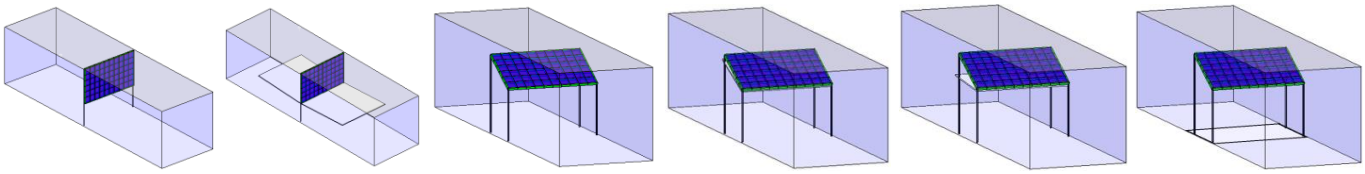

(a) **(b)** **(c)** **(d)** **(e)** **(f)**

Figure 7. A few of the simulated cases for bifacial PV to obtain yearly received irradiation for comparing various design options. **(a)** Vertical bifacial PV aligned with the pond orientation (θ_M = 0°, A_M = 222°) with no reflector, the underneath surface has the albedo of the water. **(b)** Vertical bifacial PV aligned with the pond orientation with an 80% reflective Lambertian reflector (reflector size = 1.7m × PV module length), the rest of the underneath surface has the albedo of the water. Reflectors are tilted 5° with respect to the ground. **(c)** 27° tilted bifacial PV with no reflector aligned with the pond orientation. The underneath surface has the albedo of the water. **(d)** 27° tilted bifacial PV with a close reflector aligned with the pond orientation. The reflector is tilted 5° with respect to the PV module and 80% reflective (reflector size = PV module size). **(e)** 27° tilted bifacial PV with a close reflector aligned with the pond orientation. The reflector is tilted 22° with respect to the PV module and is 80% reflective (reflector size = PV module size). **(f)** 25° tilted bifacial PV module orientated towards the South with 1m distance horizontal reflector (80% reflective, reflector size = PV module size) aligned with the pond orientation. For the South orientation and a horizontal reflector underneath, 25° is the optimum tilt. To account for the light passing between the cells, the cell size, spacing, and the arrangement of a 60-cell *LG Neon 2Bifacial* was considered. The total effective irradiation falling on the bifacial PV module surfaces calculated as: *front irradiation + (rear irradiation × bifaciality factor)*. For the bifaciality factor 0.8 was considered. For the design options (a) to (f) the simulated results for the total effective irradiation are respectively 943, 1202, 1085, 1091, 1138, and 1249 kWh/m^2/year.

2.5. Partial water soaking

Soaking a PV module in water changes the received sunlight spectrum on the PV module surface (negative effect) but reduces the working temperature (positive effect) [37]. Therefore, for water soaking applications it is always important to find the sweet spot that keeps the temperature low but does not drastically reduce the impinged irradiance. This is normally dictated by the soaking depth in the water. Therefore, for a floating PV, which is in the vicinity of the water, it is worth investigating water cooling as a design option. However, as shown in Section 2.4, using a reflector is essential to make the most out of a bifacial PV installation. This implies that soaking a bifacial PV module fully in water is not a logical approach because it would lead to a very small contribution from the rear side. Hence, to study such a possibility in this research, we investigated a partial (frame soaking) of the PV module.

COMSOL Multiphysics was used to make a comparison between a bifacial PV module placed above the water and a module with direct water contact of the lower frame (see Figure 8). Water temperature, as an input for the COMSOL model, was calculated using the empirical model suggested in [38] while the rest of the weather inputs were obtained as described in Section 2.4. Material properties of the PV module layers were obtained from the literature [39] and are shown in Table 2. Figure 8 shows a comparison for the two simulation cases for the 30th of May at 13:30 at the pond location. The temperature at the bottom part of the module is considerably lower for the case where the module is placed in contact with water, but this effect is hardly extended further to the PV cells placed at the bottom. This is due to the low thermal conductivity of both the EVA and the glass. Similar COMSOL simulations were done for the daylight hours of the hottest days of the months (data of the year 2005) and further, the differences in the electrical yield were calculated. Figure 9, shows the difference between the water and the air temperatures at the pond and the additional energy gain by lower frame soaking of the bifacial PV module. The total yearly gain is very minor, around 0.17%. Considering the low energy gain and the higher chance for the potential induced degradation (PID) effect [40], this option is left outside the perspective of a durable floating bifacial PV system.

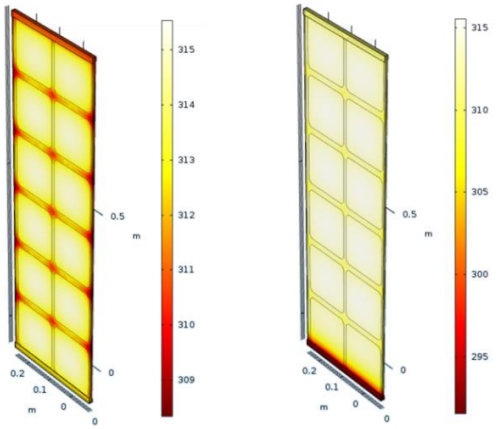

Figure 8. Temperature distribution (in Kelvin) within the bifacial PV module without contact with water (left) and with the bottom frame in contact with water (right). The two cases are simulated using the weather data of the 30th of May at 13:30 at Weurt, the Netherlands. To reduce the computation burden, the simulated module was assumed to have 2 × 6 cells. *60-cell LG Neon 2Bifacial* datasheet was used for the cell, spacing, and frame sizes. Properties of materials such as EVA and the glass were added manually using the data shown in Table 2, reported in [39]. For the simulations, weather data of the year 2005 was used.

Table 2. Properties of the main materials within the PV module, used in COMSOL simulation.

Material	Thermal conductivity κ (W/m.K)	Density ρ (kg/m^3)	Heat capacity C_P (J/kg.K)	Emissivity ε
Silicon	130	2329	700	-
Aluminium	238	2700	900	0.77
EVA	0.34	935	480	-
Glass	1.8	2700	750	0.84
Silver	429	10500	235	-

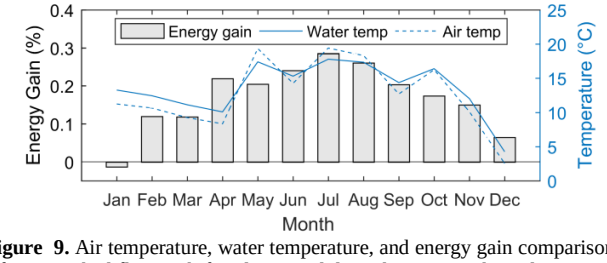

Figure 9. Air temperature, water temperature, and energy gain comparison of a frame-soaked floating bifacial PV module with a case with no direct contact with water. Hottest day of each month (year 2005) was simulated in COMSOL as the monthly representative of the PV module thermal performance. Further the electrical yield was calculated using the temperature coefficients of the *60-cell LG Neon 2Bifacial* PV module.

3. DESIGN AND REALIZATION

3.1. Previous floating PV concepts

After the first floating PV system built in 2007 in Aichi, Japan, several floating PV concepts were developed [41]. A floating PV system normally consists of floats, mooring and anchoring system, PV modules, and balance of system (BoS) components. The most common float types are (1) *pure floats* with high-density polyethylene material, and (2) *pontoons* (or hallow cubes) with metal trusses [41-43]. The first type is lightweight and thin with large water-plastic contact area (at least 50% of the plant size), which increases the chance for plastic defoliation. The lightness of the floats and large water-plastic contact area makes it vulnerable to high wind loads [44, 45] and increases the plastic defoliation possibility, respectively. Although the first type is cost-effective but has a complex mooring system, hardly customizable for sun tracking, and for a large surface it is not sufficient to anchor the system only on the perimeter. The second type suffers from high cost and complex construction [46] but brings the possibility for sun tracking.

Several concepts are introduced in the literature and patented to implement sun tracking to the floats [47-49]. They can be categorized as trackers with and without confining structure. Almost all the floating PV tracking solutions reported in the literature turns the floaters (vertical-axis Sun tracking) and do not tumble them (horizontal-axis Sun tracking), driven mainly by safety reasons (tumbling increases the wind load). However, turning an array of the PV modules (changing the azimuth) while their tilt is kept low because of the wind safely measures does not in principle contribute much in electric yield increase.

From wave point of view, there are four categories for the floating PV systems. The first three categories are for inland water areas, respectively for negligible, 1m-, and 2m-wave heights. The fourth category is the for open seas for which the floating PV systems should withstand waves up to 10 meters of height [50]. The technology readiness level is higher for the lower wave categories, however, there is still insufficient practical knowledge about the long term performance and longevity.

Further, accessibility to water areas is crucial for inland water ponds, canals, and rivers. For example, mowing activities are regularity done on inland water areas, and therefore, a sophisticated floating PV system must be movable while sustaining the maximum possible electrical yield (to have a low LCOE) while being resilient to high wind and categorized wave forces.

3.2. Introduced floating PV concepts

The available knowledge in the literature, the findings reported in Section 2, mechanical restrictions, and the requirements for water mowing activities served as inputs to converge into two new floating PV concepts: (i) *retractable system*, and (ii) *tumbler floating island*. In the design concept (i) PV modules are placed between four fixed pillars (as anchoring spots) and can be lined up and spread out (using two winches) when needed. This concept resembles shopping carts where the PV panels can be folded one against the other on a similar way as the shopping carts do in a supermarket. In the design concept (ii), however, the modules are installed on a floating island which is anchored at one spot to the bottom of the lake. The island is occupied with two tanks underneath to track the Sun (in the horizontal axis) by pumping water from one tank to another. Both design options enable regular mowing activities and access to the water surface. Both concepts are able to cope with water level variation even in extremely low-water-level seasons. The designed concepts are shown in Figure 10.

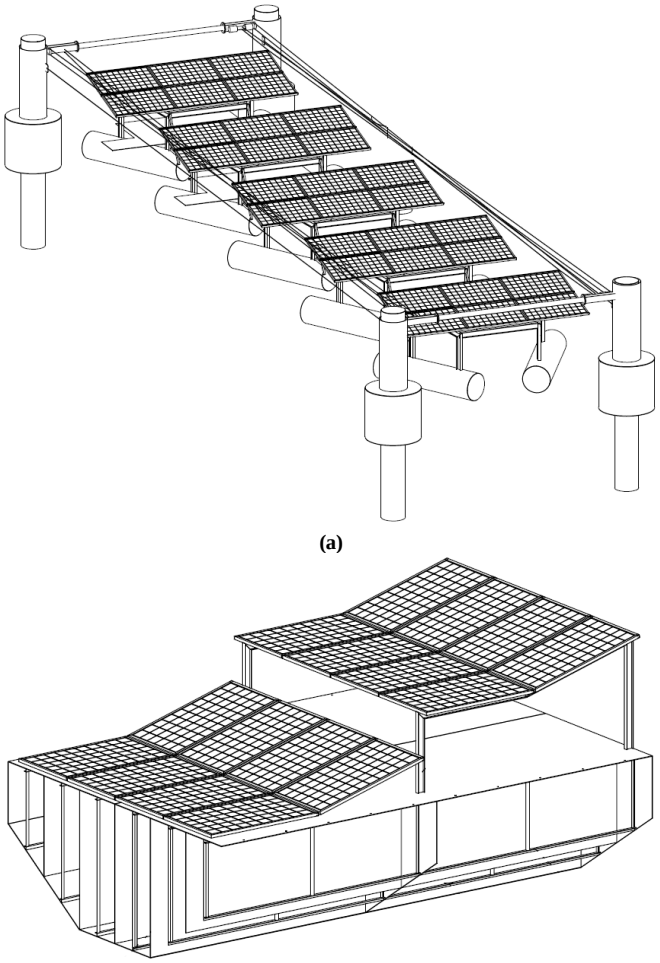

(a)

(b)

Figure 10. The developed floating PV concepts: **(a)** retractable system and **(b)** tumbler floating island. The retractable system has 5 rows of PV panels (4.94m × 2.29m, 15° tilt) each with 6 PV modules. The distance between the panels are 4.85 m. Panels can be lined up at either two ends of the system. Reflectors (aluminum reflecting coating) can be placed under any row of the system. The height of the PV panel upper edge from the reflector (trapezoidal shape with bases of 2.02 and 4.55m and height of 2.01) and the water level are 1.58m and 1.94m. The system has the overall dimension of 25.42m × 7.78m. The tumbler floating island has 4 panels (4.52m x 1.04m) of PV modules. Two rows are horizontal and the other two are tilted for 15°. The lower and upper side of the last row are positioned 1.33m and 1.05m above the island surface, which is covered by aluminum reflecting coating. The island can tumble for maximum 27° to the sides and has the overall dimension of 6.62m × 4.51m.

3.3. Realization

In summer 2019, realization of the introduced floating PV concepts was accomplished. Figures 11(a) to 11(e) show a few snapshots of the realization procedure. In order to monitor the performance of the floating PV concepts and compare it with conventional PV systems, two land-based PV systems were

also installed by the pond. In total 9 pilot systems with different features were installed, as can be seen in Figure 12.

3.4. Components and sensors

Installed mono-facial and bifacial PV modules were respectively *60-cell LG Neon 2Black (LG330N1K-V5)* and *72-cell LG Neon 2Bifacial (LG400N2T-A5)*. Each module is equipped with a *SolarEdge P5050* power optimizer and all are connected to a *SolarEdge SE17K* three-phase inverter. This arrangement made it possible to monitor the DC yield of the PV modules and reduce the effect of BoS components in the comparative study of the pilot systems.

Due to a lack of immediate supply for the desired white color reflector, orange color reflector with aluminium reflecting coating was utilized. Further, a series of indoor reflectance tests were done on the reflector sample using *LAMBDA 950* spectrophotometer. The effective albedo for the reflector was calculated as 68.5% (see Figure 13), which shows that the orange reflector has a comparable albedo with respect to a weathered white reflector.

The winch system is powered up by two PV+battery units located at the two ends of the retractable system (see Figure 14). In this way, the power from the pilot system is not being used for retracting manoeuvre. However, the power needed for tumbling the floating island is driven from the grid and to account for this energy the pump consumption was calculated. The tumbling system uses a pump to distribute water between two tanks on the two sides of the floater (each tank has two compartments). Each compartment has 1.3 m^3 of space. The tracking is based on the position of the Sun and is done every 15 minutes with the resolution of 2 degrees using a pre-defined look-up table. According to the tracking lookup table, on average it takes ~30 minutes to fully pump the water from one compartment to another (tumble the island for 27°). This requires 2.6 m^3/h of flow rate, 45 W of input power, and according to the pump performance curve will lead to 2.75m of the pump head. Thus, on average every 24 hours of tumbling for Sun tracking consumes 90 Wh resulting in 32.85kWh per year.

Various sensors were installed at the site at different times of the monitoring period, including a visual camera, a horizontal irradiance sensor, a wind speed sensor, an air temperature sensor, an irradiance sensor to measure the reflected sunlight by the water, and an irradiance sensor to measure the reflected light on the rear side of one bifacial PV panel with reflector. This sensor was placed on the retractable system. The sensors are shown in Figure 15.

4. MONITORING AND ANALYSIS

It has been reported in the literature through monitoring and simulation that the fixed floating PV systems can yield 11-13% more in comparison to land-based PV systems mainly because of lower air temperature above the water and higher wind speed. However, these studies do not show a fair comparison as the PV systems do not experience the same weather condition. In [51] the two monitored PV systems were apart for 60 km and in [8] the implied distance between the hypothetical simulated PV systems is more than 150 km. In this research, however, we placed the land-based and the

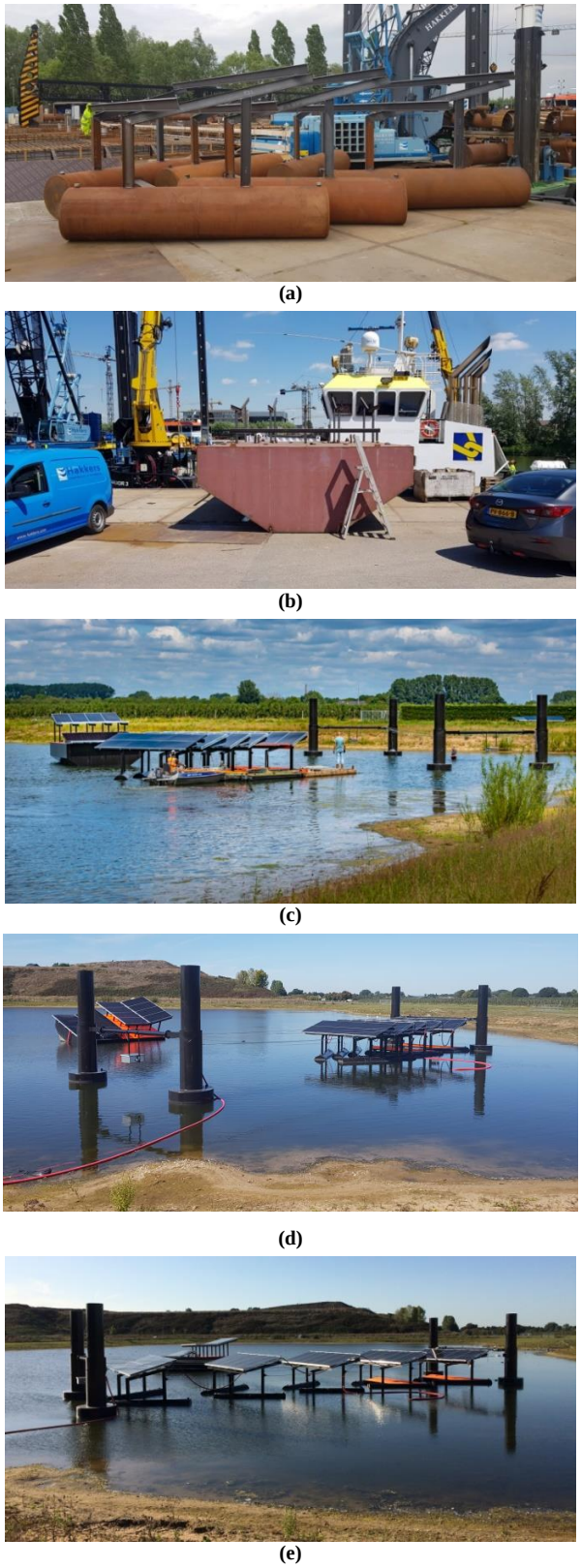

Figure 11. Snapshots of the realization procedure: **(a)** preparation of the floating pontoons and the attached metallic structures for the retractable systems, **(b)** preparation of the metallic frame for the tumbler floating island, **(c)** moving the retractable PV systems towards the installation spot in the pond, **(d)** retracting and tumbling tests on the floating concepts, and **(e)** operational retractable PV systems (front) and the floating island (rear).

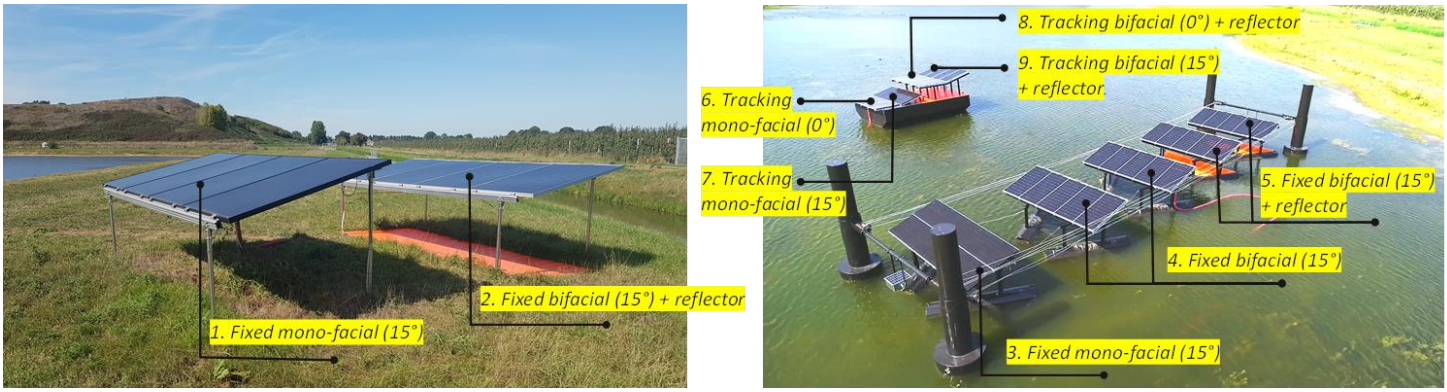

(a) **(b)**

Figure 12. Pilot systems installed at the pond: **(a)** reference ground based systems by the pond and **(b)** installed floating PV systems. There are nine systems: 1. Fixed ground based mono-facial PV system, 2. Fixed ground based bifacial PV system with reflector, 3. Fixed floating mono-facial PV system, 4. Fixed floating bifacial PV system, 5. Fixed floating bifacial PV system with reflector, 6. Horizontal-axis tracking floating mono-facial PV system (0° tilt), 7. Horizontal -axis tracking floating mono-facial PV system (15° tilt), 8. Horizontal-axis tracking floating bifacial PV system (0° tilt) with reflector, and 9. Horizontal -axis tracking floating bifacial PV system (15° tilt) with reflector.

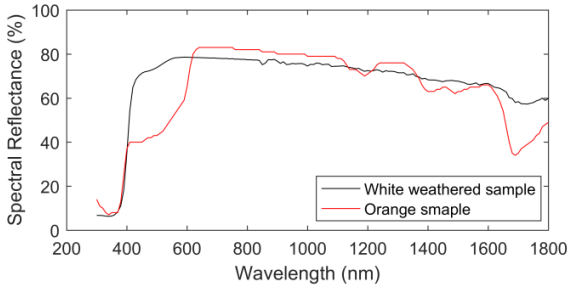

Figure 13. Measured spectral reflectance of the orange material (used in the pilot system) and a white weathered material (as a reference for comparison). The average reflectance (300-1800nm) for the orange and white samples are 63.28% and 67.34%, respectively. Considering AM 1.5 spectrum, the broadband albedo (300-1800nm) for the orange and white samples are 62.22% and 70.66% while the effective albedo (300-1200nm, considering the response of Mono-cSi) are calculated as 68.49% and 73.96%., respectively.

(a) **(b)**

Figure 14. Components for the retracting system: **(a)** winch motor and cables, **(b)** PV + Battery unit to power up the winch system.

floating PV systems close to each other which enables a fair comparison and a precise understanding of the long-term performance of the floating PV system. Moreover, a thorough performance analysis of the floating bifacial PV systems is barely reported in the literature so far, mainly because of the complexity in both modeling and monitoring. Moreover, this research practically considers reflectors and tracking systems to give a broader understanding about the performance of various land-based and floating PV systems.

The monitoring of the 9 pilot systems introduced in Section 3.3 started on 22-Sep-2019 and still is an ongoing process.

(a) **(b)** **(c)**

Figure 15. Sensors: **(a)** mete-unit consists a camera for occasional remote visual checks, anemometer to measured wind speed, temperature sensor to record ambient temperature, and a working-class reference cell to measured global horizontal irradiance, **(b)** a working class reference cell installed upside down to measure the sunlight reflected from the water, and **(c)** a working class installed at the rear side of a bifacial PV module (on the 4th panel of the retractable system) to measure the rear side irradiance.

Several interesting points were recorded, observed, and examined that are discussed in Sections 4.1 to 4.6.

4.1. Drifting pontoon

Less than one month after the installation, the modules on the 4th panel of the retractable system started to drift off and caused a drop in the electrical yield (maximum 50%) produced by that panel. This effect was noticed both via the camera at the site and by the recorded kWh by the optimizers. This issue started on the 2nd week of October, detected in two weeks, and resolved in the 2nd week of November (lasted for ~5 weeks).

4.2. Storm events:

The pilot systems experienced two storm events on 9th and 16th of February 2020, storms Ciara and Dennis [52, 53], with maximum wind gusts of 50 km/h recorded at the pond. The systems did not damage and functioned normally during and after the storms with no yield interruption. It is worth noting that during the same period, 1.5% of the Lingewaard floating PV park (moulded plastic-based pure floats), located at 10 km away from our pilot system was damaged by these storm events [44].

4.3. Visual inspection

In May 2020, after almost 8 months of operation, a series of visual and thermal checks were done on the pilot systems. Visual checks were performed using the NREL guidelines for visual inspection [54].

(1) Slight azimuth misalignment was observed between the land-based pilot systems. It could be because of the storm event and/or inaccurate installation. Also tilts of the land-based system deviated from the design (7° and 12.7° instead of 15°). However, the tilt and orientation of the floating PV concepts were correct.

(2) Birds dropping were observed at several spots on the floating PV modules. The influence of the bird presence was more intense for the surfaces that were closer to the water and less tiled. Remarkably the reflectors of the retractable system (pilot system no.5) and the horizontal mono-facial PV modules on the tumbler floating island (pilot system no.6) were heavily covered by bird droppings and even a bird nest (See Figure 16). It is worth noting that the other pilot systems were slightly soiled with no heavy shading.

A few passive actions that can be done to reduce the birds' presence effects such as increasing the distance of the reflectors from the water level and placing them slightly tilted in the retractable system and keeping the floating island tumbled during the night time. However, this observation suggests more active bird control techniques (such as laser-based bird control [55]) for inland floating PV concepts.

(3) Vicinity to water: It was observed that when the floating island tumbles with high degrees, the mono-facial modules on the (pilot systems nos. 6 and 7) almost touch the water surface. In the long-term, this might boost the possibility for PID effect. However, this cannot be confirmed as long as electroluminescence or separate I-V measurements are done on the modules. This is out of the scope of the current study and is planned to be done after the full monitoring period.

4.4. Thermal inspection

The thermal inspection was performed on the 9 pilot systems on 15-May-2020 using a *Fluke Ti32* thermal imager. Several points were observed that are mentioned here.

. The one-day thermal inspection does not bring conclusive remarks about the temperature of the floating and land-based PV system. However, it is postulated that there should not be an overall significant temperature difference between the floating and land-based PV systems when they are placed close to each other, as long as they use the same PV technology. The reason is that the main cooling mechanism in PV systems is convective cooling mainly driven by the wind flow [56], and both systems experience similar wind speeds. Moreover, due to the fact that the floating PV modules are more exposed to the bird droppings, which cause shading [57] and hotspot [58], in general, floating PV modules compare to close-located land-based PV systems can even experience higher temperature spatial variance. Figure 17(a) and (b) shows the thermal images of the mono-facial PV modules on the floating island and the land. As it can be seen, heavily fouled PV modules on the floating island experience higher spatial temperatures variance.

Another interesting aspect is the temperature difference between the front and rear sides of the floating bifacial PV modules. Figure 17(c) and (d) shows the thermal images of the front and rear side of one module on the pilot system no.9. Although the front side is experiencing a minor hotspot, the rear side has slightly (1.2°C) higher average temperature with more temperature non-uniformity.

4.5. Irradiance monitoring

The irradiance sensors were used to monitor the real-time water albedo and the irradiance reflected on the rear side of the floating bifacial modules (to evaluate the contribution of the reflectors). The sensors installed and started to operate in May 2020. Results of the irradiance monitoring from 20-May-2020 to 31-May-2020 are shown in Figure 18.

For this duration, the daily average water albedo is about 11.6% with rises in the mornings and evenings because of the high angular dependency (low Lambertian behaviour) caused by the low altitude of the Sun. Also it is interesting to observe that the water albedo increases during a cloudy day (May 24th) with respect to a clear day (May 28th) for about 4% absolute. The reflected share of the Sunlight at the rear side of the module is higher than water albedo because of the contribution of the reflector. However, this contribution is not very high mainly because of the heavy fouling and the dirt present on the reflector. The reflector performance enhances during morning and evening both because of the angular dependency and the redshift of the Sunlight light spectrum. Thus, the orange-color reflector boosts up the power more in the evening and morning helping to slightly smoothen the bifacial power production curve. On daily average, the reflected irradiance on the rear side has a share of 23.4%. This ratio slightly decreases during the cloudy day with respect to a sunny day as a result of two opposite effects: the diffuse light in cloudy days increases the albedo of contributing surfaces (by casting less shadow on the ground [23]) but on the other hand, the sunlight spectrum is less favourable for the orange-colored reflector (a cloudy day spectrum has more share in the high-frequency region [59]).

4.6. Electrical yield comparison

The specific DC yield (Wh/Wp) of the 9 pilot systems were monitored for 8 months, October 2019 until May 2020. The overall performance of the systems is shown in Figure 19 and further broken down into the monthly comparison in Figure 20. The comparison shows that the tracking bifacial modules with reflector (system no. 9) outperform all the other systems by yielding ~14% more than the reference land-based mono-facial modules (system no. 1, as a reference). In a month with more clear sky days (May 2020), this value reaches up to ~29%. The bifacial modules on the retractable floater (systems no. 4 and no. 5), however, produce less than the land-based bifacial modules (systems no. 2), proving the effect of low water albedo and severe influence of the birds' presence on the reflectors of the retractable system. It is worth noting that the pilot systems no.3 and no.6 are respectively experiencing less favourable sunlight and temperature. System no.5 is regularly shaded over a few hours a day by the front anchoring poles and system no.6 can barely benefit from backside cooling as it is attached to the surface of the floating island. The monitoring is continued to cover one full year of operation which will result in more conclusive comparisons.

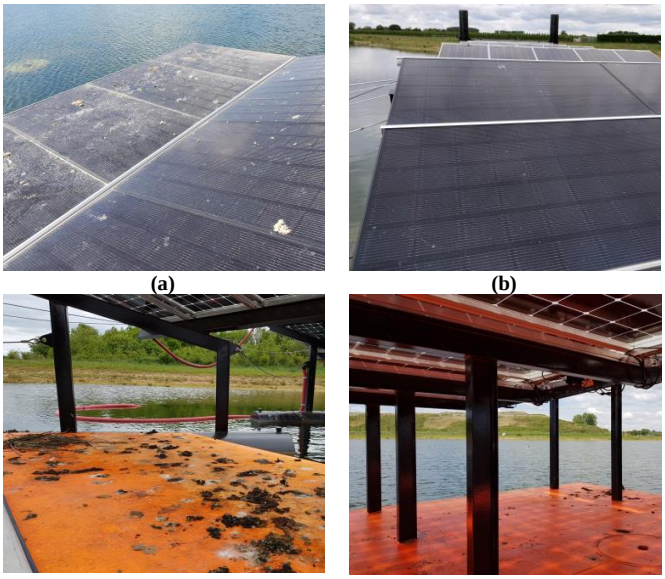

Figure 16. Birds influence on the floating pilot systems. **(a)** Horizontal pilot PV system no.6 is considerably covered by birds droppings while the tilted system on the same floater is much cleaner. **(b)** The tilted PV modules on the retractable floaters are barely influenced by birds. **(c)** Reflectors of the retractable systems which are placed horizontally and near the water level are easily accessible for the birds, and therefore, heavily fouled. On the left side of the image, a bird nest is also visible. **(d)** The reflectors on the floating island are much cleaner than the ones on the retractable system because the island reflector regularly tumbles and is more distanced from the water level.

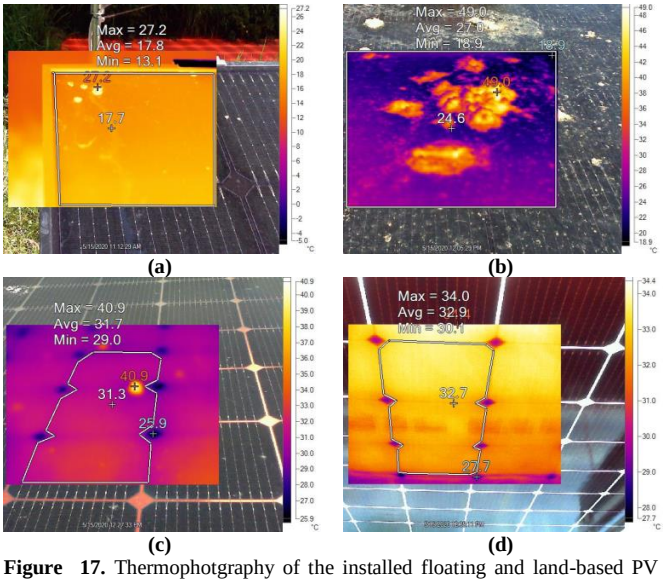

Figure 17. Thermophotgraphy of the installed floating and land-based PV modules: **(a)** Land-based mono-facial PV module, **(b)** mono-facial PV module on the floating island, **(c)** Front side of one bifacial PV module on the floating island, and **(d)** rear side of the same bifacial PV module on the floating island. The min, max, and average temperature values for the area surrounded by the polygons are shown on the images. The temperature spatial variance, which is a is a key indicator of possible defects in thermal image-based diagnostics [60], for **(a)** to **(d)** are respectively 7.38, 26.72, 1.19, and 0.97 °C^2. Fluke Ti32 with coupled with SmartView software package was used to capture and analyze the thermal images. The average GHI and ambient temperature during these measurements were respectively 768 W/m^2 and 9.5 °C.

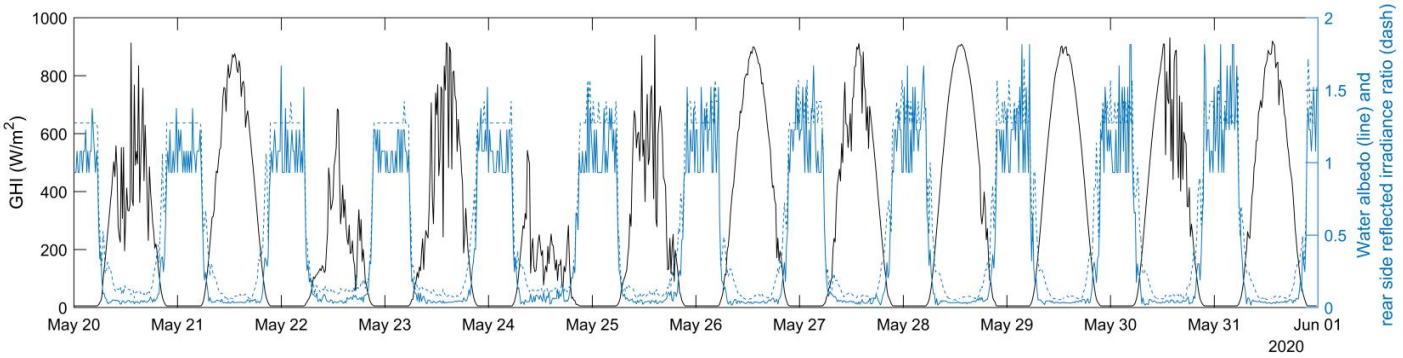

Figure 18. Global horizontal irradiance, the albedo of the water, and the ratio of the reflected light on the rear side of the bifacial PV module, from 20-May-2020 to 31-May-2020. The average daily water albedo and the rear side irradiance ratio of the floating bifacial PV module equipped with an orange-color reflector are 11.6% and 23.4%, respectively. For clear and cloudy days of May 28th and May 24th, the water albedo is respectively 10.6% and 14.6% while the rear side irradiance ratio is respectively 24.3% and 22.9%. The values were obtained excluding the night-time recordings.

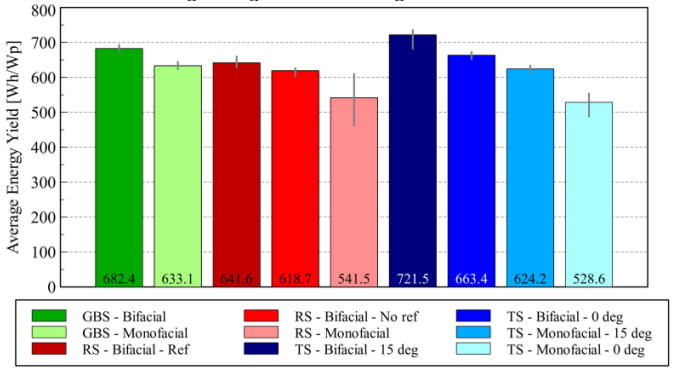

Figure 19. Comparison of the overall specific DC yields of the pilot PV systems (Oct2019 to May2020). The green bars represent the ground-based system, the red bars the retractable system and the blue bars the tracker system. The grey error bars depict the range of the minimum and the maximum energy yield of each module in the respective system. The results are however only for an 8-month period, and the overall picture can change after monitoring the summer months.

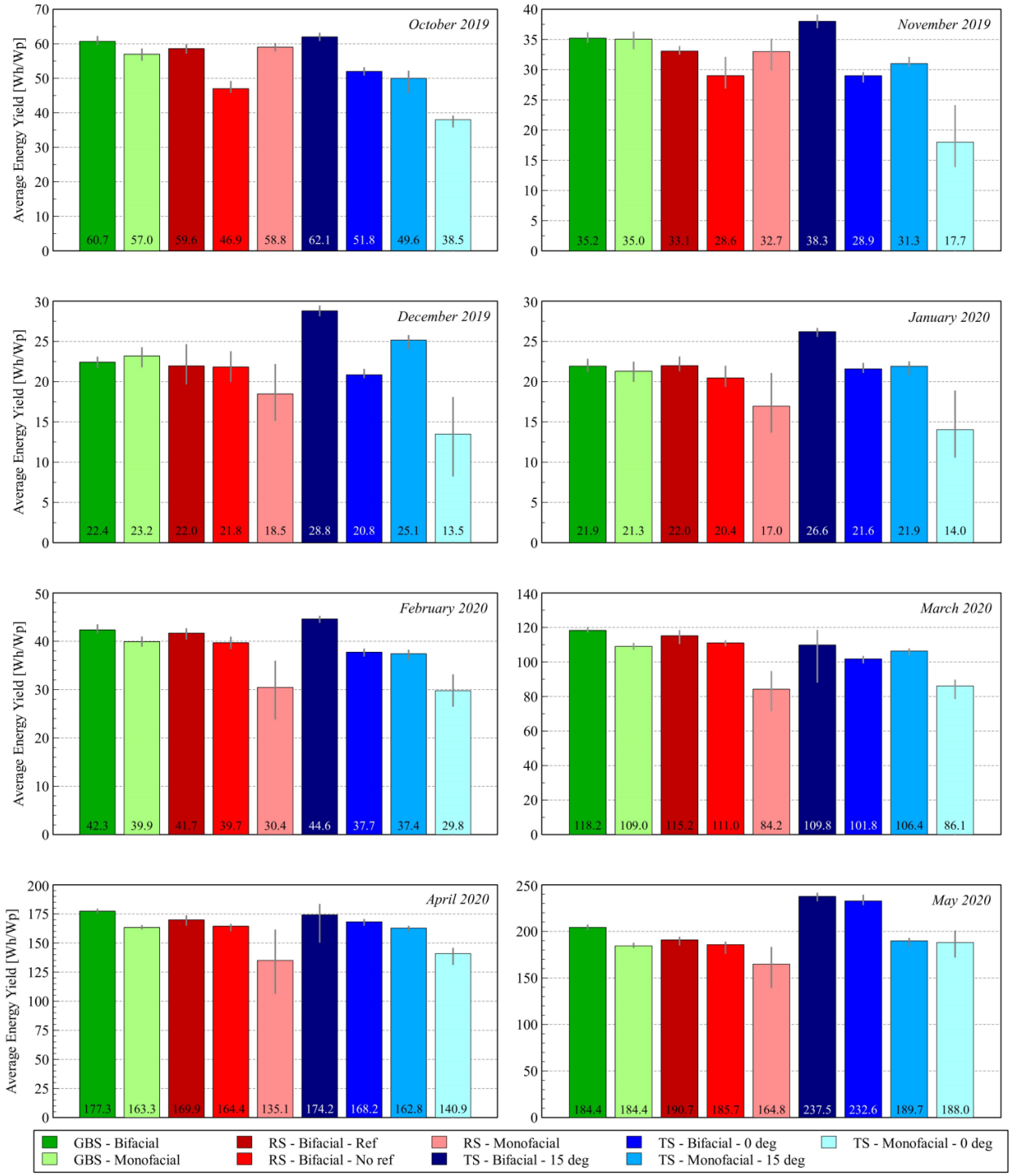

Figure 20. Monthly breakdown of the specific yield for the monitored pilot systems. The green bars represent the ground-based system, the red bars the retractable system and the blue bars the tracker system. The grey error bars depict the range of the minimum and the maximum energy yield of each module in the respective system. During the 8-month period, the pilot systems on the floating island have produced 7.47 MWh in total. This means Sun-tracking consumes 0.3% of the production (see pump consumption calculation in Section 3.4). GBS: ground-based system, TS: tracking system, RS: retractable system, ref: reflector.

5. CONCLUSION

This paper introduced two novel floating PV concepts for inland water areas: the retractable and the tumbler island. The introduced concepts can accommodate bifacial PV modules equipped with reflectors and horizontal sun-tracking. They also do not disturb mowing activities and can be moved around to enable light penetration into the water. The location survey, modelling, realization, and the results of 8 months monitoring were reported. Through the study, several myths about floating bifacial PV were debunked and are mentioned here as a summary:

1. Despite the immediate expectation, inland water areas have low effective albedo which makes water less favorable for bifacial PV installation. Therefore, including reflectors is highly recommended.
2. Frame soaking of the floating PV modules has a very minor influence on the performance and, therefore, does not bring added values.
3. Horizontal Sun tracking is possible for floating PV modules by adjusting the water content within the floater compartments by a pump.
4. The birds' presence on the floaters show its effect in the short-term. The surfaces that directly (PV) and indirectly (reflector) play a role in the FPV irradiance capturing should be kept tilted and at a higher level than that of the water. This reduces the birds' presence effects. Active bird control techniques are also recommended.
5. Floating PV system experience higher fouling rate and will suffer more from temperature spatial variance compared to close-located land-based PV systems. This will boost the ageing procedure.
6. Quantitative yield monitoring and analysis revealed that only bifacial PV with reflector and tracking can outperform considerably the conventional land-based systems.

The reported findings and the lessons learned will help the floating PV community to boost the technology readiness level further up for various categories of the water areas.

ACKNOWLEDGMENT

The work was supported by Netherlands Enterprise Agency (RVO) via the project: INNOZOWA. The authors would like to thank Nynke Hermelink (RVO), Johan Bakker (Waterschap Rivierenland), Peter van der Linde (Hakkers BV), Furkan Fatih Sönmez (TU Delft), and Andres Calcabrini (TU Delft) respectively for organizational suggestions, practical discussion, suggestions for mechanical design, help in measurements, and comments on simulations.

REFERENCES

1. Luque, A., A. Cuevas, and J. Ruiz, *Double-sided n+-p-n+ solar cell for bifacial concentration.* solar Cells, 1980. **2**(2): p. 151-166.
2. *Global bifacial module market report 2019*. 2020, Wood Mackenzie Power & Renewables.
3. Equipment, V.P., *International Technology Roadmap for Photovoltaic (ITRPV) 2019 Results*. 2020, March.
4. Abel, G.J., et al., *Meeting the Sustainable Development Goals leads to lower world population growth.* Proceedings of the National Academy of Sciences, 2016. **113**(50): p. 14294-14299.
5. *Dutch water facts*. 30-05-2020]; Available from: https://www.holland.com/global/tourism/information/general/dutch-water-facts.
6. Taboada, M., et al., *Solar water heating system and photovoltaic floating cover to reduce evaporation: Experimental results and modeling.* Renewable energy, 2017. **105**: p. 601-615.
7. *Maarten Romijn, Head of R&D, HydroPV, personal communication, March 24, 2020.*
8. Golroodbari, S.Z. and W. van Sark, *Simulation of performance differences between offshore and land-based photovoltaic systems.* Progress in Photovoltaics: Research and Applications, 2020.
9. Sharma, P., B. Muni, and D. Sen. *Design parameters of 10 KW floating solar power plant*. in *Proceedings of the International Advanced Research Journal in Science, Engineering and Technology (IARJSET), National Conference on Renewable Energy and Environment (NCREE-2015), Ghaziabad, India*. 2015.
10. Ferrer-Gisbert, C., et al., *A new photovoltaic floating cover system for water reservoirs.* Renewable Energy, 2013. **60**: p. 63-70.
11. Sahu, A., N. Yadav, and K. Sudhakar, *Floating photovoltaic power plant: A review*. Renewable and sustainable energy reviews, 2016. **66**: p. 815-824.
12. Maisch, M., *WoodMac: Bifacial module capacity will exceed 21 GW by 2024*, in *PV Magazine*. 2019.
13. *https://www.waterschaprivierenland.nl/*.
14. *https://www.hakkers.com/*.
15. *https://www.blue21.nl/*.
16. Mondol, J.D., Y.G. Yohanis, and B. Norton, *Solar radiation modelling for the simulation of photovoltaic systems.* Renewable Energy, 2008. **33**(5): p. 1109-1120.
17. Oke, T.R., *The energetic basis of the urban heat island.* Quarterly Journal of the Royal Meteorological Society, 1982. **108**(455): p. 1-24.
18. Sönmez, F.F., et al., *Fast and accurate ray-casting-based view factor estimation method for complex geometries.* Solar Energy Materials and Solar Cells, 2019. **200**: p. 109934.
19. *https://meteonorm.com/en/product/horicatcher*.
20. *Meteonorm 7.3.4*. Available from: https://meteonorm.com/en/download.
21. Steyn, D., *The calculation of view factors from fisheye-lens photographs: Research note*. 1980.
22. Keijzer, M., *A multi-surface reflected irradiance model for pyranometer corrections and PV yield calculations in complex urban geometries*. 2019, Delft University of Technology.
23. Ziar, H., et al., *A comprehensive albedo model for solar energy applications: Geometric spectral albedo.* Applied Energy, 2019. **255**: p. 113867.
24. Brennan, M., et al., *Effects of spectral albedo on solar photovoltaic devices.* Solar Energy Materials and Solar Cells, 2014. **124**: p. 111-116.
25. *Flyer: Reference cells, Spectral response of different reference cells*, I. Fraunhofer, Editor.
26. Guerrero-Lemus, R., et al., *Bifacial solar photovoltaics–A technology review*. Renewable and sustainable energy reviews, 2016. **60**: p. 1533-1549.
27. Liang, T.S., et al., *A review of crystalline silicon bifacial photovoltaic performance characterisation and simulation.* Energy & Environmental Science, 2019. **12**(1): p. 116-148.
28. Khatib, T., A. Mohamed, and K. Sopian, *A review of solar energy modeling techniques.* Renewable and Sustainable Energy Reviews, 2012. **16**(5): p. 2864-2869.

29. Standard, A., *G173-03-Standard Tables for Reference Solar Spectral Irradiances: Direct Normal and Hemispherical on 37 Tilted Surface.* Ann. Book of ASTM Standards 2003, 2012. **14**.
30. Carolus, J., et al., *Physics of potential-induced degradation in bifacial p-PERC solar cells.* Solar Energy Materials and Solar Cells, 2019. **200**: p. 109950.
31. Tim N. C. de Vries, J.B., Martijn Vermeer, Jaap C. B. Donker, 4 Sven A. Briels, Hesan Ziar, Miro Zeman, and Olindo Isabella, *A quick-scan method to assess photovoltaic 1 rooftop potential based on aerial imagery 2 and LiDAR.* Solar Energy (accepted for publication), 2020.
32. *KNMI - Koninklijk Nederlands Meteorologisch Instituut*. Available from: https://www.knmi.nl/home.
33. Watson, D.F. and G. Philip, *A refinement of inverse distance weighted interpolation.* Geo-processing, 1985. **2**(4): p. 315-327.
34. Ridley, B., J. Boland, and P. Lauret, *Modelling of diffuse solar fraction with multiple predictors.* Renewable Energy, 2010. **35**(2): p. 478-483.
35. Mishra, S., *Selection Map for PV Module Installation Based on Shading Tolerability and Temperature Coefficient*. 2018, Delft University of Technology.
36. Santbergen, R., et al., *Annual Energy Yield Simulation Toolbox and its Application to Floating Bifacial Photovoltaic Modules with Reflectors*, in *ELECTRIMACS 2019 – Salerno, Italy, 21st-23rd May 2019*. 2019.
37. Cazzaniga, R., et al., *Floating photovoltaic plants: Performance analysis and design solutions.* Renewable and Sustainable Energy Reviews, 2018. **81**: p. 1730-1741.
38. Harvey, R., et al., *The influence of air temperature on water temperature and the concentration of dissolved oxygen in Newfoundland Rivers.* Canadian Water Resources Journal, 2011. **36**(2): p. 171-192.
39. Peter, N., et al., *3D finite element method modelling and simulation of the temperature of crystalline photovoltaic module.* International Journal of Research in Engineering and Technology, 2015. **4**(9): p. 378-384.
40. Lausch, D., et al., *Potential-induced degradation (PID): Introduction of a novel test approach and explanation of increased depletion region recombination.* IEEE Journal of Photovoltaics, 2014. **4**(3): p. 834-840.
41. Trapani, K. and M. Redón Santafé, *A review of floating photovoltaic installations: 2007–2013.* Progress in Photovoltaics: Research and Applications, 2015. **23**(4): p. 524-532.
42. Schmaelzle, P.H., et al., *Deployment techniques of a floating photovoltaic power generation system*. 2017, Google Patents.
43. Water, W.S.M., *Floating Solar Market Report*. World Bank Group and SERIS, Singapore, 2018.
44. *Another damage to floating solar park Lingewaard*, in *Solar Magazine*. 2020.
45. Bellini, E., *Japan's largest floating PV plant catches fire after Typhoon Faxai impact*, in *PV Magazine*. 2019.
46. Cazzaniga, R., *Floating PV Plants-chapter 4: Floating PV Structures*. 2020: Academic Press.
47. Tina, G., M. Rosa-Clot, and P. Rosa-Clot. *Electrical behavior and optimization of panels and reflector of a photovoltaic floating plant*. in *Proceedings of the 26th European photovoltaic solar energy conference and exhibition (EU PVSEC'11)*. 2011.
48. Clot, M.R., P.R. Clot, and S. Carrara, *Apparatus and method for generating electricity using photovoltaic panels*. 2011, Google Patents.
49. Fraas, L., et al., *Solar PV Carousel Trackers for Building Flat Rooftops: Three Case Studies.* 2010.
50. Folkerts, W., et al., *Roadmap PV Systemen en Toepassingen.* 2017.
51. Choi, Y.-K., *A study on power generation analysis of floating PV system considering environmental impact.* International journal of software engineering and its applications, 2014. **8**(1): p. 75-84.
52. *https://en.wikipedia.org/wiki/Storm_Ciara*.
53. *https://en.wikipedia.org/wiki/Storm_Dennis*.
54. Packard, C.E., J.H. Wohlgemuth, and S.R. Kurtz, *Development of a visual inspection data collection tool for evaluation of fielded PV module condition*. 2012, National Renewable Energy Lab.(NREL), Golden, CO (United States).
55. *https://www.birdcontrolgroup.com/*.
56. Jones, A. and C. Underwood, *A thermal model for photovoltaic systems.* Solar energy, 2001. **70**(4): p. 349-359.
57. Ziar, H., et al., *Quantification of Shading Tolerability for Photovoltaic Modules.* IEEE Journal of Photovoltaics, 2017. **7**(5): p. 1390-1399.
58. Ziar, H., et al. *Bypass diode characteristic effect on the behavior of solar PV array at shadow condition*. in *2012 3rd Power Electronics and Drive Systems Technology (PEDSTC)*. 2012. IEEE.
59. Bird, R.E. and C. Riordan, *Simple solar spectral model for direct and diffuse irradiance on horizontal and tilted planes at the earth's surface for cloudless atmospheres.* Journal of climate and applied meteorology, 1986. **25**(1): p. 87-97.
60. Tsanakas, J. and P. Botsaris, *An infrared thermographic approach as a hot-spot detection tool for photovoltaic modules using image histogram and line profile analysis.* International Journal of Condition Monitoring, 2012. **2**(1): p. 22-30.

B

Appendix - Power Conversion Tool Manual

This Appendix contains the manual that is created in support of the newly build Power Conversion tool. The manual explains the operation and the underlying principles of the tool.

User Manual

Power conversion tool for the PVMD modeling toolbox

Developed by Tim Stark - 4631781

Date: 31/01/2020

Power Conversion tool: Version 1.1

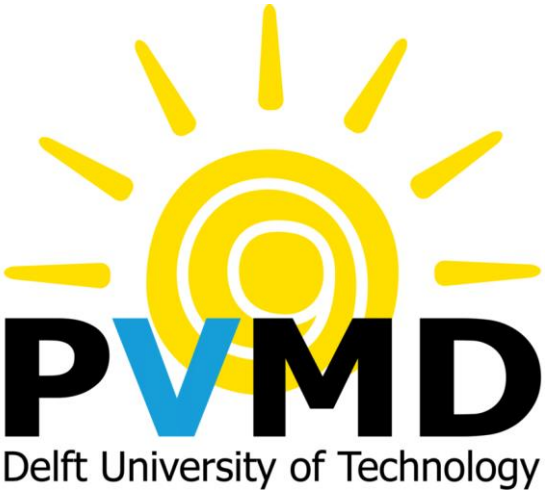

1 Introduction

This manual describes the different parts of the 'CONVERSION' tool of the PVMD Modeling Toolbox. After running the 'CELL', 'MODULE', 'WEATHER', and 'ELECTRIC' units of the toolbox, the fifth and final simulation unit of the toolbox can be run: the 'CONVERSION' unit. This unit can be accessed by clicking the CONVERSION button, shown in red in Figure 1, in the main menu. After pressing this button, a second menu shows up, shown in Figure 2. This menu allows the user to choose between four distinct power conversion architectures: A central inverter, a micro inverter, a string inverter, and a power optimizer. The following sections of this manual describe the features and underlaying principles for each of these systems.

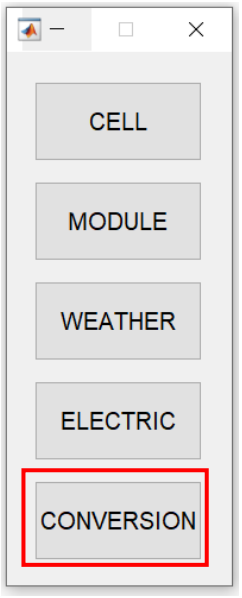

Figure 1

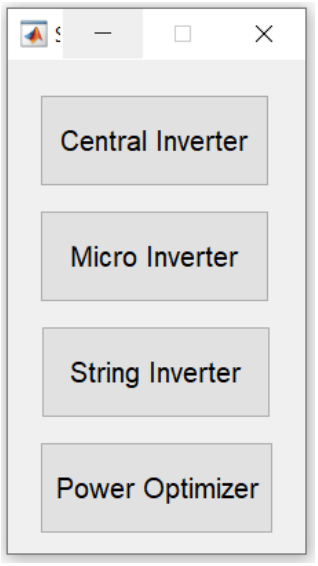

Figure 2

2 Central Inverter

This section describes the first option of the power conversion unit of the PVMD toolbox, the 'Central Inverter'. This option can be selected if the user wants to simulate a system with multiple parallel strings connected to a single inverter.

After clicking the top button of the menu shown in Figure 2, the user is asked to input the number of modules in parallel and in series (Figure 3). From this input, the simulation calculates the system voltage, current and power based on the results of the 'ELECTRIC' part. An important assumption that is made here is that each module in the array has the same output (power/voltage/current), as the current version of the PVMD toolbox can only simulate one module at the time.

```
Specify number of modules in parallel:
Specify number of modules in series:
```

Figure 3

Based on the maximum module output voltage, the tool presents a list with compatible inverter types (Figure 4). This list is created from a database with inverters that have coefficients for the SNL inverter model. The database that is used in the simulation is retrieved from the open source PV performance Modeling Collaborative, the PV_LIB Toolbox [1].

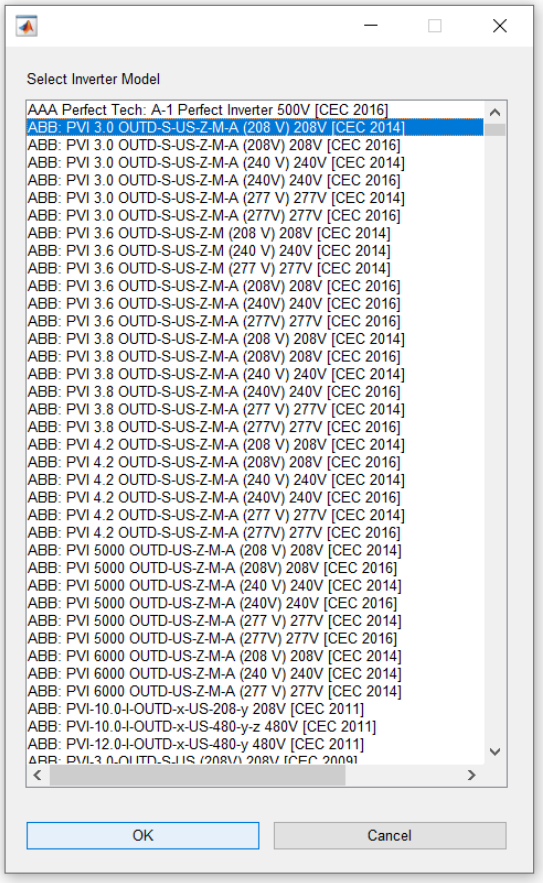

Figure 4

[1] PV Performance Modeling Collaborative, "PV_LIB Toolbox," [Online]. Available: https://pvpmc.sandia.gov/applications/pv_lib-toolbox/. [Accessed 31 01 2020].

After selecting the desired inverter type, the user is asked to include cable losses. More detail of these cable losses can be found in a separate section of this manual, Section 6.

The conversion efficiency of the inverter is calculated with the SNL model [2]. The calculations include inverter clipping and night tare losses. The final results of the simulation are stored in a struct called CONVERSION_output. In this struct the input inverter power and output inverter power, the inverter model, and the efficiency are stored.

Finally, an option is included to plot graphs. These graphs can help visualize the actual simulation. A graph for comparing the inverter input and output power is included as well as a graph for the inverter efficiency.

3 Micro Inverter

The Micro Inverter is the second power conversion option of the Conversion unit of the PVMD toolbox. The working principles are almost the same as the Central Inverter simulation, which is described in Section 2. After selecting the 'Micro Inverter' option shown in Figure 2, the user is presented with a list of inverters to choose from. It should be noted that the inverters in this list are not per definition all micro inverters. The list is based on a database with inverter models that have constants for the SNL inverter model. Since this database has no option to filter for micro inverters, an arbitrary maximum voltage of 100V is imposed as a way to filter the database. This maximum can be easily adjusted to show more or less inverter types.

After selecting the inverter type, cable losses can be added (explained in detail in Section 6) and graphs with results can be plotted. The final results of the simulation are stored in a struct called CONVERSION_output.

4 String Inverter

The String Inverter is the third power conversion option of the Conversion unit of the PVMD toolbox. The working principles are mostly the same as the two previous inverter simulations. After selecting the 'Micro Inverter' option shown in Figure 2, the user is presented with a list of inverters to choose from. It should be noted that the inverters in this list are not all string inverters. The list is based on a database with inverter models that have constants for the SNL inverter model. Since this database has no option to filter for string inverters, the list is only filtered based on the maximum module output voltage.

After selecting the inverter type, cable losses can be added (explained in detail in Section 6) and graphs with results can be plotted. The final results of the simulation are stored in a struct called CONVERSION_output.

[2] D. L. King, S. Gonzalez, G. M. Galbraith and W. E. Boyson, "Performance Model for Grid-Connected Photovoltaic Inverters," Sandia National Laboratories, Albuquerque, New Mexico 87185 and Livermore, California 94550, September 2007.

5 Power Optimizers

This section describes the fourth option of the power conversion tool for the PVMD toolbox; the power optimizer. This option can be selected to simulate systems that use power optimizers on module level. The simulation calculates the DC output power of the power optimizer based on the efficiency curves of the manufacturer. Finally, the user is able to add a complementary inverter and cable losses.

After clicking the 'Power Optimizer' button, shown in Figure 2, the user is asked to select the manufacturer of the power optimizer that they want to use (Figure 5). At this moment only one manufacturer is available in the tool, SolarEdge. After selecting the manufacturer, the user has to select the power optimizer type (Figure 6).

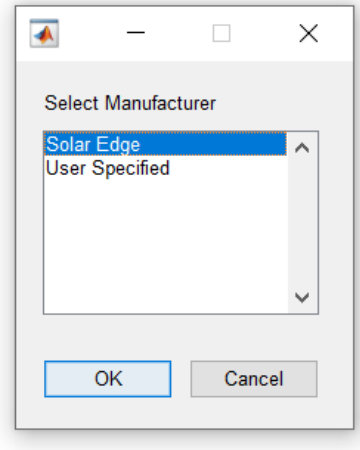

Figure 5

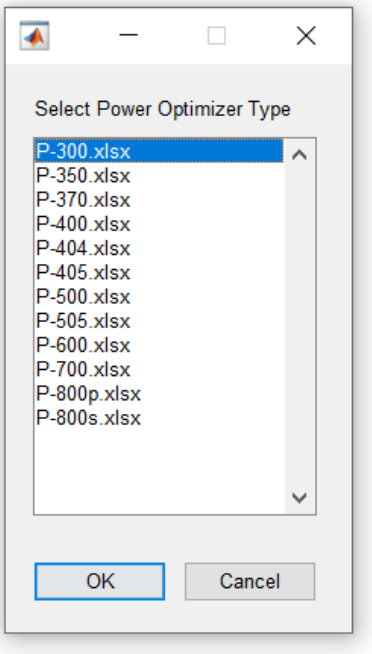

Figure 6

The power optimizer type that the user selects corresponds with an Excel file. This file contains the tabular data for three efficiency curves, where each curve corresponds to a certain input voltage. An example of such an efficiency curve for a power optimizer of SolarEdge is shown in Figure 7. The user can easily add a new manufacturer with different models by adding a new folder within the existing folder structure. In the 'User Specified' folder, a template is provided to easily add custom efficiency curves.

The simulations automatically check whether the maximum module output voltage exceeds the maximum input voltage of the selected power optimizer model. This could for example result in the following warning:

```
Warning: Max module output voltage exceeds vendor specified max input voltage
of 48V.
```

After some basic interpolation calculations between the provided curves, the tool calculates the power output and efficiency of the power optimizer. The output is stored in the workspace as a struct under CONVERSION_output and is shown in the Command Window, like the example below:

```
The predicted Power Optimizer output energy yield is 521.3712 Wh.
```

```
The overall Power Optimizer efficiency is 98.1994 %
```

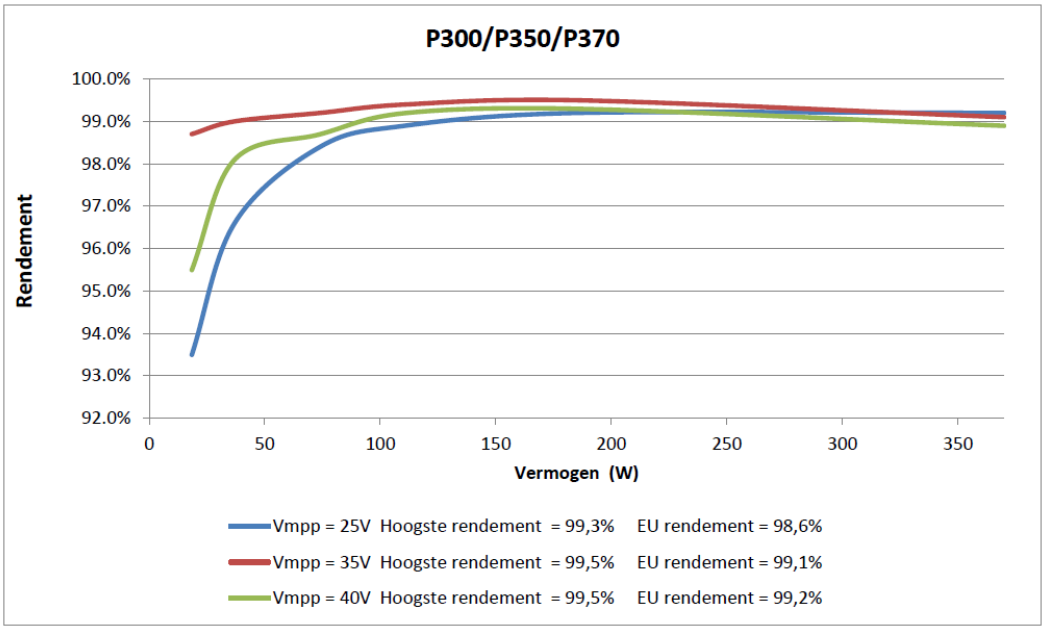

Figure 7 [3]

The simulations only work properly if the tabular data that is provided starts at y = 0. This is for example not the case in the example of Figure 7. In this case the code automatically calculates a new point at y = 0 based on the assumption that the graph is linear at low levels of input power.

After calculating the output power of the power optimizer, the user has the option to add a complementary central inverter (Figure 8). If 'Yes' is selected in this menu, the user is asked to input the number of modules in series and parallel (Figure 3). After providing this information, the user has to select an inverter manufacturer and inverter type (Figure 9 & Figure 10).

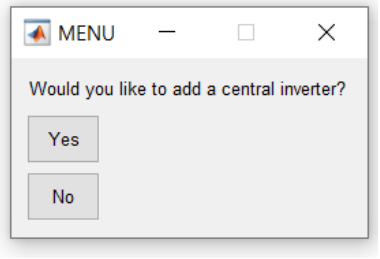

Figure 8

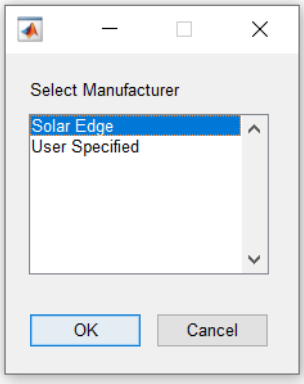

Figure 9

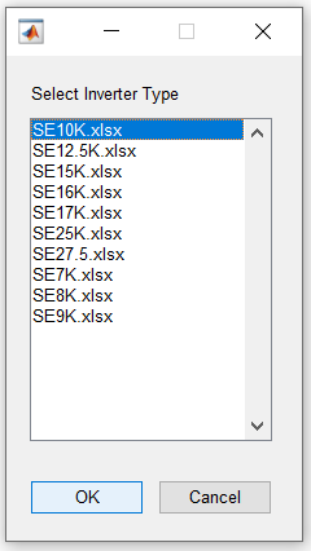

Figure 10

[3] SolarEdge, "Downloads," [Online]. Available: https://www.solaredge.com/nl/downloads#/. [Accessed 31 01 2020]

The inverter that is selected corresponds to an Excel file containing the inverter efficiency curve. The SNL model is not used in these calculations since these are special inverters that are complementary with the power optimizers and thus don't have DC-DC conversion and MPPT. Therefore, the choice was made to include company specific efficiency curves. The user can easily add custom efficiency curves within the existing folder structure using the Template.xslx file.

If a SolarEdge inverter type is chosen, the simulation checks if the number of power optimizers in the string is according to the regulations set by that company [4]. For this check to be carried out the user inputs the peak power generation of a single module (Figure 11). This check could result in a warning, e.g.:

```
Warning: The number of power optimizers in the string should be between 15
and 33.
```

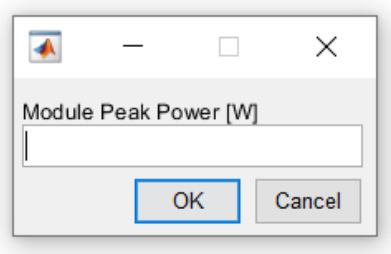

Figure 11

After selecting an inverter, the user has the option to include cable losses. Consider at least 2 meters of cable for each optimizer that is added to the system. The detailed procedure for the cable losses calculations are given in more detail in Section 6. Finally, an option is included to create graphs of the simulation results.

[4] SolarEdge, "Application Note SolarEdge String Sizing, EU Regulations"

6 Cable losses

In the previous sections, an option to include cable losses in the simulation was briefly mentioned. In this section this cable losses calculation is explained in some detail.

When running either the central, micro, or string inverter simulation or when adding a central inverter to a system with power optimizers, the user is asked to include cable losses by the means of a menu, shown in Figure 12.

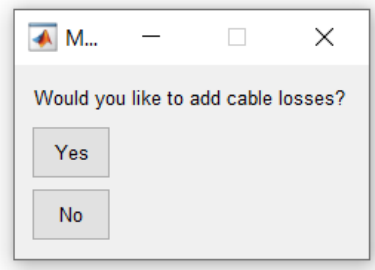

Figure 12

When 'no' is selected, the simulation carries on without including cable losses. When 'yes' is selected in this menu a second menu is presented to the user, shown in Figure 13.

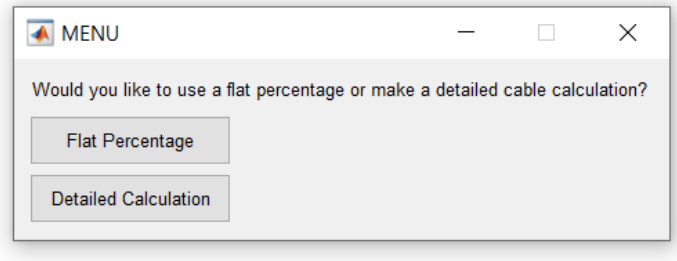

Figure 13

In this menu the user can choose between a simple calculation using a fixed loss percentage or a detailed cable loss calculation. When the 'fixed percentage' option is selected by the user, a menu is presented in which the user can specify an overall cable loss percentage (Figure 14). By default, this percentage is set at 1%. This percentage is subsequently used to calculate the DC input power of the inverter.

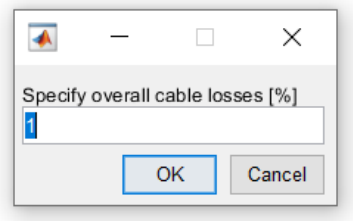

Figure 14

When the 'Detailed Calculation' option is selected, a new script is run in which these calculations are made. The calculations of the detailed cable losses are based on a relatively simple cable lay-out. A schematic of this lay-out is shown in Figure 15. In this schematic, multiple strings are connected to a junction box. This junction box is connected with a cable to the inverter. This lay-out provides the

flexibility to calculate independently the heat dissipated in the string cable and the cable to the inverter. Finally, these numbers are added to have a final value for the heat that is dissipated in all the cables of the system.

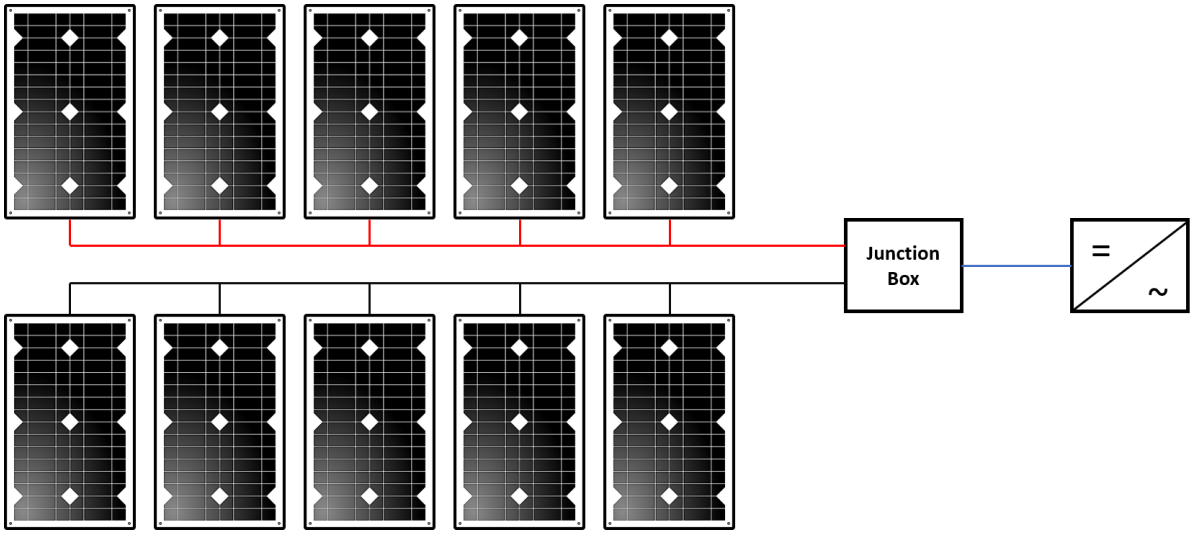

Figure 15 – Schematic overview cable calculations

The first step in the calculation is to specify the cable characteristics of a single string, in the schematic of Figure 15 shown in red. In the menu shown in Figure 17 the user selects the material (either copper or aluminum), the cable cross-section (based on industry standards) and the total cable length of a single string.

N.B.: Please consider the entire length of the cable, as the tool does not multiply the cable length with a factor of 2.

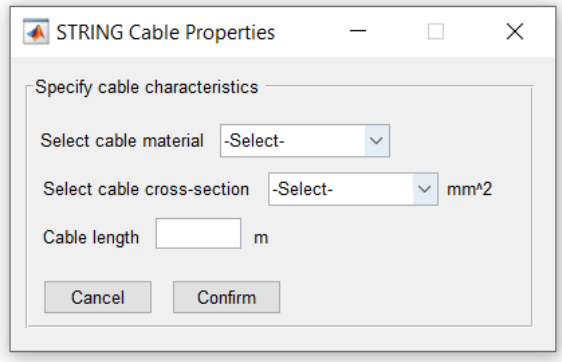

Figure 16

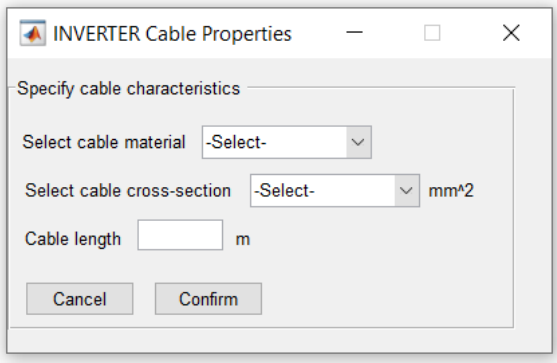

Figure 17

If there are multiple stings with modules the user has the option to include a second cable type. This cable is shown in blue in Figure 15. The user can again select the characteristics of this cable by the means of a menu, shown in Figure 17. If there are multiple strings but this cable section is not desired the user can input can simply put-in a 0 for the cable length.

In the tool, the wire sizing is indicated, from a scientific standpoint, with mm^2, while in the industry the American Wire Gauge (AWG) is typically used. Please consider Table 1 for the conversion between these two standards.

Table 1 – Cable standards [5]

Wire Cross-Section Area (mm^2)	Wire Size (AWG)	Maximum Rating (A)
0.5	20	5
0.75	18	7
1	-	-
1.5	16	10
2.5	14	15
4	12	20
6	10	30
10	8	50
16	6	65
25	4	85
35	2	115

Finally, the detailed cable calculation includes a check for the percentage of power that is lost in the cables. If this percentage exceeds 2%, the user is warned and advised to select a larger cable diameter:

```
Warning: Cable losses are above 2%. Consider a larger diameter cable.
```

The results of the cable loss calculations are independently stored in the workspace in a struct called CABLE_output. In this struct the percentual cable losses [%] and the power loss [W] are stored.

[5] H. Ziar, S. Farhangi and B. Asaei, "Modification to Wiring and Protection Standards," *IEEE JOURNAL OF PHOTOVOLTAICS,* vol. 4, no. 6, pp. 1603 - 1609, 2014.

7 Change Log

[1.1] - 2020-03-12
Added
- Change log to the manual
- Add comment about cable length
- Conversion table to manual
- 0.5 and 0.75 mm^2 cable cross-sections to the cable menu's
- Note about minimum cable length for optimizers

Changed
- Flat percentage to Fixed percentage
- INVERTER to INVERTER input
- Schematic overview of system

Removed
- Some of the larger cable diameters from the drop-down list

[1.0] - 2020-01-31
Added
- Power conversion tool. Features: simulation of power optimizers, inverters and cable losses based on user inputs.
- Power conversion user manual

- `Added` for new features.
- `Changed` for changes in existing functionality.
- `Deprecated` for soon-to-be removed features.
- `Removed` for now removed features.
- `Fixed` for any bug fixes.
- `Security` in case of vulnerabilities.

C

Appendix - NREL Module Inspection Questionnaire

To conduct the visual inspection of the modules of the INNOZOWA PV pilot system, an NREL questionnaire is used [51]. In this Appendix, such a completely filled-out questionnaire can be found. In total nine forms were filled-out, one for every INNOZOWA study case.

Monofacial, 0 deg tilt, Tracker System

Documentation of module condition

Date 15/05/2020 Name of data recorder TiM

Location RWZI, Weurt

Latitude 51.851 Longitude 5.795 Altitude -

1. System Data

System design: ☐ single module ☑ multiple modules (a.) ☐ unknown

(a.) Multiple module system:

Module location/number in a series string (from negative) ?

# of modules in series (string) 24 # of strings in parallel (array) -

# of bypass diodes - # of modules per bypass diode -

System Bias: ☐ open circuit ☐ resistive load ☑ max. power tracked ☐ short circuit ☐ unknown

System Grounding: ☐ grounded (a.) ☐ not grounded ☑ unknown

(a.) ☐ negative ☐ positive ☐ center of string ☑ unknown

BEGIN INSPECTION AT BACK SIDE OF MODULE

2. Module Data

Technology: ☑ mono Si ☐ multi Si ☐ a--Si ☐ CdTe ☐ CIGS/CIS ☐ other: _____

Certification: ☐ unknown ☐ UL 1703 ☑ IEC 61215 ☐ IEC 61646 ☑ IEC 61730 ☐ other: IEC 62701

Estimated deployment date Sep - 2019

Photo taken of nameplate: ☐ **yes** ☑ **no**

Manufacturer LG

Model # LG330N1K-V5

Serial # _____

Installation Site/Facility Serial # Weurt, 1271126

Width 101.6 cm Length 168.6 cm

Nameplate: ☐ nameplate missing

P_{max} 330 V_{oc} 41,0 I_{sc} 10.27

Sys Volt 750V V_{max} 750 I_{max} _____

Bypass diode, I_f -

Series fuse 20A

3. Rear-side Glass: ☑ **not applicable** ☐ **applicable**

Damage: ☐ no damage ☐ small, localized ☐ extensive

Damage Type (mark all that apply):
☐ crazing or other non--crack damage
☐ shattered (tempered) ☐ shattered (non-tempered) ☐ cracked (a.) ☐ chipped (b.)
(a.) Cracks (#):☐ 1 ☐ 2 ☐ 3 ☐ 4--10 ☐ >10
Crack(s) start from: ☐ module corner ☐ module edge ☐ cell ☐ junction box
☐ foreign body impact location
(b.) Chips (#): ☐ 1 ☐ 2 ☐ 3 ☐ 4--10 ☐ >10
Chipping location: ☐ module corner ☐ module edge

4. Backsheet: ☐ **not applicable** ☑ **applicable** → not Possible to check

Appearance: ☐ like new ☐ minor discoloration ☐ major discoloration
Texture: ☐ like new ☐ wavy (not delaminated) ☐ wavy (delaminated) ☐ dented
Material quality --chalking: ☐ none ☐ slight ☐ substantial
Damage: ☐ no damage ☐ small, localized ☐ extensive
Damage Type (mark all that apply):
☐ burn marks (a.) ☐ bubbles (b.) ☐ delamination (c.) ☐ cracks/scratches (d.)

(a.)Burn marks (#):☐ 1 ☐ 2 ☐ 3 ☐ 4--10 ☐ >10
Fraction of area burned:
☐ <5% ☐ 5--25% ☐ 50% ☐ 75% --100% (consistent overall)
(b.) Bubbles(#): ☐ 1 ☐ 2 ☐ 3 ☐ 4--10 ☐ >10
Average bubble dimension: ☐ <5mm ☐ 5--30mm ☐ >30mm
Fraction of area with bubbles > 5 mm:
☐ <5% ☐ 5--25% ☐ 50% ☐ 75% --100% (consistent overall)
(c.) Fraction of area delaminated:
☐ <5% ☐ 5--25% ☐ 50% ☐ 75% --100% (consistent overall)
Fraction of delamination that exposes circuit or cell(s)
☐ <5% ☐ 5--25% ☐ 50% ☐ 75% --100% (consistent overall)
(d.) Cracks/scratches (#): ☐ 1 ☐ 2 ☐ 3 ☐ 4--10 ☐ >10
Cracks/scratches location: ☐ random/no pattern ☐ over cells ☐ between cells
Fraction of area affected by cracks/scratches (approx.):
☐ <5% ☐ 5--25% ☐ 50% ☐ 75% --100% (consistent overall)
Fraction of cracks/scratches that expose circuit (approx.):
☐ 0% ☐ 25% ☐ 50% ☐ 75% ☐ 100%

5. Wires/Connectors:

Wires: ☐ not applicable ☑ like new ☐ pliable, but degraded ☐ embrittled
(mark all that apply): ☐ cracked/disintegrated insulation ☐ burnt
☐ corroded ☐ animal bites/marks
Connectors: ☐ not applicable ☑ like new ☐ pliable, but degraded ☐ embrittled
Type: ☐ unsure ☑ MC3 or MC4 ☐ Tyco Solarlok ☐ other _____

(mark all that apply): ☐ cracked/disintegrated insulation ☐ burnt ☐ corroded

6. Junction Box:

Junction box itself: ☐ **not applicable/observable** ☑ **applicable**
Physical state: ☑ intact ☐ unsound structure
(mark all that apply): ☐ weathered ☐ cracked ☐ burnt ☐ warped
Lid: ☐ intact/potted ☐ loose ☐ fell off ☐ cracked
Junction box adhesive: ☐ **not applicable/observable** ☑ **applicable**
Attachment: ☑ well attached ☐ loose/brittle ☐ fell off
Pliability: ☐ like new ☐ pliable, but degraded ☐ embrittled
Junction box wire attachments: ☐ **not applicable/observable** ☑ **applicable**
Attachment: ☑ well attached ☐ loose ☐ fell off
Seal: ☐ good seal ☐ seal will leak
other: ☐ arced/started a fire

7. Frame Grounding:

Original state: ☐ Wired ground ☐ Resistive ground ☐ No ground ☑ unknown
Appearance: ☑ Not applicable ☐ Like new ☐ Some corrosion ☐ Major corrosion
Function: ☑ Well grounded ☐ No connection

Photos taken of ☑ **back, label, and junction box** Partly

CONTINUE INSPECTION ON FRONT SIDE OF MODULE

8. Frame: ☐ **not applicable** ☑ **applicable**

Appearance: ☑ like new ☐ damaged (a.) ☐ missing
(a.) (mark all that apply): ☐ minor corrosion ☐ major corrosion ☐ frame joint separation
☐ frame cracking ☐ bent frame ☐ discoloration
Frame Adhesive: ☑ like new/not visible ☐ degraded (a.)
(a.) (mark all that apply): ☐ adhesive oozed out ☐ adhesive missing in areas

9. Frameless Edge Seal: ☑ **not applicable** ☐ **applicable**

Appearance: ☐ like new ☐ discoloration (a.) ☐ visibly degraded
(a.) Fraction affected by discoloration:
☐ <5% ☐ 5--25% ☐ 50% ☐ 75% --100% (consistent overall)
Material problems:
☐ squeezed/pinched out ☐ shows signs of moisture penetration
Delamination: ☐ none ☐ area(s) delaminated (a.)
(a.) Fraction Delaminated:
☐ <5% ☐ 5--25% ☐ 50% ☐ 75% --100% (consistent overall)

10. Glass/Polymer (front):

Material: ☐ glass ☐ polymer ☐ glass/polymer composite ☐ unknown
Features: ☐ smooth ☐ slightly textured ☐ pyramid/wave texture
☐ antireflection coating
Appearance: ☐ clean ☐ lightly soiled ☐ heavily soiled
Location of soiling:
☐ locally soiled near frame:
☐ left ☐ right ☐ top ☐ bottom ☐ all sides
☐ locally soiled on glass /bird droppings
Damage: ☐ no damage ☐ small, localized ☐ extensive
Damage Type (mark all that apply):
☐ crazing or other non--crack damage
☐ shattered (tempered) ☐ shattered (non--tempered) ☐ Cracked (a.)
☐ Chipped (b.) ☐ milky discoloration (c.)
(a.) Cracks (#): ☐ 1 ☐ 2 ☐ 3 ☐ 4--10 ☐ >10
Crack(s) start from: ☐ module corner ☐ module edge ☐ cell ☐ junction box
☐ foreign body impact location
(b.) Chips (#): ☐ 1 ☐ 2 ☐ 3 ☐ 4--10 ☐ >10
Chipping location: ☐ module corner ☐ module edge
(c.) Fraction of area:
☐ <5% ☐ 5-25% ☐ 50% ☐ 75% -- 100% (consistent overall)

11. Metallization:

Gridlines/Fingers: ☐ not applicable/barely observable ☐ applicable
Appearance: ☐ like new ☐ light discoloration(a.) ☐ dark discoloration(a.)
(a.) Fraction of discoloration:
☐ <5% ☐ 5-25% ☐ 50% ☐ 75% - 100% (consistent overall)
Busbars: ☐ not applicable/not observable ☐ applicable
Appearance: ☐ like new ☐ light discoloration(a.) ☐ dark discoloration(a.)
(a.) Fraction of discoloration:
☐ <5% ☐ 5-25% ☐ 50% ☐ 75% - 100% (consistent overall)
(mark all that apply): ☐ obvious corrosion ☐ diffuse burn mark(s) ☐ misaligned
Cell Interconnect Ribbon: ☐ not applicable/not observable ☐ applicable
Appearance: ☐ like new ☐ light discoloration(a.) ☐ dark discoloration(a.)
(a.) Fraction of discoloration:
☐ <5% ☐ 5-25% ☐ 50% ☐ 75% - 100% (consistent overall)
(mark all that apply): ☐ obvious corrosion ☐burn marks ☐ breaks
String Interconnect: ☐ not applicable/not observable ☐ applicable
Appearance: ☐ like new ☐ light discoloration(a.) ☐ dark discoloration(a.)
(a.) Fraction of discoloration:
☐ <5% ☐ 5-25% ☐ 50% ☐ 75% - 100% (consistent overall)
(mark all that apply): ☐ obvious corrosion ☐ burn marks ☐ breaks
☐ arc tracks (thin, small burns)

12. Silicon (mono or multi) module: ☐ **not applicable** ☑ **applicable**

Number of:
Cells in module 60
Cells in series/string 60
Strings in parallel –
Cell size: Width 16,17 cm Length 16,17 cm
Distance between frame and cell: ☐ >10 mm ☐ <10 mm
Distance between cells in a string: ☐ >1 mm ☐ <1 mm
Discoloration: ☐ none/like new ☑ light discoloration ☐ dark discoloration
Number of cells with any discoloration: hard to observe due to dirtyness
of those, average % discolored area:
☐ <5% ☐ 5-25% ☐ 50% ☑ 75% - 100% (consistent overall)
Discoloration location(s) (mark all that apply): ↳ cause: dirtyness
☐ module center ☐ module edges ☐ cell centers ☐ cell edges
☐ over gridlines ☐ over busbars ☐ over tabbing ☐ between cells
☐ individual cell(s)darker than others ☐ partial cell discoloration
Junction box area: ☐ same as elsewhere ☐ more affected ☐ less affected
Damage: ☑ none hard to observe.
(mark all that apply): ☐ burn mark (a.) ☐ cracking (b.) ☐ moisture
☐ worm marks/snail tracks (c.) ☐ foreign particle embedded
(a.) Burns (#): ☐ 1 ☐ 2 ☐ 3 ☐ 4-10 ☐ >10
(b.) Number of cells cracked: _____
(c.) Number of cells with worm marks/snail tracks: _____
Delamination: ☑ none ☐ from edges ☐ uniform ☐ corner(s) ☐ near junction box
☐ between cells (a.) ☐ over cells (b.) ☐ near cell or string interconnect
(a.) Fraction delaminated between cells:
☐ <5% ☐ 5-25% ☐ 50% ☐ 75-100% (consistent overall)
(b.) Fraction delaminated over cells:
☐ <5% ☐ 5-25% ☐ 50% ☐ 75-100% (consistent overall)
Likely interface (choose 2):
☐ glass ☐ semiconductor ☐ encapsulant ☐ back sheet ☐ busbar

13. Thin film module: ☑ **not applicable** ☐ **applicable**

Number of cells:
Number of cells in module _____
Number of cells in series/string _____
Number of strings in parallel _____
Cell size: Width _____ cm Length _____ cm
Distance between frame and cell: ☐ >10 mm ☐ <10 mm
Appearance: ☐ like new ☐ minor/light discoloration ☐ major/dark discoloration
Discoloration type (mark all that apply):
☐ spotted degradation ☐ haze (encapsulant browning) ☐ other

Discoloration location (mark all that apply):
☐ overall/no location pattern ☐ module center ☐ module edge(s)
☐ cell center ☐ cell edges ☐ near crack(s)

Damage: ☐ no damage ☐ small, localized ☐ extensive

Damage Type (mark all that apply): ☐ burn mark(s) ☐ cracking
☐ possible moisture ☐ foreign particle embedded

Delamination: ☐ no delamination ☐ small, localized ☐ extensive

Location: ☐ from edges ☐ uniform ☐ corner(s) ☐ near junction box ☐ near busbar
☐ along scribe lines

Delamination Type: ☐ absorber delamination ☐ AR coating delamination ☐ other

Photos taken of ☑ front and defects

14. Electronic Records ☐ not applicable ☑ applicable

Photographs and I--V curves recorded electronically--list file names in blanks

Photo files See Report

I--V curve Datasheet

Connector function: ☑ functions ☐ no longer mates ☐ exposed

Irradiance ~ 500 - 800 W/m² Sensor _____

Temperature ~ 15°C Sensor _____

EL picture -

IR picture Yes

Bypass Diode Test: ☑ not applicable ☐ applicable

Number of diodes:

In total 3, shorted 0, open 0

OTHER

* Modules heavily failed
* hard to check damage on gluss / cell / metallization due to dirt
* module azimuth changing due to one anchor point.

D

Appendix - Module Orientation

This Appendix contains the images used to determine the orientation of the modules of the Ground-based System. Figure D.1 shows a bird's-eye overview of the INNOZOWA PV pilot system. This overview is overlaid with Figure D.2, which is a schematic overview of the system. On this schematic overview all subsystems have a southward azimuth. Figure D.3 shows the overlaid image. The Retractable System of both figures is exactly placed on top of each other. The Retractable System is used as calibration because from the on-site inspection it is concluded that although the azimuth of individual panels can deviate, the overall system has a southward azimuth. From this final figure it can be concluded that the Ground-based system is not in its original intended place while its azimuth is not perfectly southwards. It is determined, from this figure, that the deviation is about 15 degrees.

Figure D.1: Bird's-eye view of the INNOZOWA PV Pilot system. Adapted from: https://www.youtube.com/watch?v=wZT82wGl9ck.

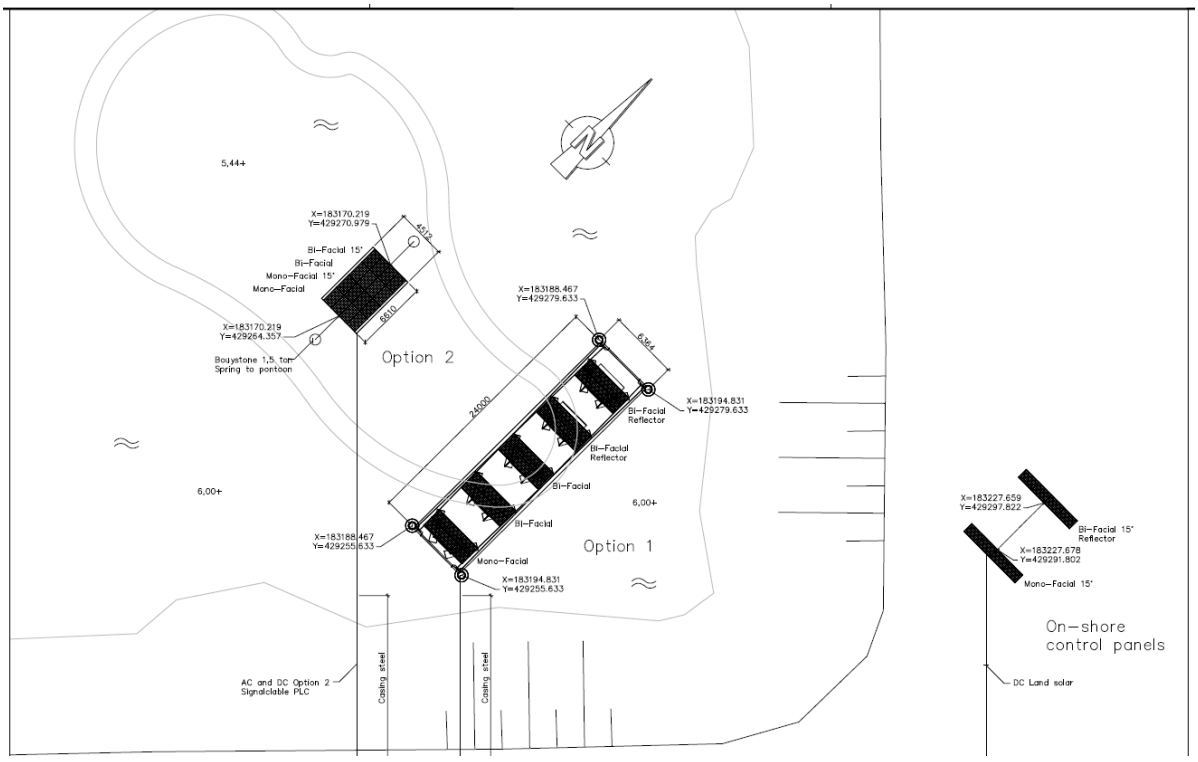

Figure D.2: Schematic overview of the pilot site.

Figure D.3: Bird's-eye overview of the PV pilot site overlaid with the schematic overview from which follows that the difference between the intended azimuth and the azimuth of the installed modules is about 15 degrees.